NTNU – Trondheim
Norwegian University of
Science and Technology

# Parametric Design

A Search for Membrane Structures

Daniel Smenes Eika

Civil and Environmental Engineering
Submission date: July 2012
Supervisor: Anders Rönnquist, KT
Co-supervisor: Pasi Olav Aalto, Institutt for byggekunst, historie og teknologi

Norwegian University of Science and Technology
Department of Structural Engineering

# PARAMETRIC DESIGN

## A SEARCH FOR MEMBRANE STRUCTURES

Daniel Smenes Eika

July 26, 2012


Norwegian University of Science and Technology

Faculty of Engineering Science and Technology

Department of Structural Engineering

TKT 4915 – Computational Mechanics, Master Thesis

# Problem Description

The thesis is aimed on the implementation of theories on Structural Engineering in the geometrical outcome of structures, and how to optimize the design thereafter. The student will to this by:

1. Studying and acquiring competence on relevant software
2. Establishing mathematical descriptions for the optimization
3. Using the software to run a selection of beam-arch problems
4. Using the software to run a selection of shell problems

The framework for this is an automatic, iterative process that finds solutions based on variations of selected geometrical parameters.

# Abstract

This report deals with shape optimization. Curved beams and thin shells are optimized with respect to internal bending moments. The shape optimization focuses solely on the shape of centroidal axes and middle surfaces, i.e. cross sections and shell thicknesses remain constant. The main part of the report is a presentation of three different cases, each with their own objectives. The scenarios are simplified and the criteria for success is internal bending moments alone; however, the methodology and the lessons learned are transferable also to other cases. 1. Curved beams in general. Optimum shapes are derived analytically for a variety of load cases and methods for estimating continuous optimum shapes are exhibited. Software which optimizes structures based on variations in the values of parameters is then applied. A brief study is done to get familiarized with approaches to the use of the software. Some of the shapes found analytically work as benchmarks. 2. An axisymmetric shell, the dome. Classical theories are studied for determining the internal bending moments of different dome shapes. After establishing the bending moments for a selection of shapes, the software is applied to accommodate the calculations and help determine what is the optimum one. An objective is to get familiarized with the assembling of 3 dimensional models within the software interface. 3. A double curvature shell. With the aid of the software, different suggestions are made to a hypothetical architect regarding the shape of the shell.

The author derives an effective method for estimating optimum shapes for curved beams. He comes to the perception that analytical approaches might not outweigh the constructive benefits of alternative methods when the complexity of the cases increases. The software proves itself an invaluable tool for form finding; however, it does not offer the same accuracy and possibilities to intervene with the algorithm of the FEA solver as other software. The general understanding of the approaches tested is that independent points and points defined by an interpolation curve are successful and that parameters assigned some level of interdependence is less successful.

Some suggestions for further work and possible improvements with regards to the process of structural optimization are presented at the end. These include mainly topology optimization, implementation of constructive measures (discrete) and how to best benefit from a conjunction of methods and types of software.

# Sammendrag (Abstract for Norwegian Readers)

Denne rapporten omhandler optimalisering av former. Buede bjelker og tynne skall blir optimalisert mht. indre bøyemomenter. Selve optimaliseringen fokuseres utelukkende på formen til tyngepunktsakser og midtre flater. Tverrsnitt og skalltykkelser forblir m.a.o. konstante. Hovedvekten til rapporten er lagt vekt på å presentere tre forskjellige case som hver har sine målsetninger. Tilfellene er forenklede og suksessfaktoren er kun indre bøyemoment, men metodikken og lærdommen er overførbar også til andre scenarioer. 1. Buede bjelker generelt. Optimaliserte former blir funnet analytisk for et utvalg av lasttilfeller og metoder for å estimere kontinuerlige, optimale former er fremvist. Programvare som optimaliserer strukturer basert på variasjoner i parametere blir så anvendt. En grunnleggende studie er utført for å bli kjent med tilnærmelser til programvaren. Noen av formene som er funnet analytisk fungerer som sammenligningsgrunnlag. 2. Rotasjonssymmetriske skall, kuppelen. Tidløse teorier studeres for å kunne fastslå de indre bøyemomentene til ulike former på kuppelen. Etter å ha etablert bøyemomentene til et utvalg av former er programvaren anvendt for å tilgodese utregningene og hjelpe til å bestemme hva som er den optimale formen. En målsetning er å bli kjent med hvordan man setter opp 3 dimensjonale modeller i programmet. 3. Et skall med dobbel kurvatur. Med hjelp av programmet presenteres forskjellige forslag som angår formen på skallet ovenfor en fiktiv arkitekt.

Forfatteren kommer frem til en effektiv metode for å estimere optimale former på buede bjelker. Han kommer til den oppfatning at analytiske tilnærmelser ikke veier opp for de konstruktive fordelene til alternative metoder når problemene blir mer omfattende. Programvaren viser seg å være et uvurderlig hjelpemiddel til å finne former, dog tilbyr den ikke samme grad av nøyaktighet og muligheter til å manipulere algoritmen til utregningene som andre, mer avanserte elementanalyseprogrammer. Blant de forskjellige tilnærmelsene forsøkt i denne studien har blant annet uavhengige punkter og punkter definert av en interpoleringskurve vist seg å være suksessfulle, mens parametere som er pålagt en eller annen form for avhengighet mellom seg har vist seg å være mindre vellykket.

Avslutningsvis blir noen forslag til videre arbeid og mulige forbedringer mht. prosessen til strukturoptimalisering fremvist. Dette inkluderer i hovedsak topologisk optimalisering, implementering av konstruktive faktorer (diskré) og hvordan best å utnytte samhandlingen mellom forskjellige metoder og typer programvare.

# Preface

The study presented here constitutes the Master Thesis; subject 'TKT 4915 – Computational Mechanics, Master Thesis', at the Norwegian University of Science and Technology (NTNU). The thesis is the final part of the program of study that is Civil Engineering, Computational Mechanics. The student is given 20 weeks to complete all phases of the project, from defining aims and acquiring literature to delivery. The thesis makes up the final 30 ECTS[1] of the total 300 ECTS of the program. Upon completion of the program, the student achieves the degree Master of Science.

The project is performed by one individual student; see the undersigned, with the guidance of supervisor, associate professor Anders Rønnquist at the Department for Structural Engineering and co- supervisor, assistant professor Pasi Aalto at the Department of Architectural Design, History and Technology.

The challenge at hand is to optimize structures with the aid of modern software. The study is confined to shape optimization.

I have, for as long as I can remember had an inherent interest for geometry and 'mathematically correct' shapes. The mere aesthetics of continuous structures that successfully serve as transmitters of forces appeal to me in a way that makes the problem at hand a natural choice for my Master Thesis. It is a wish of mine to be able to utilize the theories acquired through my education in the early stages of construction projects. The interchanging of ideas with architects and the potential synergy that might result from it intrigues me.
After being introduced to the software used in this research, it has been a motivation of mine to be able to manage and comprehend its potential. Fur-

[1] European Credit Transfer and Accumulation System

thermore, the intention has been to reach a certain level of insight as to what fields and specializations play a role in the wide spectrum that is Structural Optimization.

My key experiences and - competences related to this project are obtained through the courses offered at NTNU. The preceding semester, I completed a specialization project which focused on optimizing a quasi-static simulation in Abaqus FEA.

Some logistical challenges involved the procurement of the individual pieces of software needed to complete the study, and a personal computer equipped to run the optimizations. Due to external circumstances, the delivery date for the thesis was set to be in the middle of the Norwegian summer vacation. This required a certain level of independence during its completion. A number of libraries in Norway were closed during this period, prolonging the waiting period for relevant last minute literature.

The experience of writing the thesis has been exciting. The more I have investigated the more interesting fields and approaches I have come across.

During the 20 weeks spent writing this report several updates to all pieces of the software have been published, significantly improving both work flow and possibilities to solving the problems. The road to discovering the world of the software family that is Rhino, Grasshopper and Karamba and associated programs has been a true journey; one I hope I get to pursue in my working profession, future studies and other future endeavors.

Daniel Smenes Eika, July 26, 2012

# Acknowledgments

It was my supervisor, associate professor Anders Rønnquist at the Department for Structural Engineering, who first introduced me to the topic of parametric design and supported me in proceeding with parametric design for my master thesis. I thank him for his guidance throughout the semester and for his advice on matters stretching beyond the realms of the report. It was he who got me in contact with assistant professor Pasi Aalto at the Department of Architectural Design, History and Technology. Aalto's advice and insight on applicable software have been indispensable and his input from an architectural point of view has been highly motivating.

Special thanks go to Prof. Dr. Ing. Kai- Uwe Bletzinger, professor at Technische Universität München, for sharing his lecture notes and papers on structural optimization. Further thanks go to Ing. Tomás del Carril, professor at the Faculty of Engineering at la Universidad de Buenos Aires, for his literary advice.

David Rutten and Clemens Preisinger, authors of the software, have provided for an impeccable customer service and great thanks go to them for helping clarify any doubts related to its application.

A mandatory regard goes to my grandmother, Birgit Eika, for moral support and for leaving her house at my disposal during the completion of the thesis. Finally, I would like to thank my reading committee, M.Sc. Offshore Engineering Åsmund Eika and Dr. Johan Elling Tausjø, for academic feedback and for feedback on the language respectively.

You have all, each in your own way, contributed to making this learning experience both rewarding and enjoyable.

# List of Tables

# List of Figures

# Nomenclature

## Acronyms

| | |
|---|---|
| BIM | Building Information Modeling |
| CAD | Computer Aided Design |
| FEA | Finite Element Analysis |
| NTNU | Norwegian University of Technology and Science |
| NURBS | Non-Uniform Rational B-Spline |

## Symbols[2]

| | |
|---|---|
| $a, b$ | temporarly assigned variables |
| A,B,C,D | geometric ends or corners |
| $A, B$ | Lamé parameters (when related to double curvature shells) |
| $C$ | constant of integration |
| $\mathbf{e}$ | unit vector |
| $e$ | axis of revolution |
| $i$ | imaginary number, $\sqrt{-1}$ |

[2]some symbols that are given explicit explanations in the text or considered obvious to the reader are not included

| | |
|---|---|
| $k$ | number of beam elements |
| $N$ | internal axial force |
| $p$ | surface load |
| $q$ | line load |
| $S$ | beam length along centroidal axis |
| $T$ | internal membrane force |
| $u, v, w$ | displacements in local coordinates |
| $x, y, z$ | global, Cartesian coordinates |
| $\frac{1}{R}$ | initial curvature |
| $\kappa$ | change in curvature |
| $\varphi$ | parallel angle |
| $\psi$ | meridional angle |
| $\tilde{(-)}$ | projected onto the x,y- plane |
| $I, II$ | curvilinear coordinates |

Vectors are given a bold font.

**Sub- indices**

| | |
|---|---|
| $a$ | approximated |
| $a, b$ | initial shape assumptions, analytical convergence |
| $c$ | catenary |
| $n$ | normal |
| $p$ | parabola (if related to shape) |
| $p$ | projected (if related to load) |

| | |
|---|---|
| $q$ | quarter circle |
| $x, y, z$ | global, Cartesian directions |
| $\varphi$ | parallel direction (except for $R_\varphi$) |
| $\psi$ | meridional direction (except for $R_\psi$) |
| $\parallel$ | parallel direction |
| $\perp$ | perpendicular direction |
| $0, 1, ..i, ..k$ | point or node identities |
| $1, 2, ..i, ..k$ | line or beam element identities |
| $1, 2, 3..i, ..$ | analytical iterations |
| $1, 2$ | principal directions (when related to double curvature shells) |
| $3$ | normal direction (when related to double curvature shells) |

# Contents

# Chapter 1

# INTRODUCTION

## 1.1 Description

In coherence with the problem description, this report will examine ways to optimize structures by applying modern software. The optimization is limited to the geometric features of structures. Curved beams and shells will be investigated. Some solutions will be derived analytically for the sake of comparison as well as for the sake of establishing an academic foundation.

## 1.2 Focus

There are several criteria by which one might measure the success of a project or a design. Since the intention is to be able to delve into the topic of structural optimization, the variety of problems and criteria for optimization for this report becomes limited. The idea is that the methodology to some extent is transferable to other types of structural challenges. In this investigation, beam and shell cases are limited to cases where the overall axial and membrane stresses are compressive. The optimization is solely chosen to reduce the bending moments within the structures, to strive for a membrane state. A reason for this is the high efficiency in terms of internal work reached by such a solution. - How to determine the internal bending moments of curved beams and shells? It is chosen to focus on optimizing geometric parameters that influence the shape of the centroidal axes of the structures; i.e. cross

sections remain constant. - How to reduce bending moments of a structure by modifications to its shape? - To what extent is this possible by applying the software available today?

**Challenge:** Finding structures subjected to only axial or membrane stresses

**Measure of success:** Absolute bending moment $\rightarrow 0$

## 1.3 Strategy

To be able to answer the questions in section 1.2, the following steps will be taken:

1. Establish a theoretical foundation. Timeless theories will be investigated through classical literature and customized to the needs of this research. Some methods will be derived by the writer
2. Present a general outline of the software
3. Attempt to reach solutions analytically for curved beams and axisymmetric shells
4. Reach solutions for the curved beams and axisymmetric shells with the aid of the software. The purpose of this is to investigate approaches to the software and get familiarized with its possibilities and challenges
5. Apply the software with the purpose of finding optimum shapes for a double curvature shell

Results, discussions and intermediate conclusions will be presented consecutively in accordance to the individual objectives and purposes of each case and section, for the reader to more easily be able to follow the line of reasoning.

# Chapter 2

# THEORETICAL BACKGROUND

## 2.1 Some Basic Assumptions

Both beams and shells obey Hooke's law. Displacements are small relative to the other dimensions of the beams and shells, including the (thin) shell thickness.

All shell calculations follow theories considered valid for thin shells. This implies that the thickness of the shell is (or at least should be) less than 5% of the smallest radius of curvature at any point on the shell, [Novozhilov64]. Kirchhoff's statements apply. 1) The straight fibers of a plate which are perpendicular to the middle surface before deformation remain so after deformation and do not change their length. 2) The normal stresses acting on planes parallel to the middle surface may be neglected in comparison with the other stresses. Some methods derived from references are based on a disregard of the term $\frac{t}{R}$ where $t$ and $R$ are the thickness and radius of curvature of the shell respectively.

Higher order terms are disregarded without being stated explicitly. A consequence of this is; e.g., changes in curvature may be derived from a second order derivation of the normal displacements.

Some assumptions remain implicit when considered obvious to the reader.

## 2.2 Geometrical Descriptions

### 2.2.1 The Curved Beam

The curved beam problems are in this research reduced to cases where the beam endpoints are positioned at the Cartesian coordinates $(0, 0)$ and $(\Delta y, \Delta x)$ with $\Delta y \cap \Delta x > 0$. The centroidal axis of the beam is denoted $y(x)$.

#### Remarks Regarding the Curved Beam

One key feature of the curved beam is that the centroidal axis does not coincide with the neutral axis, [Cook99]. The neutral axis within a beam makes up the positions where the circumferential strain due to bending moment is zero. Consequently, an optimum homogeneous cross section for a curved beam made up of a linear elastic, isotropic material would generally be thicker in the z- direction on the side of the centroidal axis closer to the center of curvature. This is independent of whether the bending moment is negative or positive. Optimization of cross sections is not included in this study; however, this feature is considered so essential that it is mentioned as such.

### 2.2.2 The Axisymmetric Shell

To describe an axisymmetric shell, it is found convenient to define the location and curvature at a given point on its surface by its meridional angle $\psi$, parallel angle $\varphi$ and principal radius of curvature $R_\psi$ and $R_\varphi$. $R_\psi$ and $R_0$ are the radius of curvature of the meridional and parallel curves, figure 2.1 *(a)* and *(b)*.

As a consequence of this notation, an infinitesimal part of the shell's surface can be written in the following manner

$$dA = R_\psi \cdot d\psi \cdot R_0 \cdot d\varphi \tag{2.1}$$

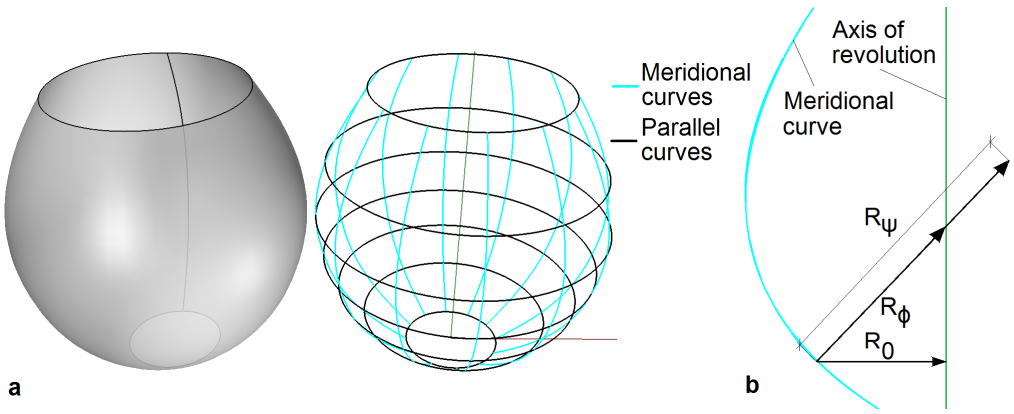


Figure 2.1: *(a) Axisymmetric surface with corresponding meridional and parallel curves (b) Meridional plane with the principal radius of curvature and the radius of curvature of the parallel curve at a point on the surface*

In cases where the meridional radius of curvature can be expressed by the radius of the parallel curves, and the coordinate on the axis of revolution is $e$, the following notation can be adapted

$$R_\psi\left(R_0\right) = -\frac{\left(1+e(R_0)^{'2}\right)^{\frac{3}{2}}}{e(R_0)^{''}} \tag{2.2}$$

where $e(R_0)^{(n)} = \frac{d^n e(R_0)}{dR_0^n}$. The sign of the curvature implies that it is positive when the inclination of the meridional curve decreases as $R_0$ increases.

The relation between the global, Cartesian coordinates $x, y, z$ and the meridional angle $\psi$ and the principal curves are given and demonstrated in the proceeding example.

*Example*

We want to describe a roof shaped as a revolved parabola, figure 2.2.

In this case $R_0 = x$ and the meridional curve is given by $e = y = b\left(1 - \left[\frac{x}{a}\right]^2\right)$; hence, the meridional angle is given by

$$\psi = -atan(\frac{dy}{dx}) = atan(\frac{2b}{a^2}x) \tag{2.3}$$

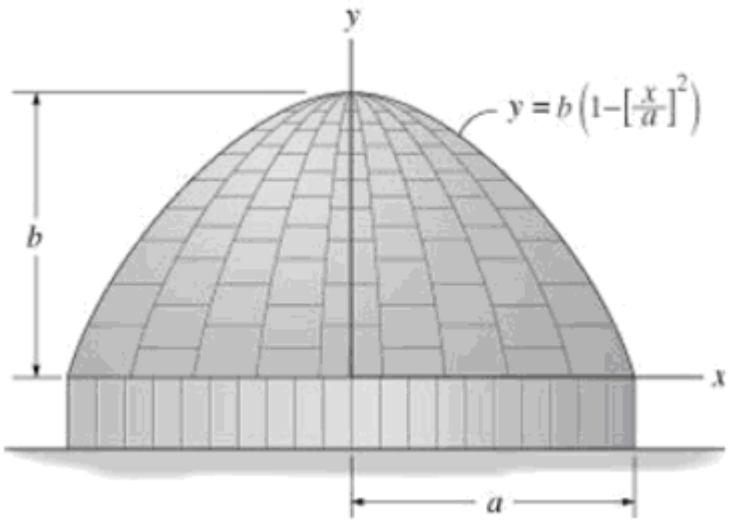


Figure 2.2: *http://www.solutioninn.com. Roof with the shape of a revolved parabola*

and the meridional radius of curvature is

$$R_\psi = \frac{(1 + (\frac{2b}{a^2}x)^2)^{\frac{3}{2}}}{\frac{2b}{a^2}} = \frac{a^2}{2b}(1 + (\frac{2b}{a^2}x)^2)^{\frac{3}{2}} \tag{2.4}$$

$\psi$ spans from the y- axis; i.e., where the surface intersects the axis of revolution, $R_0 = \psi = 0$.

The other principal radius of curvature $R_\varphi$ is

$$R_\varphi = \frac{R_0}{sin(\psi)} = \sqrt{x^2 + (\frac{a^2}{2b})^2} \tag{2.5}$$

□

Note that the terminology 'axisymmetric' and 'rotational symmetric' will be used interchangeably, though all cases in this research are axisymmetric.

## 2.3 Theories from Structural Mechanics

In this report, the terminology 'membrane state' applies to both beams and shells and refers to a state where the structure is subjected to only axial or membrane stresses.

### 2.3.1 The Curved Beam

An infinitesimal part of the centroidal axis of the curved beam $dS$ is given the lateral and vertical components $dx$ and $dy$. Correspondingly, a distributed load $q_n$ acting perpendicularly over the same part has the components $q_x = q_n\frac{dy}{dS}$ and $q_y = q_n\frac{dx}{dS}$. By projecting these load components onto the x- and y- axes; $q_{xp} \cdot dy = q_x \cdot dS$ and $q_{yp} \cdot dx = q_y \cdot dS$, the following relation is found

$$q_n(y(x)) = q_{xp}(y) = q_{yp}(x) \tag{2.6}$$

for any point $[x, y(x)]$.

A load $q_y(y(x))$ acting strictly vertically over the same part has the projection

$$q_{yp}(x) = q_y(y(x))\frac{dS}{dx} = \frac{q_y(y(x))}{cos(atan(\frac{dy}{dx}))} = q_y(y(x))\sqrt{(\frac{dy}{dx})^2 + 1} \tag{2.7}$$

acting over the infinitesimal distance $dx$.

### 2.3.2 The Axisymmetric Shell

Theories dealing with membrane and bending stresses in axisymmetric thin shells will be presented. When dealing with axisymmetric cases, the material properties, boundary conditions, lines of distortion and geometry all are restricted to the cylindrical symmetry. If any of these conditions are not met, the case ceases to comply with the following theories, as shear stresses as well as membrane and bending stresses will be present, [Ugural81], p. 201.

#### 2.3.2.1 External forces

The external load component normal to an infinitesimal part of the surface is denoted $p_n$. The components tangent to the meridional and parallel curves are denoted $p_\psi$ and $p_\varphi$. $P_e$ is the resultant of the load, and is always pointing in the direction of the axis of revolution.

#### 2.3.2.2 Membrane Theory

In the following it is attempted to establish the equations of equilibrium for the membrane forces $T_\psi$ and $T_\varphi$, corresponding to the forces in the meridional and parallel directions.

In the plane of the parallel curves, the internal forces are independent from the angle $\varphi$ as there is neither variation in neither geometry nor external load in that direction. However, in the meridional direction the variation must be accounted for. By treating the two directions separately we can derive from equation 2.1 that the internal forces occurring within an infinitesimal part of the shell are equal to $T_\psi \cdot R_0 \cdot d\varphi$ and $T_\varphi \cdot R_\psi \cdot d\psi$. The variation in the meridional direction over the same infinitesimal part is then noted $\frac{\delta T_\psi \cdot R_0 \cdot d\varphi}{\delta \varphi} d\varphi$.

The resultant of the internal forces over the same infinitesimal part is pointing in the direction normal to the surface, figure 2.3. From the illustration, it is observed that the resultants of the forces are equal to $2T_\psi \cdot R_0 \cdot d\varphi \cdot sin(\frac{d\psi}{2}) \approx T_\psi \cdot R_0 \cdot d\varphi \cdot d\psi$ and $T_\varphi \cdot R_\psi \cdot d\psi \cdot sin(\frac{d\varphi}{2}) \approx T_\varphi \cdot R_\psi \cdot d\psi \cdot d\varphi$. The equation of equilibrium for the forces acting perpendicularly to the surface is then as follows

$$p_n \cdot dA - T_\psi \cdot R_0 \cdot d\varphi \cdot d\psi - T_\varphi \cdot R_\psi \cdot d\psi \cdot d\varphi \cdot sin(\psi) = 0$$

Combined with equation 2.1, this then reveals the following relation

$$\frac{T_\psi}{R_\psi} + \frac{T_\varphi}{R_\varphi} = p_n \tag{2.8}$$

Parallel to the axis of revolution, only the forces in the meridional direction contributes to the equilibrium. By looking at an axisymmetric shell intersected by a plane in the parallel direction, it is shown that

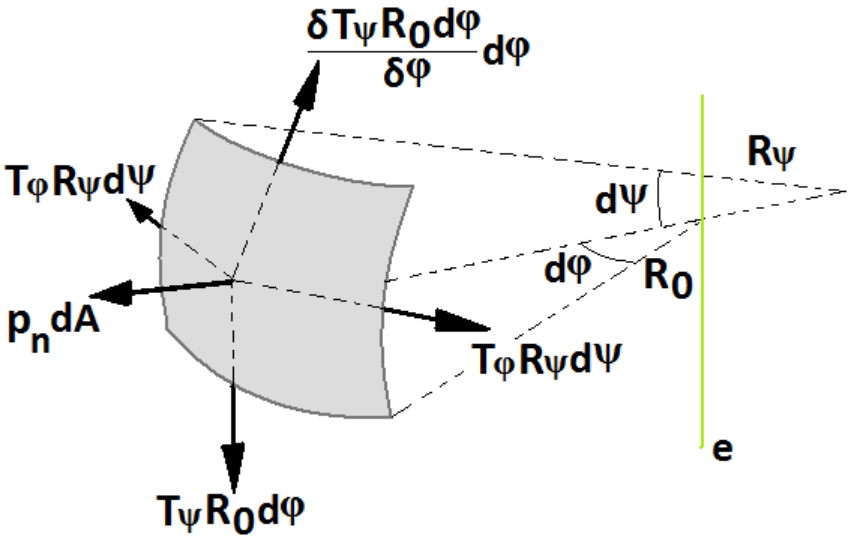


Figure 2.3: *Membrane shell element of an axisymmetric shell*

$$P_e + T_\psi \cdot R_0 \cdot 2\pi \cdot sin(\psi) = 0$$

This leads to the following equation of equilibrium

$$T_\psi = -\frac{P_e}{R_0 \cdot 2\pi \cdot sin(\psi)} \tag{2.9}$$

**Remarks Regarding the Membrane State** The membrane state is no longer current at- and in close proximity to lines of distortion. The lines of distortion refer to parallel lines where shear forces appear. These are due to the following:

1. Borders and boundary conditions where the displacements are incompatible with the angles of support
2. Concentrated loads, or loads with discontinuities
3. Abrupt changes in curvature, 'kinks'
4. Abrupt changes in stiffness

To account for the shear forces, one has to introduce flexural theories. Recommended reading on this subject is [Flügge60], an invariable reference on shell calculations.

If an axisymmetric shell is subjected to an asymmetric load (e.g. wind loading), one can include membrane shearing forces $T_{\psi\varphi}$ and $T_{\varphi\psi}$ in the membrane theory, as proposed in [Ugural81], chapter 10.7. This scenario is not included in the form finding studied here.

For thin shells of revolution, it can be shown that the accuracy of the membrane theory is adequate for most design purposes. Both stresses and displacements ascertained from membrane theory differ little from that ascertained when including the bending theory with the exception of lines of distortion, [Ugural81], p. 243. In accordance with the aim of this study; however, the bending theory plays an important role for optimizing structures with respect to bending moments.

#### 2.3.2.3 Bending Theory

In addition to the normal forces $T_\psi$ and $T_\varphi$, there are three unknown stress resultants $Q_\psi$, $M_\psi$ and $M_\varphi$ being the shearing force in the meridional direction and the moments about the parallel and meridional tangents, figure 2.4. Note that there are no shearing forces in the parallel direction, and that $\frac{dT_\varphi}{d\varphi} = \frac{dM_\varphi}{d\varphi} = 0$. By following the same analogy as with the membrane theory, the equilibrium normal- and tangent to the meridional curve and about the parallel curve respectively are expressed;

$$p_n \cdot dA - T_\psi \cdot R_0 \cdot d\varphi \cdot d\psi - T_\varphi \cdot R_\psi \cdot d\psi \cdot d\varphi \cdot sin(\psi) - \frac{d(Q_\psi \cdot R_0 \cdot d\varphi)}{d\psi} d\psi = 0$$

$$p_\psi \cdot dA + Q_\psi \cdot R_0 \cdot d\varphi \cdot d\psi + T_\varphi \cdot R_\psi \cdot d\psi \cdot d\varphi \cdot cos(\psi) - \frac{d(T_\psi \cdot R_0 \cdot d\varphi)}{d\psi} d\psi = 0$$

$$Q_\psi \cdot dA + M_\varphi \cdot R_\psi \cdot d\psi \cdot d\varphi \cdot cos(\psi) - \frac{d(M_\psi \cdot R_0 \cdot d\varphi)}{d\psi} d\psi = 0$$

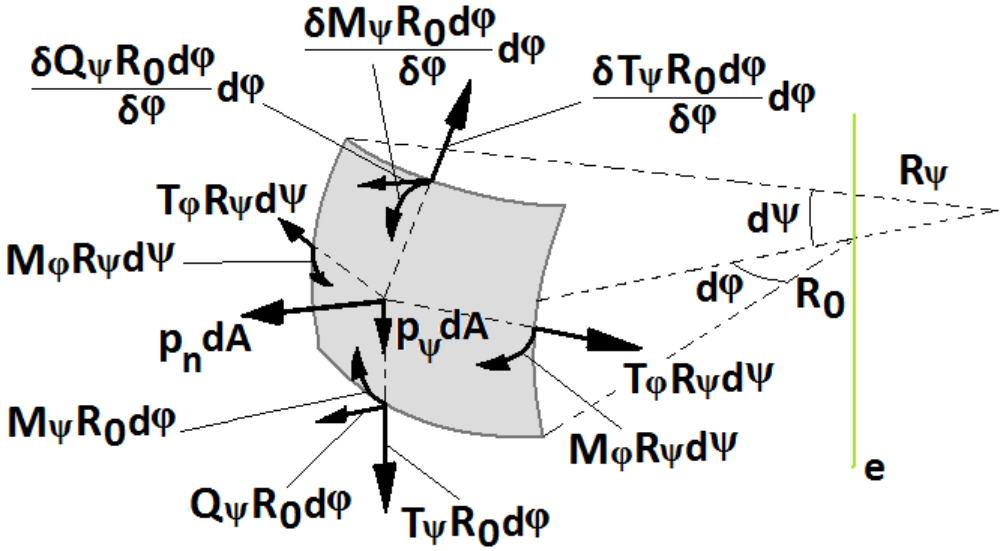


Figure 2.4: *Shell element of an axisymmetric shell included bending theory*

where $M_\varphi \cdot R_\psi \cdot d\psi \cdot d\varphi \cdot cos(\psi)$ is the resultant of the moments acting on each meridional side of the infinitesimal part, diverging at an angle $d\varphi$.

Introducing equation 2.1, the governing equations of equilibrium are revealed

$$\frac{T_\psi}{R_\psi} + \frac{T_\varphi}{R_0} sin(\psi) + \frac{d(Q_\psi \cdot R_0)}{d\psi} \frac{1}{R_\psi \cdot R_0} = p_n \tag{2.10}$$

$$\frac{Q_\psi}{R_\psi} + \frac{T_\varphi}{R_0} \cdot cos(\psi) - \frac{d(T_\psi \cdot R_0)}{d\psi} \frac{1}{R_\psi \cdot R_0} = -p_\psi \tag{2.11}$$

$$Q_\psi + \frac{M_\varphi}{R_0} \cdot cos(\psi) - \frac{d(M_\psi \cdot R_0)}{d\psi} \frac{1}{R_\psi \cdot R_0} = 0 \tag{2.12}$$

Displacements parallel to the meridional tangent and normal to the surface are denoted $u$ and $w$ respectively. By further introducing kinematic relations, equation 2.13, material laws for isotropic materials in plane stress, equation 2.14, and moment- curvature relations, equation 2.15, the number of unknowns is reduced to three.

$$\begin{bmatrix} \varepsilon_\psi \\ \varepsilon_\varphi \end{bmatrix} = \begin{bmatrix} \frac{1}{R_\psi}\frac{du}{d\psi} - \frac{w}{R_\psi} \\ \frac{u}{R_\varphi}cot(\psi) - \frac{w}{R_\varphi} \end{bmatrix} \tag{2.13}$$

$$\begin{bmatrix} \sigma_\psi \\ \sigma_\varphi \end{bmatrix} = \frac{1}{t}\begin{bmatrix} T_\psi \\ T_\varphi \end{bmatrix} = \frac{E}{1-\nu^2}\begin{bmatrix} \varepsilon_\psi + \nu \cdot \varepsilon_\varphi \\ \varepsilon_\varphi + \nu \cdot \varepsilon_\psi \end{bmatrix} \tag{2.14}$$

$$\begin{bmatrix} M_\psi \\ M_\varphi \end{bmatrix} = -D\begin{bmatrix} \kappa_\psi + \nu \cdot \kappa_\varphi \\ \kappa_\varphi + \nu \cdot \kappa_\psi \end{bmatrix} \tag{2.15}$$

$\varepsilon$, $\nu$, $t$ and $E$ are the strains, Poisson's ratio, shell thickness and Young's modulus correspondingly. The shell rigidity is $D = \frac{E \cdot t^3}{12(1-\nu^2)}$. The change in curvature is given the following relations; $\kappa_\psi = \frac{1}{R_\psi}\frac{d}{d\psi}(\frac{u}{R_\psi} + \frac{dw}{R_\psi \cdot d\psi})$ and $\kappa_\varphi = (\frac{u}{R_\psi} + \frac{dw}{R_\psi \cdot d\psi})\frac{cos(\psi)}{R_0}$, [Ugural81]. The equations for the bending moments are of interest, and consequently they are exhibited:

$$M_\psi = -D[\frac{1}{R_\psi}\frac{d}{d\psi}(\frac{u}{R_\psi} + \frac{dw}{R_\psi \cdot d\psi}) + \frac{\nu \cdot cos(\psi)}{R_0}(\frac{u}{R_\psi} + \frac{dw}{R_\psi \cdot d\psi})] \tag{2.16}$$

$$M_\varphi = -D[(\frac{u}{R_\psi} + \frac{dw}{R_\psi \cdot d\psi})\frac{cos(\psi)}{R_0} + \frac{\nu}{R_\psi}\frac{d}{d\psi}(\frac{u}{R_\psi} + \frac{dw}{R_\psi \cdot d\psi})] \tag{2.17}$$

Hooke's law, which is a mere alternative to equation 2.14, is presented

$$\begin{bmatrix} \varepsilon_\psi \\ \varepsilon_\varphi \end{bmatrix} = \frac{1}{E}\begin{bmatrix} \sigma_\psi - \nu \cdot \sigma_\varphi \\ \sigma_\varphi - \nu \cdot \sigma_\psi \end{bmatrix} \tag{2.18}$$

# Chapter 3

# SOFTWARE

It is desired to optimize the shape of the structures. In order to run the optimization, four pieces of software have been adopted. Rhinoceros is a modeling tool. Grasshopper is a plug-in for Rhinoceros, and enables the user to create models based on parameters and relations between them. Karamba is a Finite Element program that runs within the Grasshopper interface. The optimization itself is run by Galapagos. Galapagos is an Evolutionary Solver included in the Grasshopper plug-in.

In the proceeding sections, key features of the software will be presented briefly.

## 3.1 Rhinoceros 5.0

Rhinoceros, or Rhino for short, is one of the more advanced options of designing tools on the market today. In this research, attention is given the software for its well established application amongst architects. Rhino provides an interface for a series of third party plug-ins suited for a variety of purposes. Grasshopper is an example which is suited for the purpose of parameterization.

Rhino has been in the forefront in the field of Non- Uniform Rational B-Splines (NURBS) geometry, [Altmann], [Rw06], [Schneider]. NURBS has proven itself advantageous in representing free form, 3 dimensional geometry for its flexibility and accuracy. NURBS is a key feature in isogeometric

analysis partly due to its infinite smoothness, [Cottrell09]. When working in a 3 dimensional environment projected on to a 2 dimensional screen, and when manipulating NURBS geometry, the understanding of homogeneous coordinates is relevant, [Anh05], [Wildberger09].

For more information, visit http://www.rhino3d.com/.

## 3.2 Grasshopper 0.9.0001

Grasshopper provides for an interactive way of modeling. On a canvas one lays out all parameters, geometries, data, functions, conversions, and any other feature one might think of. Between these components one draws the wires that connect them, mapping out the relations between them. Most components are designed with inputs and outputs representing the input data and the corresponding data outputs. There might be several data outputs on a component. If any of the components contain geometric data, the geometry is drawn in the Rhino interface. One component in particular allows for dynamic updates, and is used for the evolutionary solver; namely, the slider. On the slider is a value within a defined range. This value can be modified by dragging its position up and down the slider. By doing so, all components that depend on this value update dynamically. Consequently, the geometry shown in the Rhino interface also updates in real- time. In figure 3.1 is a simple example including two points whose coordinates are defined by the values on sliders.

Any one component might contain large amounts of data. This can among other things be single values, vectors, multidimensional matrices, Boolean values, geometries and generic data. When dealing with matrices or lists of data, one refers to data trees and paths. The handling and manipulation of such lists is essential to the Grasshopper workflow, [Payne09]. In figure 3.1 is a simple example showing that two individual point components give the same data as one point component containing two points.

Third parties continuously develop new components that enhance the workflow and possibilities of Grasshopper. In order to accomplish what is demonstrated in this research, an add-on called MeshEdit was installed for more components related to mesh editing. The add-on is developed by a third party called [uto], http://www.grasshopper3d.com/group/geco.

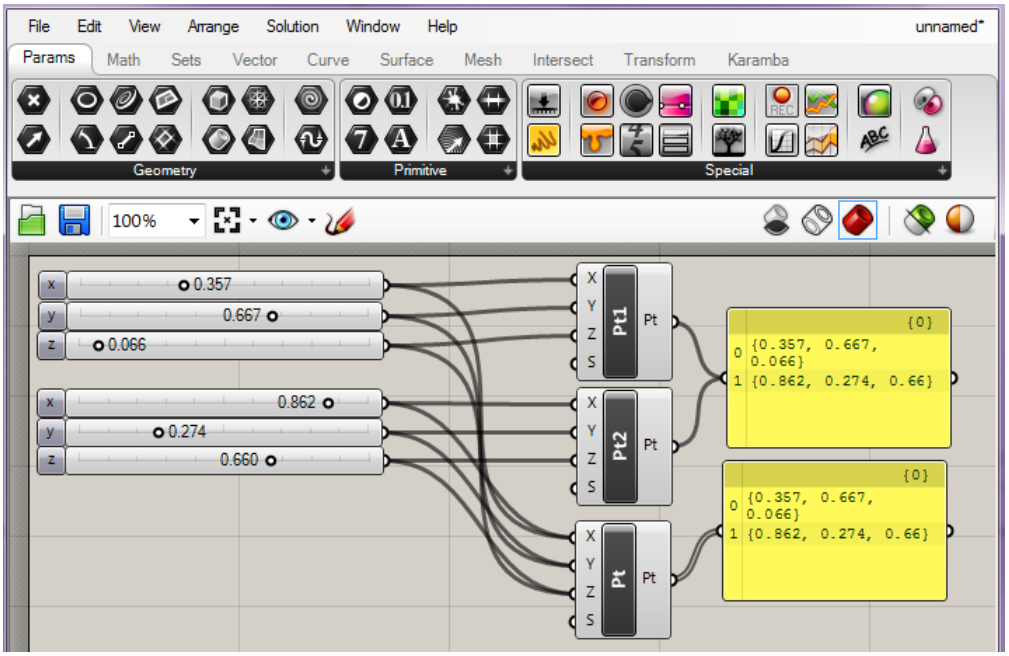


Figure 3.1: *Simple example of sliders and data management in Grasshopper*

As Grasshopper is a plug-in for Rhino, its geometry is represented by NURBS; and thus, any interpolation is also represented by NURBS curves and surfaces. Knowing this is important when manipulating the models, as the geometrical outcome is a result of the features of such a framework. One trait investigated here is the curve degree. By increasing the curve degree of an interpolated curve, one increases its ability to 'wiggle' and it is given more freedom. This may result in curves that more easily make sudden turns, or even loops. The degree refers to the number of control points surrounding a given point on the curve that contribute to its shape, [Rutten12]. The number of control points for a curve is greater than or equal to the degree of the curve plus one. Hence, by increasing the curve degree, in some cases, one increases the number of control points needed to make the interpolation.

For more examples; a selection of the models used in the research is included in appendix C.

For more information, visit http://www.grasshopper3d.com/.

| The Karamba Beam Element | |
|---|---|
| **Geometry** | Cylinder, circular profile |
| Outer diameter | $10cm$ |
| Wall thickness | $0.33cm$ |
| **Material** | Steel, S235 |
| **Interpolation** | Hermitian |

Table 3.1: *Features of the default beam element used in Karamba*

## 3.3 Karamba 0.9.0084

Karamba is, as mentioned, a Finite Element program that works within the Grasshopper interface. In practice, it is a set of new components that allows for structural analysis on the models developed in Grasshopper. Among other things, it defines and assembles the loads, geometry and support conditions for the analysis.

At the time of investigation only beam elements are provided by the software; however, a version that includes shell elements is only weeks away from being published [Preisinger12#2]. To compensate for this, triangular beam grids are suggested by its developers. In this research, no modifications are done to the default element. Its features are presented in table 3.1, [Preisinger12#1].

Each load component applied in this research provides for the opportunity to toggle whether the load is perpendicular to the element, defined by global coordinates and distributed on to the beam, or if it is defined by global coordinates and projected. In either case, the user is left only to decide its absolute value and global direction. Two different load components have been used. The first one is a line load. Investigation confirms that its load does transfer to both point loads and moments about its nodes. The second one is called a mesh load. The mesh load component is given a surface mesh established in Grasshopper. From the surface mesh, it distributes the load acting over its surface onto points defined by the user. The size of a point load acting on a point depends on the distributed load acting over the area closest to it. Investigation confirms that the mesh load does not translate to bending moments about its nodes.

The software is deliberately limited to that necessary in the early design phase to enhance the speed of calculation, [Mira12]. This is one of the rea-

sons why isoparametric elements are not employed. The Finite Element Analysis (FEA) performed by Karamba is strictly linear elastic, and applicable only to beam elements with straight axes. However, geometrical nonlinearity is partly accounted for by a large deformation component. The component allows for incremental increases of the load, where the geometry updates after each increment. The estimation obtained with such a method will inevitably drift away from the exact solution, and the error is only reduced by decreasing the size of the increments, [Preisinger12#1]. The large deformation analysis is one approach to form finding, but is not included in the current research as the intentions of the research is solely to study the optimization of parameters.

By default, all element joints are stiff. For more information on hinged joints, it is referred to [Mira12], which examines deployable scissor structures modeled using Karamba.

The software also includes calculations of eigenmodes, a feature not further examined in this investigation.

For more information, visit http://www.karamba3d.com/.

## 3.4 Galapagos

Within the Grasshopper interface exists a component which is the Evolutionary Solver called Galapagos. This component relates to a selection of parameters to be optimized and a fitness parameter. The fitness parameter is the measure for the optimization. The user is free to select any output and define it as the fitness parameter. If the output chosen as the fitness parameter contains more than one value, Galapagos uses its average by default, [Rutten10]. One can choose for Galapagos to either maximize or minimize the fitness. The task of the Evolutionary Solver is to vary the parameters to be optimized in order to find the global maxima or minima of the fitness, respectively.

Without going into details about the Evolutionary Algorithms, some advantages and disadvantages will be mentioned. A pedagogical introduction to the topic with a humorous touch is recommended, [Rutten10]. The pros and cons as mentioned by [Rutten10] are as follows:

### Cons

1. They are slow. If an iteration takes 1 minute and consists of 50 individuals and it is run for 50 generations, one is looking into a two-day run time. For the most complex (but still simple) problems presented in this research, the completion of one generation lasts about 30 seconds.

2. They do not guarantee a solution. If no 'good enough' value is prescribed, they will tend to run indefinitely.

### Pros

1. They are flexible. They are able to tackle a wide variety of problems. Most the problems one encounter on a daily basis falls into the 'evolutionary solvable' category.

2. They are forgiving. They will happily chew on problems that have been poorly formulated. Due its progressive process, any intermediate solution can be harvested and called a result of sorts.

3. They allow for a high degree of interaction with the user. The run time process is highly transparent and the solver can be coached and goaded with the aid of human intelligence.

# Chapter 4

# CASE: CURVED BEAMS

In this case, a simply supported curved beam is studied. The end of the beam at point $(0, 0)$ is named A and the other extreme is named B, positioned at $(\Delta x, \Delta y)$. The shape of the beam is represented by its centroidal axis $y(x)$. The goal is to find shapes for the beam that give zero bending moment $M_z(x, y(x)) = 0$ for a variety of load cases. All loads are acting in the x, y-plane; hence, the solutions are restricted to $z = 0$.

Firstly, some analytical solutions will be established. Some of the solutions will then work as benchmarks when applying the software.

## 4.1 Loads and Boundary Conditions

The beam is pinned in A. The boundary forces in A are denoted $A_x$ and $A_y$ and defined as positive when acting in the direction of the x- and y- axes. In B, the beam is only restricted against lateral movement. The boundary force is denoted $B_x$ and defined as positive when acting in the negative x-direction. An advantage of the chosen boundary conditions is that upon the attainment of such a zero moment shape, the solution can be mirrored about the axis $(\Delta x, 0), (\Delta x, \Delta y)$ to form an arch with only axial internal forces.

For the sake of simplicity, all loads are decomposed into vertical and lateral components that are projected parallelly to the x- and y- axes correspondingly. In cases where the magnitude and/or direction of the load depends on the surface it is acting on, a load acting perpendicularly to $y(x)$ is projected

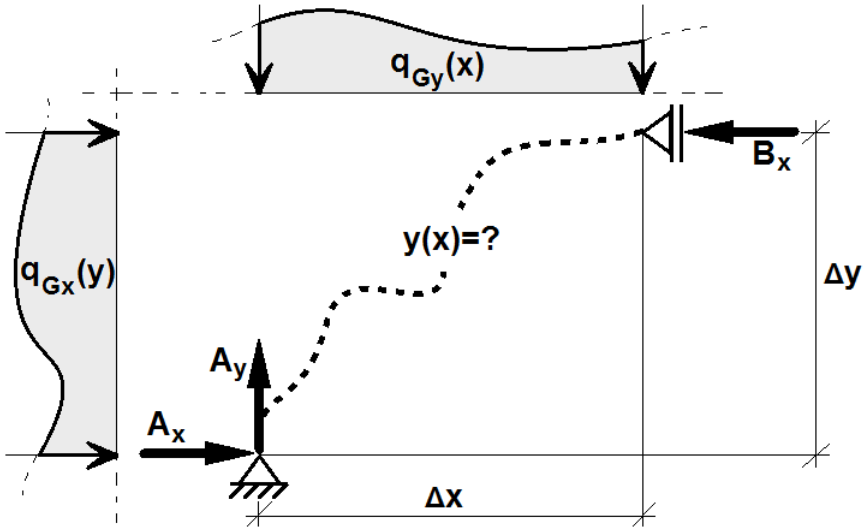


Figure 4.1: *Loads and boundary conditions for the curved beam scenarios*

in accordance with equation 2.6. Loads acting vertically over the centroidal axis are decomposed in accordance with equation 2.7. The sum of all decomposed and projected loads are referred to as global loads $q_{Gx}(y)$ and $q_{Gy}(x)$, figure 4.1. $q_{Gx}$ is defined as positive when acting in the positive x- direction and $q_{Gy}$ is defined as positive when acting in the negative y- direction.

## 4.2 Analytical Solutions

For the sake of notation, $y = y(x)$ and $M = M_z$ for the remainder of this chapter unless explicitly stated otherwise.

### 4.2.1 When the Global Loads Are Given

A method for deriving zero moment shapes when the global loads are given will be investigated.

As a statically determinate system, the boundary forces can be calculated from the equilibrium equations alone. $\sum F_y = 0$ reveals that $A_y = \int_0^{\Delta x} q_{Gy}(x)dx$ and $\sum M_A = 0$ reveals that $B_x = \frac{1}{\Delta y}(\int_0^{\Delta y} q_{Gx}(y) \cdot ydy + \int_0^{\Delta x} q_{Gy}(x) \cdot xdx)$.

In turn, $\sum F_x = 0$ gives that $A_x = B_x - \int_0^{\Delta y} q_{Gx}(y)dy = \int_0^{\Delta y} q_{Gx}(y) \cdot (\frac{y}{\Delta y} - 1)dy + \frac{1}{\Delta y}\int_0^{\Delta x} q_{Gy}(x) \cdot xdx$. The bending moment $M(x, y)$ due the loads $q_{Gx}(y)$ and $q_{Gy}(x)$ are denoted $M_{qx}(y)$ and $M_{qy}(x)$ correspondingly.

$$M_{qx}(y) = \int_0^y q_{Gx}(\psi) \cdot (y - \psi)d\psi \tag{4.1}$$

$$M_{qy}(x) = \int_0^x q_{Gy}(\chi) \cdot (x - \chi)d\chi \tag{4.2}$$

Knowing this, the moment distribution can be calculated for an arbitrary shape $y(x)$ starting in A:

$$M(x, y) = A_x \cdot y - A_y \cdot x + M_{qx}(y) + M_{qy}(x) \tag{4.3}$$

As defined by the goal, it is desired to find a solution for $M(x, y) = 0$. By doing so, and further moving all terms dependent on 'y' on the left side of the equation, and all terms dependent on 'x' on the other, an implicit form of the solution is obtained.

$$A_x \cdot y + M_{qx}(y) = A_y \cdot x - M_{qy}(x) \tag{4.4}$$

#### 4.2.1.1 Uniform Global Load Acting at an Angle

It is desired to reach an analytical solution for a constant global load $q_{G\alpha}$ acting at an angle $0 < \alpha \leq \frac{\pi}{2}$ to the x- axis. As a consequence, $\alpha = 0$ indicates that $q_{Gy}(x) = 0$ and $q_{Gx}(y) = q_{G\alpha}$, and $\alpha = \frac{\pi}{2}$ means that $q_{Gy}(x) = q_{G\alpha}$ and $q_{Gx}(y) = 0$.

From this approach one can derive shapes for a variety of carrying structures. The most intuitive load equivalent would perhaps be that of evenly spaced truss-like structures or ropes. Varying the position of the supports corresponds to changing the direction of the load relative to the global axes x and y described later in this section.

Before proceeding, the scenario $\alpha = \frac{\pi}{2}$ is investigated. The solution is open for input values $\Delta x$ and $\Delta y$, leaving the boundary forces to be $A_y = q_{G\alpha} \cdot \Delta x$ and $B_x = A_x = \frac{1}{2} q_{G\alpha} \frac{\Delta x^2}{\Delta y}$. The bending moment contributions from the

| Angle, $\alpha$ | $y(x, \Delta x, \Delta y)$ | $y(x, 1.0, 1.5)$ |
|---|---|---|
| $\frac{\pi}{2}$ | $x\frac{\Delta y}{\Delta x}(2 - \frac{x}{\Delta x})$ | $1.5x(2 - x)$ |

Table 4.1: *Solution for a constant global load at* $\alpha = \frac{\pi}{2}$

global load are $M_{qx}(y) = 0$ and $M_{qy}(x) = \frac{1}{2}q_{G\alpha} \cdot x^2$. Adding these results to equation 4.4 and solving for '$y$', reveals the solution shown in table 4.1. As an example, the solution for $\Delta x = 1.0$ and $\Delta y = 1.5$ is included.

This shows that the parabola is the shape that carries a constant global load without being subject to bending moments about the axis perpendicular to its plane. The axis of symmetry of the parabola is parallel to the direction of the load. Knowing this, a general solution for a load acting at an angle $\alpha$ can be explored. It is advantageous to transform the coordinate system by rotating it about the end point 'A' so that the directions of its axes are parallel and perpendicular to the load. Its coordinates are denoted $r_{\parallel}$ and $r_{\perp}$ and relate to $x$ and $y$ in the following manner

$$\begin{Bmatrix} r_{\parallel}(x, y, \alpha) \\ r_{\perp}(x, y, \alpha) \end{Bmatrix} = \begin{bmatrix} -cos(\alpha) & sin(\alpha) \\ sin(\alpha) & cos(\alpha) \end{bmatrix} \cdot \begin{Bmatrix} x \\ y \end{Bmatrix} \tag{4.5}$$

As with $\Delta x$ and $\Delta y$, the distances between A and B parallel and perpendicular to the newly established axes are expressed; $\{\Delta r_{\parallel}(\alpha), \Delta r_{\perp}(\alpha)\}^T = \{r_{\parallel}(\Delta x, \Delta y, \alpha), r_{\perp}(\Delta x, \Delta y, \alpha)\}^T$. In order to use the solution found for $\alpha = \frac{\pi}{2}$, the curved beam is pinned in B and added a hinge at its peak $C$, located at the maximum value of $r_{\parallel}(r_{\perp})$, figure 4.2. Additional information regarding the admissible height of the curved beam is required. Relating this height to the globally defined coordinate '$y$' has proven itself quite cumbersome, and is not recommended. It is chosen to define the coordinate in $C$ parallel to the load; $\Delta r_{\parallel AC}(\alpha)$, by an accepted interpolation for $\alpha \in [0, \frac{\pi}{2}]$. Naturally it is given that $\Delta r_{\parallel AC}(0) = 0$ and $\Delta r_{\parallel AC}(\frac{\pi}{2}) = \Delta r_{\parallel}(\frac{\pi}{2}) = \Delta y$. The choice for interpolation can easily be modified in compliance with the problem at hand, whether being in terms of geometrical restrictions or restrictions regarding the internal axial forces of the beam. What is yet to determine is the coordinate in $C$ perpendicular to the load; $\Delta r_{\perp AC}(\alpha)$. As a statically determinate system, the boundary forces for each of the beam members $AC$ and $CB$ can be calculated separately as shown in section 4.2.1. By adding

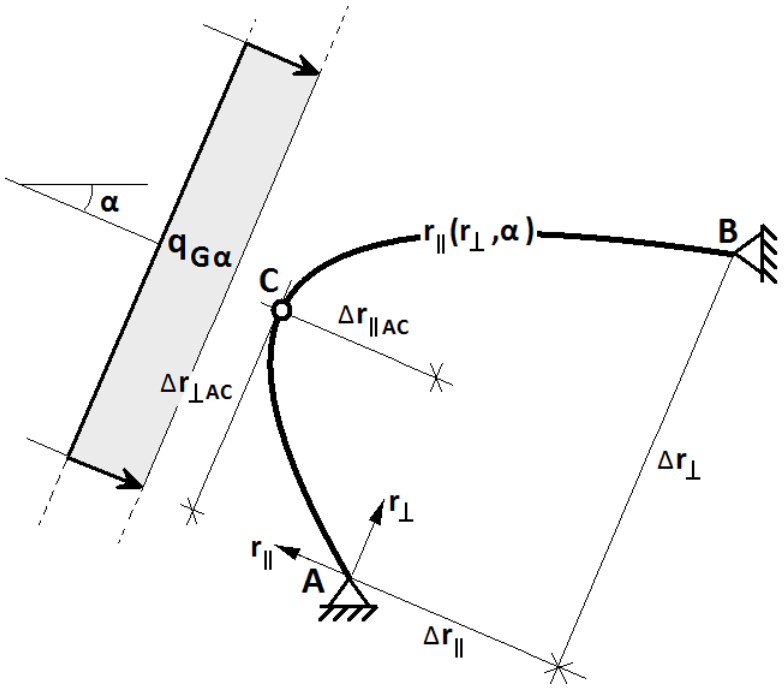


Figure 4.2: *Loads, boundary conditions and coordinate system for the scenario of the constant global load acting at an angle*

the requirement that the boundary forces perpendicular to the load need to be equal; $A_{\perp} = C_{\perp} = B_{\perp}$, it is defined that

$$\Delta r_{\perp AC}(\alpha) = \Delta r_{\perp}(\alpha)\frac{\Delta r_{\parallel AC}(\alpha)}{\Delta r_{\parallel}(\alpha)} \left\{ \begin{array}{c} 1+\sqrt{1-\frac{\Delta r_{\parallel}(\alpha)}{\Delta r_{\parallel AC}(\alpha)}} \\ 1-\sqrt{1-\frac{\Delta r_{\parallel}(\alpha)}{\Delta r_{\parallel AC}(\alpha)}} \end{array} \right\} \tag{4.6}$$

However, $\Delta r_{\perp AC}(\alpha)_1$ will not be given any more attention as it implies that $\Delta r_{\perp AC}(\alpha) \geq \Delta r_{\perp}(\alpha)$; thus, leaving $\Delta r_{\perp AC}(\alpha) \leftarrow \Delta r_{\perp AC}(\alpha)_2$.

Having identified all variables, the curved beam expressed in coordinates '$r_{\parallel}(r_{\perp})$' and '$r_{\perp}$' is as follows

$$r_{\parallel}(r_{\perp},\alpha) = -\frac{\Delta r_{\parallel AC}(\alpha)}{\Delta r_{\perp AC}(\alpha)^2} r_{\perp}^2 + 2\frac{\Delta r_{\parallel AC}(\alpha)}{\Delta r_{\perp AC}(\alpha)} r_{\perp} \tag{4.7}$$

| Angle, $\alpha$ | $y(x, \Delta x \leftarrow 1.0, \Delta y \leftarrow 1.5)$ |
|---|---|
| $\frac{\pi}{2}$ | $1.5x(2-x)$ |
| $\frac{5\pi}{12}$ | $3.678 - 3.732x - 4.904(0.919 + \left\{ \begin{array}{c} \sqrt{0.029 + 1.500x} \\ -\sqrt{0.029 + 1.500x} \end{array} \right\})$ |
| $\frac{\pi}{3}$ | $1.995 - 1.732x - 1.535(0.864 + \left\{ \begin{array}{c} \sqrt{0.190 + 2.598x} \\ -\sqrt{0.190 + 2.598x} \end{array} \right\})$ |
| $\frac{\pi}{4}$ | $1.376 - 1.000x - 0.918(0.688 + \left\{ \begin{array}{c} \sqrt{0.659 + 3.000x} \\ -\sqrt{0.659 + 3.000x} \end{array} \right\})$ |
| $\frac{\pi}{6}$ | $1.001 - 0.577x - 0.771(0.434 + \left\{ \begin{array}{c} \sqrt{0.749 + 2.598x} \\ -\sqrt{0.749 + 2.598x} \end{array} \right\})$ |
| $\frac{\pi}{12}$ | $0.686 - 0.268x - 0.915(0.171 + \left\{ \begin{array}{c} \sqrt{0.335 + 1.500x} \\ -\sqrt{0.335 + 1.500x} \end{array} \right\})$ |

Table 4.2: *Solutions for beams with zero bending moment pinned in* $(0, 0)$ *and* $(1.0, 1.5)$ *and subjected to a constant global load acting at various angles* $\alpha$*. Height defined by* $\Delta r_{\parallel AC}(\alpha) = \Delta y \cdot sin(\alpha)$

Transforming the general solution back to global coordinates '$x$' and '$y$', equation 4.5 and solving for $y$ gives the final expression for the beam

$$y(x, \alpha) = \frac{\Delta r_{\perp AC}(\alpha) - x \cdot sin(\alpha)}{cos(\alpha)} - \frac{\Delta r_{\perp AC}(\alpha)}{2\Delta r_{\parallel AC}(\alpha) \cdot cos(\alpha)^2}[\Delta r_{\perp AC}(\alpha) \cdot sin(\alpha) + (\star)] \tag{4.8}$$

$$(\star) = \left\{ \begin{array}{c} \sqrt{(\Delta r_{\perp AC}(\alpha) \cdot sin(\alpha) - 2\Delta r_{\parallel AC}(\alpha) \cdot cos(\alpha))^2 + 4x \cdot \Delta r_{\parallel AC}(\alpha) \cdot cos(\alpha)} \\ -\sqrt{(\Delta r_{\perp AC}(\alpha) \cdot sin(\alpha) - 2\Delta r_{\parallel AC}(\alpha) \cdot cos(\alpha))^2 + 4x \cdot \Delta r_{\parallel AC}(\alpha) \cdot cos(\alpha)} \end{array} \right\}$$

As previously stated, the interpolation for $\Delta r_{\parallel AC}(\alpha)$ can be chosen freely. This case advances with the following suggestion; $\Delta r_{\parallel AC}(\alpha) = \Delta y \cdot sin(\alpha)$. Table 4.2 shows the solutions for this interpolation with the constant load acting at various angles '$\alpha$' for the scenario $\Delta x = 1.0$ and $\Delta y = 1.5$. The general formulas can be found in appendix A.1. Figure 4.3 illustrates the centroidal axes $y(x)$ for the same solutions.

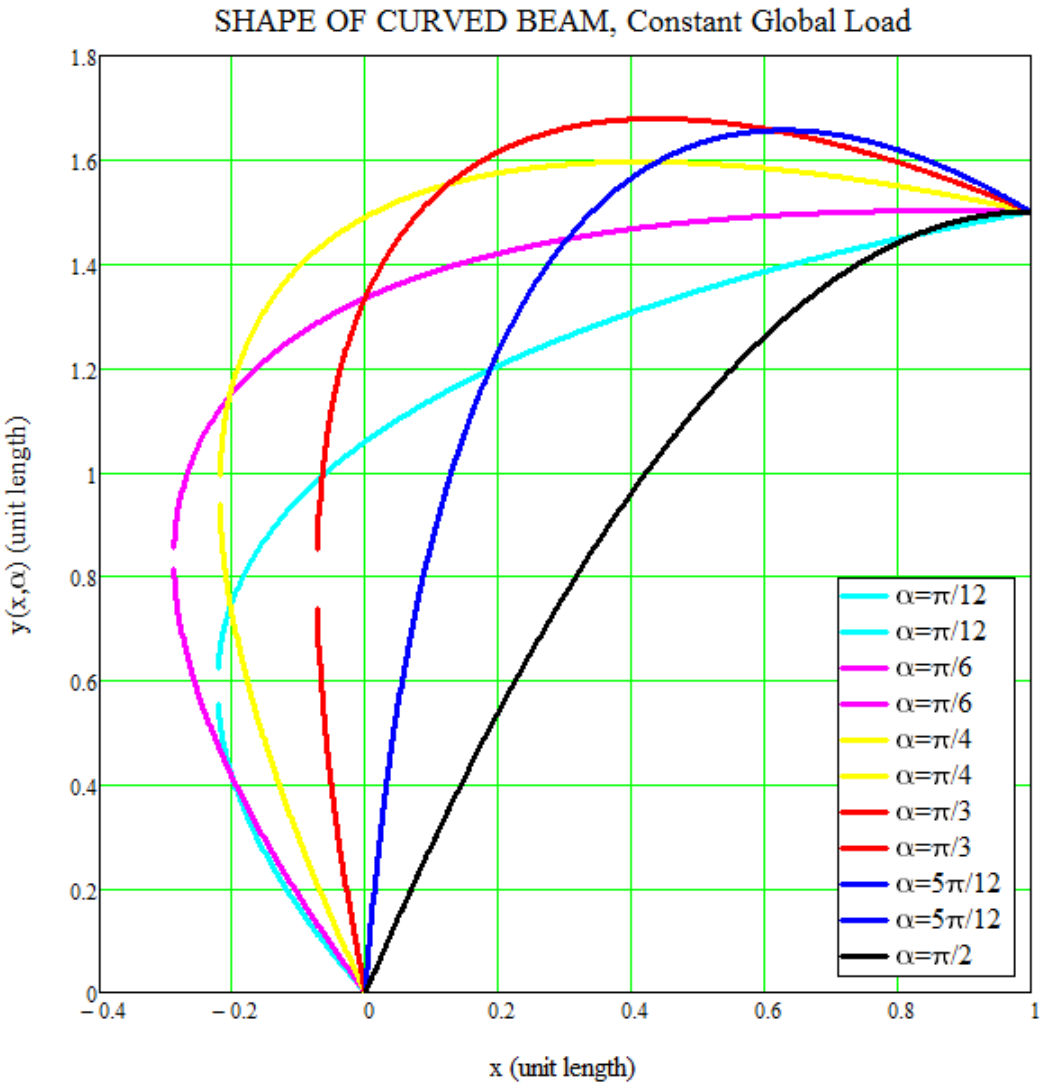


Figure 4.3: *Centroidal axes of beams with zero bending moment pinned in* $(0, 0)$ *and* $(1.0, 1.5)$ *and subjected to a constant global load acting at various angles* $\alpha$. *Height defined by* $\Delta r_{\|AC}(\alpha) = \Delta y \cdot sin(\alpha)$

| $\Delta x$ | $\Delta y$ | $y(x, \Delta x, \Delta y)$ |
|---|---|---|
| 1.0 | 0.5 | $-0.75 + 1.0 \cdot \left\{ \begin{array}{c} \sqrt{0.5625 + 1.0 \cdot x(2.0 - x)} \\ -\sqrt{0.5625 + 1.0 \cdot x(2.0 - x)} \end{array} \right\}$ |
| 1.0 | 1.0 | $\left\{ \begin{array}{c} \sqrt{x(2.0 - x)} \\ -\sqrt{x(2.0 - x)} \end{array} \right\}$ |
| 1.0 | 1.5 | $1.25 + 0.3333 \cdot \left\{ \begin{array}{c} \sqrt{0.5625 + 9.0 \cdot x(2.0 - x)} \\ -\sqrt{0.5625 + 9.0 \cdot x(2.0 - x)} \end{array} \right\}$ |

Table 4.3: *Solutions for beams undergoing solely axial internal forces when subjected to a uniform load acting perpendicular to its centroidal axis* $y(x, \Delta x, \Delta y)$

#### 4.2.1.2 Constant Perpendicular Load

The intention now is to reach a solution for a uniform load $q_n$ acting normally to the centroidal axis, independent of its shape. One could argue that this does not qualify as a known global load; however, as demonstrated by equation 2.6, the projected loads $q_{xp}$ and $q_{yp}$ are both constant if $q_n$ is constant. This load is typically transferable to air pressure or water pressure at a given depth.

The boundary forces are as follows; $A_y = q_n \cdot \Delta x$, $B_x = \frac{q_n}{2\Delta y}(\Delta x^2 + \Delta y^2)$ and $A_x = \frac{q_n}{2\Delta y}(\Delta x^2 - \Delta y^2)$. The moment contributions from the load are $M_{qx}(y) = \frac{q_n}{2}y^2$ and $M_{qy}(x) = \frac{q_n}{2}x^2$. By using equation 4.4 and solving for '$y$', it is found that

$$y(x, \Delta x, \Delta y) = \Delta y^2 - \Delta x^2 + \frac{1}{2\Delta y} \left\{ \begin{array}{c} \sqrt{(\Delta x^2 - \Delta y^2)^2 + 4\Delta y^2 \cdot x(2\Delta x - x)} \\ -\sqrt{(\Delta x^2 - \Delta y^2)^2 + 4\Delta y^2 \cdot x(2\Delta x - x)} \end{array} \right\} \tag{4.9}$$

Three scenarios are investigated; $\Delta y < \Delta x$, $\Delta y = \Delta x$ and $\Delta y > \Delta x$. Correspondingly, the values chosen are $\Delta x = 1.0$ and $\Delta y = 0.5, 1.0 \cap 1.5$, which leads to the results shown in table 4.3. The shapes are displayed in figure 4.4.

As one might expect, the case $\Delta y = \Delta x$ reveals a quarter circle.

It is assumed that $\int q_{yp}(x)dx \approx 0$ for $x < 0$ when determining $A_y$ for the case $\Delta y = 1.5\Delta x$.

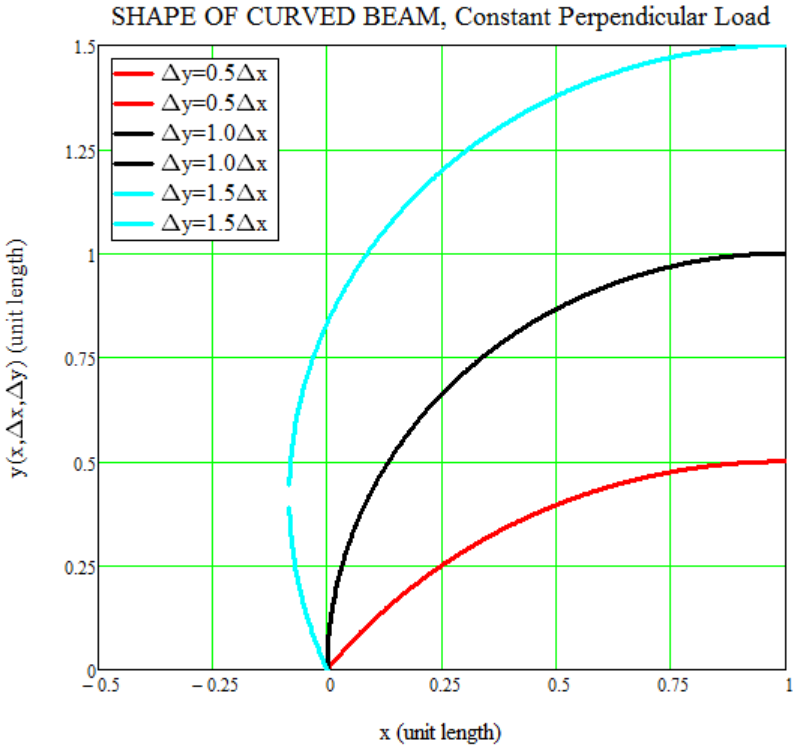


Figure 4.4: *Shapes for beams undergoing solely axial internal forces when subjected to a uniform load acting perpendicular to its centroidal axis* $y(x, \Delta x, \Delta y)$

#### 4.2.1.3 Discussion Regarding Form Finding When Global Loads Are Given

When the global loads are given, it appears quite straight forward to derive a shape with zero internal bending moments. Only continuous load cases are investigated in this study. However, it is mentioned that parts of a beam not subject to any perpendicular load would constitute straight segments as the attainment of a membrane state implies that only axial forces are acting in their endpoints. The straight segments would then be tangent to the adjacent curved segments in the joints. Point loads would be compensated by 'kinks', analogue to any truss structure.

One drawback with the method is the arising sizes of the shape functions, in particular, the general shape functions where certain variables remain

unknown, like those given in table A.1. Still, any computer aided calculation should handle this without much difficulty.

### 4.2.2 When the Global Loads Depend on the Shape of the Beam

When the forces acting on the beam depend on its shape, its projections; and thus its boundary forces, remain unknown until the final shape is given. Most of these scenarios qualify as non-linear problems and will not be dealt with here; however, a small selection will be presented.

#### 4.2.2.1 Constant Vertical Load Acting Over the Beam Length

**Analytical approach.** Some problems can be solved when knowing the incremental changes in load and internal forces that occur along the beam. For instance, when the beam is subject to only vertical loading, it is given that the horizontal component of the internal forces is constant and equal to $A_x$ which in turn is equal to $B_x$, independent of its shape. In this section, the intention is to reach a solution for a constant vertical load $q_y$ acting over the length of the beam. This would correspond to the dead weight of the beam (uniform cross section) or the weight of snow on top of the beam when the height of the snow is constant.

In this case it is convenient to change the origin of the coordinate system to the location of B and change the direction of the axes. The solution will later be transformed back to its original orientation. By letting the distance along the beam from B to an intermediate point on the beam be noted '$S$' and its internal forces '$N_x$' and '$N_y$', it is given that $N_x = A_x = B_x$ and that $N_y = q_y \cdot S$. The scenario is illustrated in figure 4.5. With no shear forces within in the beam, it follows that $\frac{dy}{dx} = \frac{N_y}{N_x} = \frac{q_y \cdot S}{A_x}$.

From $\frac{dS}{dx} = \sqrt{(\frac{dy}{dx})^2 + 1} = \sqrt{(\frac{q_y \cdot S}{A_x})^2 + 1}$, the relation between $S$ and its corresponding coordinate $x$ is as follows

$$x(S) = \int \frac{1}{\sqrt{(\frac{q_y \cdot S}{A_x})^2 + 1}} dS = \frac{A_x}{q_y} ln(\frac{q_y}{A_x} S + \sqrt{(\frac{q_y \cdot S}{A_x})^2 + 1}) \tag{4.10}$$

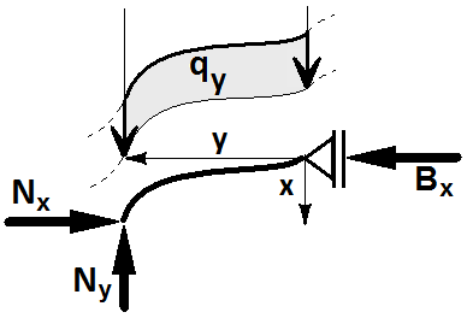


Figure 4.5: *Loads, boundary conditions and coordinate system for the scenario of the constant vertical load acting over the beam length*

The indeterminate constant of the integral was here determined from $x(0) = 0$.

In the same manner it is found from $dy = \frac{q_y \cdot S}{A_x} dx = \frac{q_y \cdot S}{A_x} \frac{dx}{dS} dS$ that

$$y(S) = \frac{q_y}{A_x} \cdot \int \frac{S}{\sqrt{(\frac{q_y \cdot S}{A_x})^2 + 1}} dS = \frac{A_x}{q_y} (\sqrt{(\frac{q_y \cdot S}{A_x})^2 + 1} - 1) \tag{4.11}$$

The indeterminate constant of the integral was determined from $y(0) = 0$.

Solving equations 4.10 and 4.11 for '$S$' and then eliminating it reveals that

$$\sqrt{y^2 + 2\frac{A_x}{q_y} y} = \frac{A_x}{q_y} sinh(\frac{q_y \cdot x}{A_x}) \tag{4.12}$$

Solving equation 4.12 for '$y$' and only considering the positive result exposes the temporary solution of the problem

$$y(x) = \frac{A_x}{q_y} \cdot (cosh(\frac{q_y \cdot x}{A_x}) - 1) \tag{4.13}$$

It is necessary for the desired solution of the problem to meet with the criteria $y(\Delta x) = \Delta y$. The relation $\frac{A_x}{q_y}$ is found graphically for three cases, figure 4.6, solving for

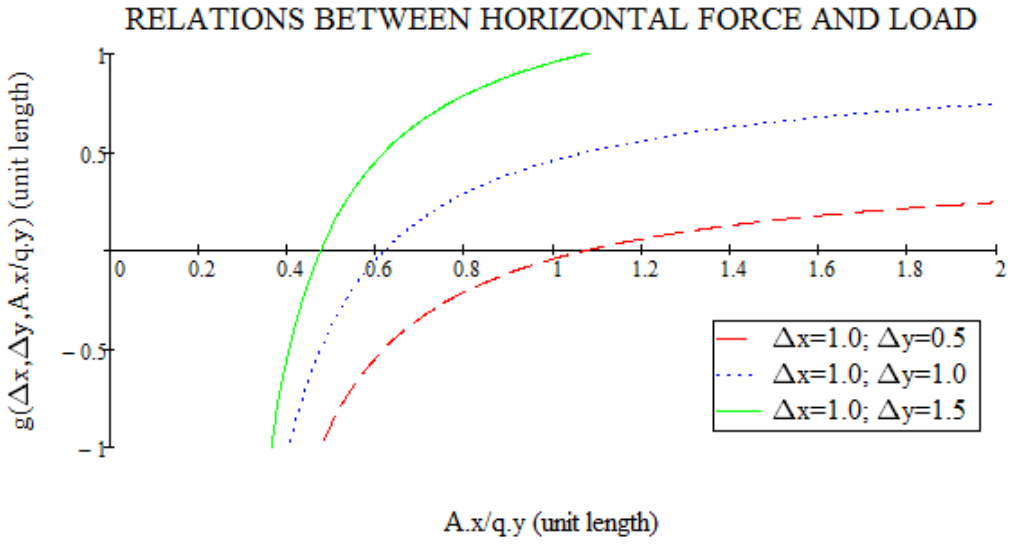


Figure 4.6: *Function 4.14 for a selection of different positions for end B. The intersections between the graphs and the horizontal axis give the relation* $\frac{A_x}{q_y}$ *that satisfy the criteria* $y(\Delta x) = \Delta y$

$$g(\Delta x, \Delta y, \frac{A_x}{q_y}) = \Delta y - \frac{A_x}{q_y} \cdot (cosh(\frac{q_y \cdot \Delta x}{A_x}) - 1) = 0 \tag{4.14}$$

The relation for the case $(\Delta x, \Delta y) = (1.0, 1.5)$ is found to be $\frac{A_x}{q_y} = 0.47568$ unit lengths (five decimal places). It is important to note that maintaining a constant relation $\frac{\Delta x}{\Delta y}$ does not uniquely define the relation $\frac{A_x}{q_y}$, i.e. $(\Delta x, \Delta y) = (2.0, 3.0)$ does not reach the same conclusion. Adding this result to equation 4.13 and transforming the equation according to the original coordinate system gives the final beam shape for this case

$$y(x) = -0.47568 \cdot (cosh(\frac{x - 1.0}{0.47568}) - 1) + 1.5 \tag{4.15}$$

As might expected, the result exposes an up-side-down catenary, the shape one would find in a hanging rope, later illustrated in figure 4.7 *(a)*.

Knowing the shape of the beam, one can assign the global load projections according to equation 2.7. With a load $q_y = 1$ the boundary forces are

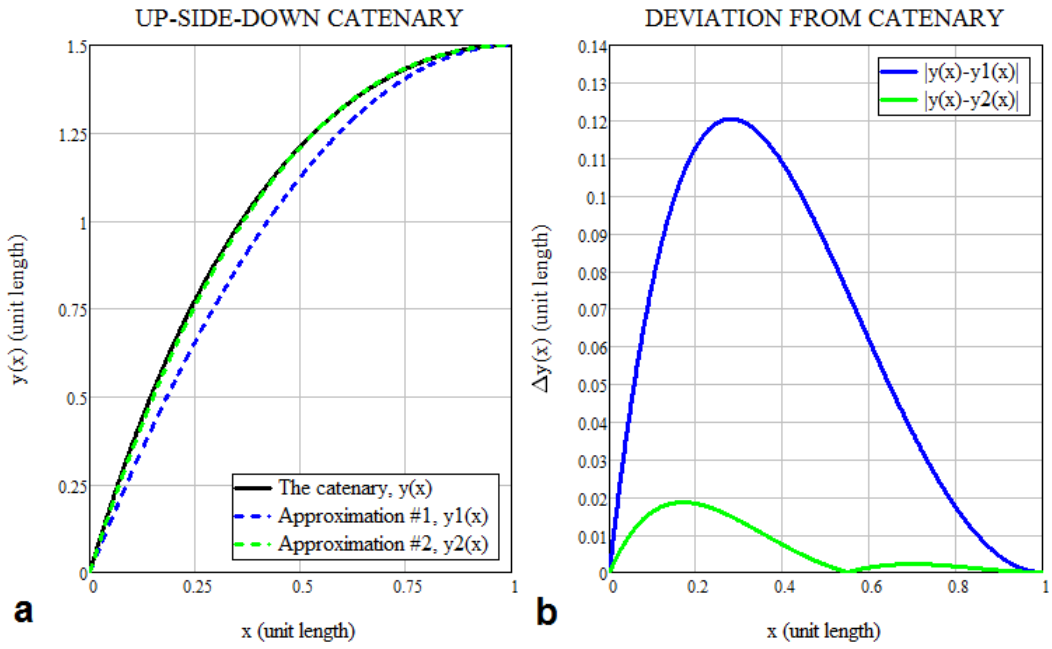


Figure 4.7: *(a) The catenary found analytically, $1^{st}$ approximation (a parabola) and $2^{nd}$ approximation found from one- time analytical iteration (b) Deviation between the approximations and the desired solution*

$(A_x, A_y) = (0.47568, 1.91747)$. Equation 4.3 verifies then that $M(x, y) < 1 \times 10^{-4}$ for the whole section $[0, \Delta x]$ with a maximum of $9.28 \times 10^{-5}$.

**Approximation using analytical convergence.** An alternative method for finding shapes with zero bending moment (or any other criteria) is the use of analytical convergence. The idea is to assume a shape $y_1(x)$ with zero bending moment, given the load- and boundary conditions at hand. For this shape, one can calculate the global loads $q_{Gx.1}(y)$ and $q_{Gy.1}(x)$. Having established these, one can proceed with the equations and methods from section 4.2.1 to find a new shape $y_2(x)$. This shape can be used to repeat the process and find $y_3(x), y_4(x)...y_i(x)$; which, if successful, will converge towards the solution of the problem. If $y_1(x)$ in fact is the correct solution of the problem, $y_1(x)$=$y_2(x)$=...=$y_i(x)$.

It is desired to find a shape for the case $(\Delta x, \Delta y) = (1.0, 1.5)$ given the

constant load $q_y$.

A common approximation for the up-side down catenary is a parabola. Temporarily assuming that the parabola is the correct solution for the problem leaves $y_1(x) = \frac{\Delta y}{\Delta x}x(2 - \frac{x}{\Delta x})$. The global loads are then $q_{Gx.1}(y) = 0$ and $q_{Gy.1}(x) = \sqrt{9(1-x)^2+1}$. By following the equations and methods as described in section 4.2.1,

$$y_2(x) = 1 + 0.23390(1-x)ln(3(x-1) + \sqrt{9x(x-2)+10}) + (\star) \quad (4.16)$$

$$(\star) = \sqrt{9x(x-2)+10}(x(0.46781 - 0.23390x) - 0.18192)$$

$y_1(x)$, $y_2(x)$ and $y(x)$ as defined by equation 4.15 are graphed in figure 4.7 *(a)*. Using equation 4.15 as a benchmark, the difference between the desired solution and $y_1(x)$ and $y_2(x)$ is illustrated in figure 4.7 *(b)*.

The maximum vertical difference between the parabola and the catenary is in this case $\approx 0.12 = 8\%\Delta y$. Iterating one time according to section 4.2.1 reduced this error with $\approx 85\%$.

#### 4.2.2.2 Perpendicular Load Depending on 'x'

It is desired to investigate the quality of assumptions for $y_1(x)$ when performing the analytical convergence, and how dependent the iterations are on the initial shape. In this case, a load linearly dependent on 'x' and perpendicular to the centroidal axis is studied. This would for instance correspond to pressure from a liquid where the coordinate 'x' refers to the depth.

The case in question is assigned the values $(\Delta x, \Delta y) = (1.0, 1.0)$. At position A, $q_n(0) = q_{nA}$ and at B, $q_n(\Delta x) = q_{nB}$ leaving the load distribution $q_n(x) = q_{nA} + \frac{x}{\Delta x}(q_{nB} - q_{nA})$. It is further assumed that $(q_{nA}, q_{nB}) = (0, 1)$. This would correspond to a beam positioned to barely touch the surface of the liquid. In order to visually be able to interpret the vertical axis as the direction of gravity, the functions for the centroidal axis will be expressed by $x(y)$; and hence, the approximations by $x_i(y)$.

Two initial assumptions for $x_1(y)$ will be investigated, one further away from- and one closer to what might be expected as the correct solution $x(y)$. The first one, $x_{1a}(y) = y\frac{\Delta x}{\Delta y}$ represents a straight beam between point A and

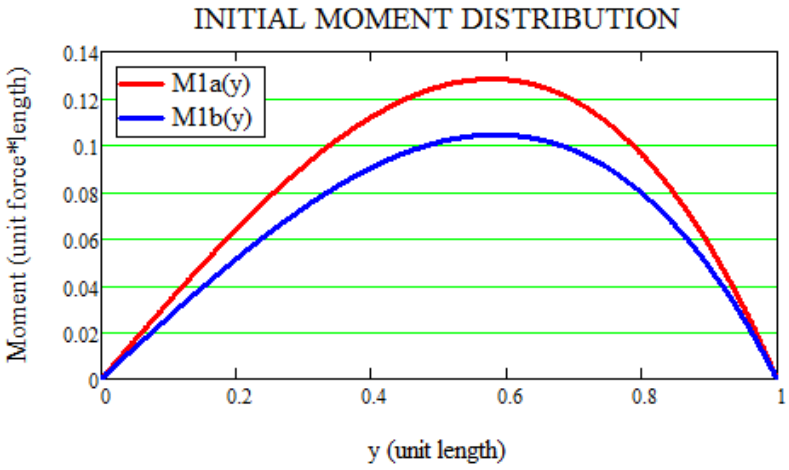


Figure 4.8: *Bending moment in a straight beam and a parabola subjected to the perpendicular load* $q_n(x)$

B. The straight beam does not accommodate the boundary conditions in B, and the tangent line at any point on the beam is perpendicular to the load distribution at all other points on the beam. The second one, $x_{1b}(y) = \Delta x(1 - \sqrt{1 - \frac{y}{\Delta y}})$ represents a parabola that accommodates the boundary conditions in B, meaning that $\frac{d(x_{1b}(y))}{dy}|_{y=\Delta y} \to \infty$.

For both cases, $q_{Gy.1}(x) = q_n(x) = x$.

$q_{Gx.1a}(y) = q_n(x_{1a}(y)) = y$ and $q_{Gx.1b}(y) = q_n(x_{1b}(y)) = 1 - \sqrt{1-y}$ which leads to the following moment distributions;

$$M_{1a}(y) = -\frac{y}{3}\left(y^2 - 1\right) \tag{4.17}$$

$$M_{1b}(y) = \frac{y}{2}(\frac{28}{15} - y - \frac{y^2}{3}) - \frac{4}{15}\left[1 - (1-y)^{\frac{5}{2}}\right] \tag{4.18}$$

As seen in figure 4.8, the difference in moment distribution is not substantial; however, one can argue that it is noteworthy.

Following the equations and methods described in section 4.2.1 one time, the approximated shapes $x_{2a}(y)$ and $x_{2b}(y)$ are as illustrated in figure 4.9,

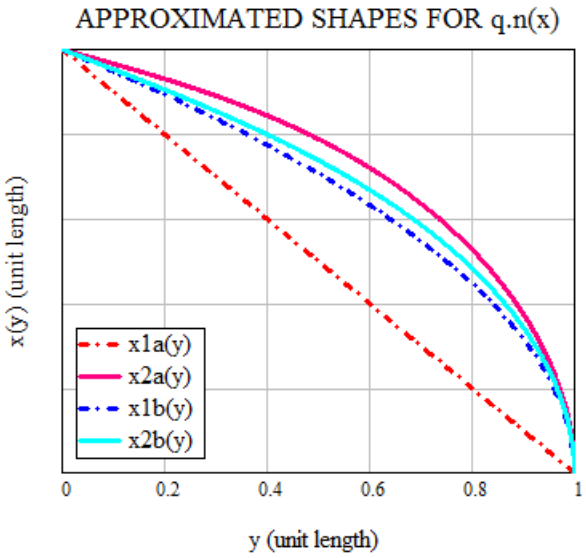


Figure 4.9: *Approximated shapes for the load* $q_n(x)$

represented by the functions given in appendix A.2. From the graph one can draw the conclusion that both initial shapes tend towards the same shape with a relatively close proximity even after only one iteration.

To check the quality of the approximations $x_{2a}(y)$ and $x_{2b}(y)$, the steps in section 4.2.1 are followed until having reached equation 4.3 which reveals the moment distribution within the beams. As illustrated in figure 4.10, the total bending moment after one time iteration based on the parabola is approximately 10% of that found from the straight beam. This is in spite of a relatively similar shape. Both outcomes; however, show a significant drop in the overall bending moment distribution with $\approx 75\%$ and $\approx 95\%$ for $x_{1a}(y)$ and $x_{1b}(y)$ correspondingly. The graph in figure 4.10 was made on the basis of the script found in appendix C.2.

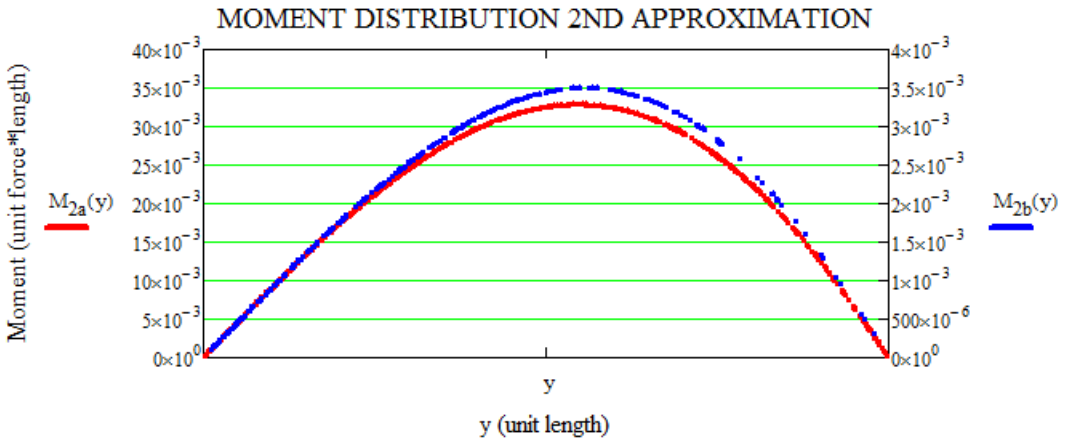


Figure 4.10: *New moment distributions of the straight beam and the parabola from figure 4.8 after one iteration*

#### 4.2.2.3 Discussion Regarding the Use of Analytical Convergence

The use of analytical convergence exhibits some strong advantages as well as disadvantages which ought to be taken into account when dealing with a problem.

An immediate drawback with the method is the vastly growing complexity of the shape functions for each iteration. As demonstrated in this chapter, seemingly "clean" shapes give rise to relatively large shape functions even after one single iteration. Advancing to further iterations increase this complexity exponentially. The solution found may result in a conjunction of solutions, where $y(x_a) = [y_1, y_2]$ for some intervals of $x$. Advancing from this type of results can become cumbersome, as the functions need to be solved piece-wise or, if possible, to be inverted to be expressed as $x(y)$. Furthermore, in spite of finding a successful shape function $y_i(x)$ it can be shown it can be be cumbersome to derive a continuous moment distribution, as one has to continue the iteration for $y_{i+1}(x)$ half-way until having reached the expression for $M(x, y)$, equation 4.3.

Nevertheless, the method has proven itself quite resourceful in terms of form finding. For any given load case, the method seems to rapidly converge towards the solution of the problem regardless of the initial assumption of the shape. The fact that the iteration allows for a conjunction of new shapes

$y_i(x) = [y_i(x)_1, y_i(x)_2...]$ makes the method a powerful tool when investigating zero moment shapes. It seems that the direction in which the iteration is heading is quite unambiguous. For each successful shape function one can easily idealize it as a "cleaner" function and repeat the iteration. The method is also a strong tool for quickly investigating the quality of an assumed shape, measured by the deviation between $y_1(x)$ and $y_2(x)$.

A one-time iteration without further attempting to reach a continuous moment distribution is for the most part an undemanding process. For quick design improvements and/or shape investigations, the method can prove itself to be of great aid. In combination with other methods, e.g. numerical methods, one can resolve difficulties like determining the moment distribution. Based on figure 4.10 one can draw the conclusion that small differences in the apparent shape of the beam can give rise to relatively large differences in the bending moment.

| Name | $y(x)$ | Description |
|---|---|---|
| $y_p(x)$ | $10m(1-\frac{x^2}{100m^2})$ | A parabola, for sustaining the constant load $q_{Gy}$ |
| $y_q(x)$ | $\sqrt{100m^2-x^2}$ | A quarter circle, for sustaining the constant load $q_n$ |
| $y_c(x)$ | $10m+6.18579m(1-cosh(\frac{x}{6.18759m}))$ | A catenary, for sustaining the constant load $q_y$ |

Table 4.4: *Benchmark beam shapes for solutions found by the software*

## 4.3 Optimization Results from Software

The purpose of this section is to get familiarized with the software and different approaches for its optimization process. Before using the software to solve more complex problems, different strategies are tested on these relatively simple 2 dimensional curved beam cases. The parameter study is relatively brief, and primarily intended to reach a general understanding of duration and quality of the various approaches.

All beam cases are given the values $(\Delta x, \Delta y) = (10m, 10m)$. The start- and endpoints on the beams are located at $(0, \Delta y)$ and $(\Delta x, 0)$ respectively. They are pinned in their endpoints and prevented horizontal movement in their starting points. They are investigated with an absolute load density of $1\frac{kN}{m}$. The real world equivalent of this load is about 20 times the dead weight the beam if it was made of aluminum. From section 4.2, it is assumed that the parabola, the quarter circle and the up-side-down catenary are the ideal shapes in terms of bending moment for a vertical constant global load, constant perpendicular load and constant vertical load acting over the beam length respectively. Hence, the benchmark shapes for these beams are as described by the functions in table 4.4. The relation $\frac{A_x}{q_y}$ for the catenary is approximated to 5 decimal places; $6.18759m$, leaving the bending moment $M_c(x) < 3 \times 10^{-11} kNm$ for the whole beam section according to equation 4.3.

The discretized, approximated shape function found by the software is named $y_a(x)$.

The default settings of the evolutionary algorithm are not altered. The fitness parameter is defined by the absolute value of the output bending moment

about the z-axis in all the nodes unless explicitly stated otherwise. The fitness objective is set to minimize the input. The initial values of all the parameters are set to zero unless explicitly stated otherwise.

### 4.3.1 Global Load

Various approaches to solving the case of the uniform vertical global load are studied.

#### 4.3.1.1 Evenly Spaced Declining Points, Node Density

First off, the density of nodes is examined. Straight beam elements are assigned between points. They are all evenly separated on the x- axis. The points are interdependent in the following manner: The y- coordinate of a point $y_i$ on the beam is defined as a factor $a_i \in [0, 1]$ times $y_{i-1}$. The parameters to be optimized are then $a_1, a_2, a_3 ... a_{k-1}$ where $k$ is the number of beam elements. The scenarios $k = 3, 10, 20$ are investigated. In figure 4.11 the difference between the obtained solutions $y_a(x)$ and the parabola $y_p(x)$ is illustrated.

The start- and endpoints on the beams are the same as the beam element nodes in the FEA Solver. By taking a closer look at the cases $k = 3, k = 10$ in figure 4.11 one can observe that the nodes are positioned at the parabola with a marginal error. The node positions are illustrated by the "peaks" on the graphs. The overall error of the two solutions is as expected, greater with a lower density of beams, illustrated by the "valleys" on the graphs. With 20 beam elements, the optimization process ended with three nodes deviating significantly compared to the rest. One node is 'off' with almost 80 cm. One generation took about 1 second to complete on a personal laptop. The three cases finished after 60, 940 and 1350 generations respectively.

The moment distribution for $k = 3, k = 10$ is graphed in figure 4.12 with linear interpolation between the nodes. The maximum bending moment for $k = 20$ is about 100 times that of $k = 10$; and thus, not included in the figure.

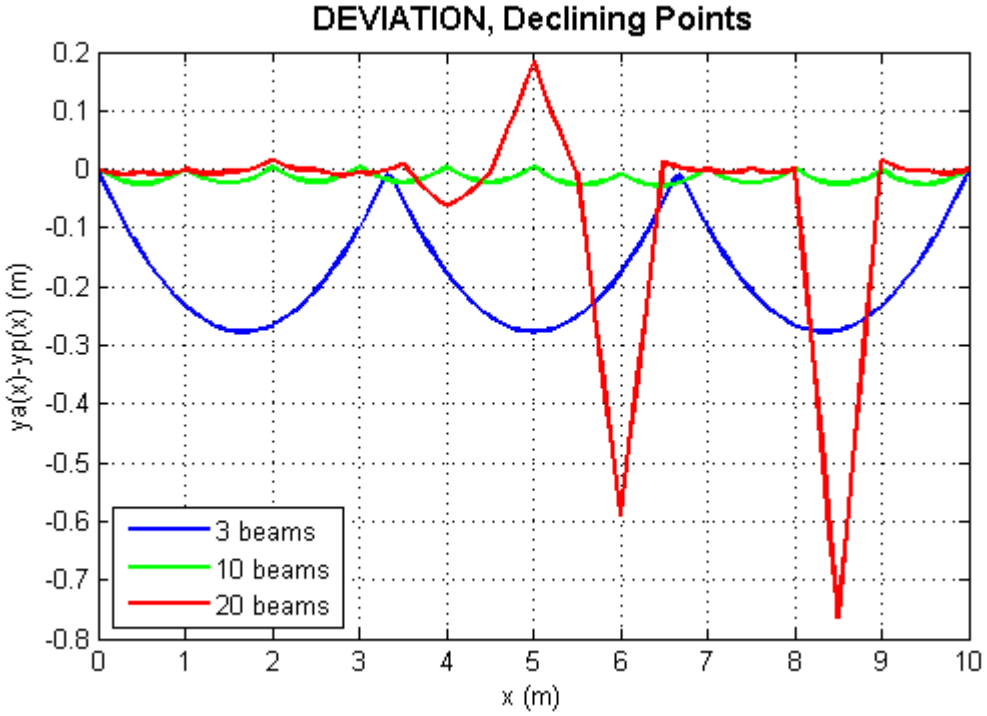


Figure 4.11: *Deviation of approximated shapes attained by the software. Uniform global vertical load, interdependent parameters*

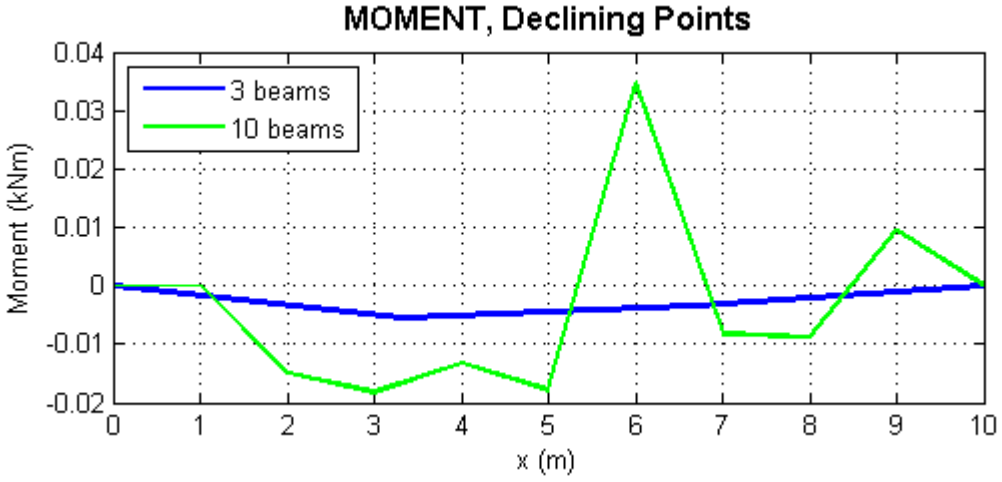


Figure 4.12: *Bending moment of approximated shapes attained by the software. Uniform global vertical load, interdependent parameters*

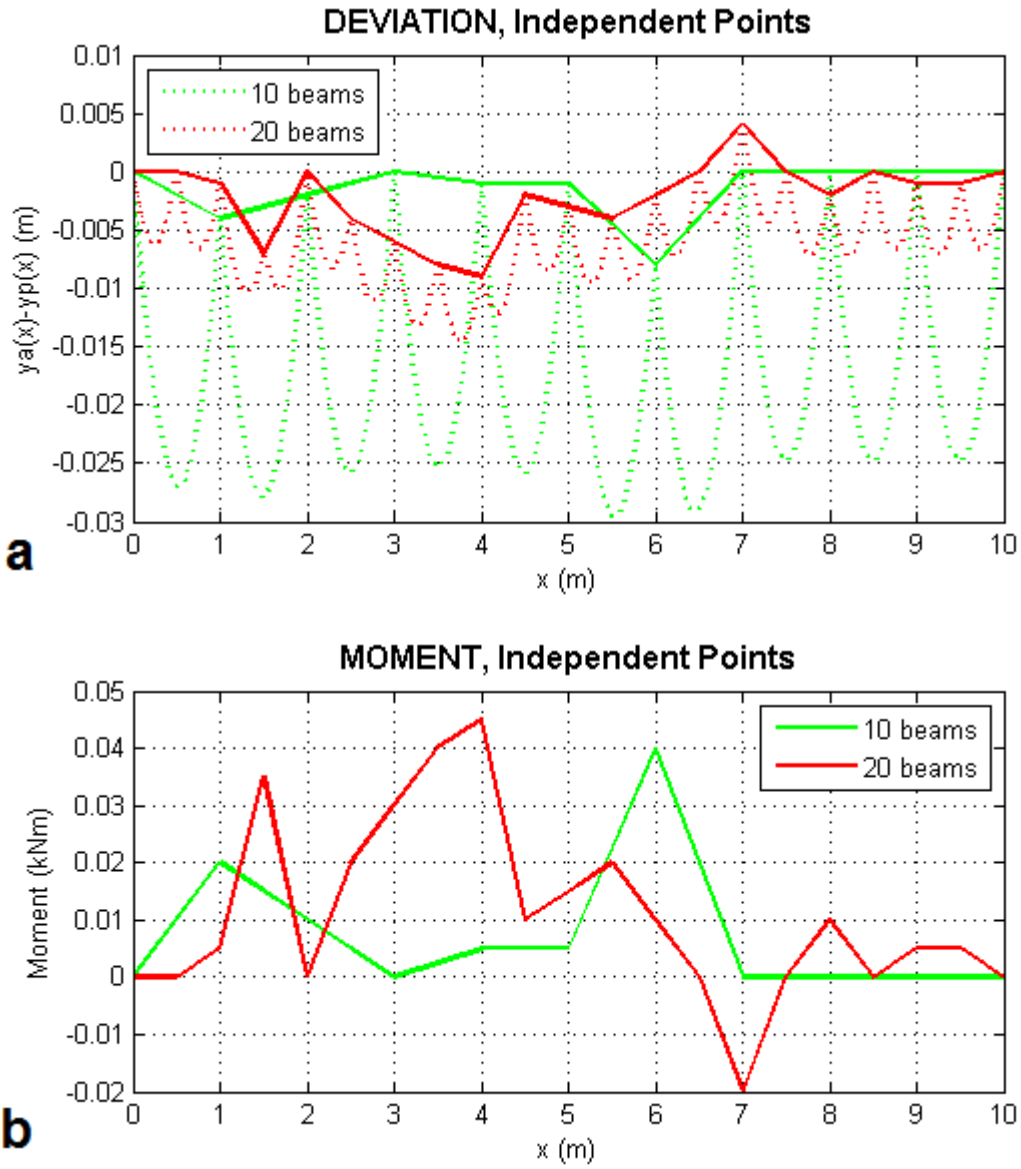


Figure 4.13: *(a) Deviation and (b) Moment of approximated shapes attained by the software. Constant global vertical load, independent parameters*

#### 4.3.1.2 Evenly Spaced Independent Points

It is in the following attempted to investigate the consequence of removing the interdependence between the parameters. I.e. the y- coordinates of the points $y_{i=1,2...k-1}$ are all defined by a value $\in [0, 10]$. These coordinates are then the parameters to be optimized. One of the features of interest is the duration of the optimization process. The cases are therefore limited to $k = 10, k = 20$. The deviation between the results and the benchmark is graphed with dotted lines in figure 4.13 *(a)*. The solid lines are the linear interpolation between the nodes.

The process was in this case completed in 270 and 800 generations correspondingly. This is a noteworthy improvement from the case with the declining points. The moment distribution is illustrated in figure 4.13 *(b)*. In terms of both deviation and bending moment, the quality of $k = 10$ is comparable using the two approaches; however, for $k = 20$ a feasible solution was only found with the independent points.

One can observe a matching pattern between the deviation and the bending moment, indicating that the benchmark is indeed the desired shape for the optimization.

#### 4.3.1.3 1 Interpolation Point, Various Beam Segments

Interpolation is a strong tool for enforcing smoothness of a curve represented by few points. The interpolation used defines a NURBS curve. In this section, only one interpolation point is used. Its location is defined by $x \in [0, 10]$ and $y \in [0, 10]$ being the parameters to optimize. On the interpolated curve, evenly spaced points are placed with different densities. These mark the start- and endpoints of the beam elements used in the model. Note that the points are evenly spaced on the curve itself, independent of the distribution projected on to the x- and y- axes.

Figure 4.14 *(a)* and *(b)* show the deviation and moment for these cases. The optimization processes all required 110-140 generations. Even though both the deviation and the moment are greater in this case than with the previous approaches, the smoothness is enhanced. Moreover, the duration of the process is significantly improved. The increase in beam element density from 10 to 20 did not result in much difference.

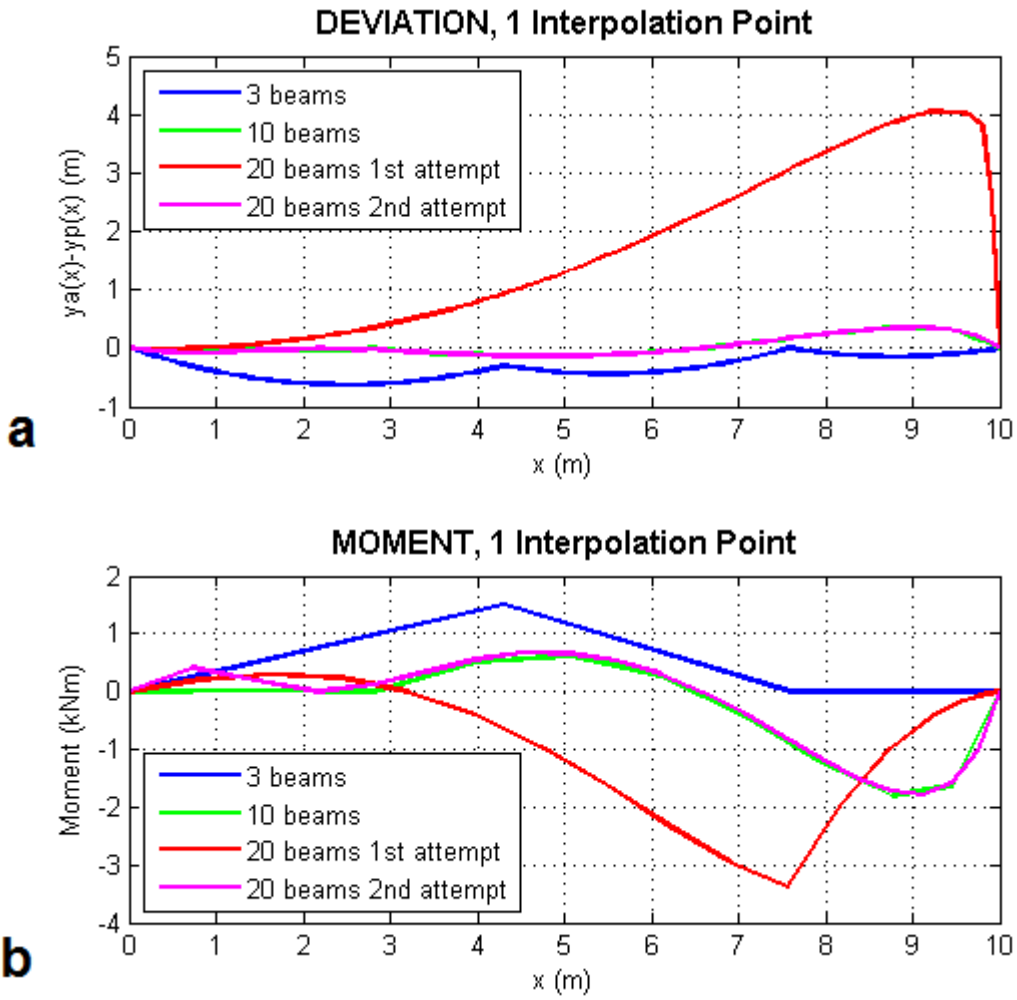


Figure 4.14: *(a) Deviation and (b) Moment of approximated shapes attained by the software. Constant global vertical load, 1 variable interpolation point*

The first optimization for $k = 20$ ended prematurely with a vertical deviation as high as 4m. In the second attempt no changes were made to the model; still, its outcome was appreciably different. Attempts beyond what is documented here confirm the observation that the models can converge in adverse directions. Thus, the results obtained after one optimization process alone are not completely unambiguous and need to be treated as such.

#### 4.3.1.4 Various Interpolation Points and -Degrees, 10 Beam Segments

The investigation advances with multiple interpolation points and varying the degree of interpolation. The number of beam elements remains 10. The nodes are evenly spaced on the curve as in the case with only one interpolation point. The x- coordinates of the interpolation points are evenly distributed on the x- axis, leaving only the y- coordinates as variable parameters.

By increasing the number of interpolation points to 2 points, the bending moment is reduced with more than half, figure 4.15 *(b)*. Further increasing the degree of the curve does not seem to have had any noteworthy impact on the result. One can clearly see a drop in both deviation and bending moment by further increasing the number of interpolation points to 9. Doing so came at cost of duration, which increased from less than 90 to more than 400 generations. With a $5^{\text{th}}$ degree interpolation, the process ended with about 50 generation more, but it accounted for the one node deviating with 15 cm, figure 4.15 *(a)*.

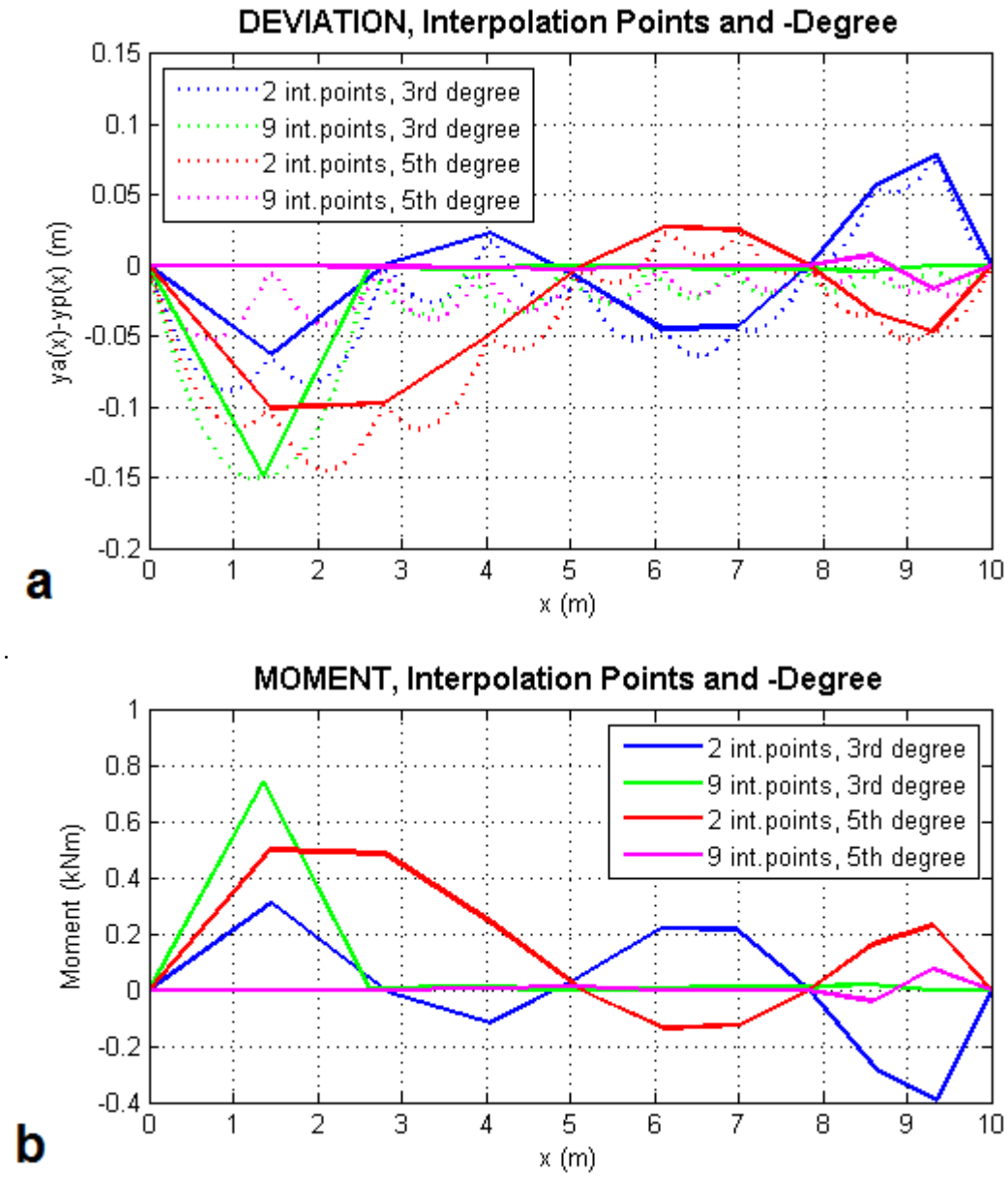


Figure 4.15: *(a) Deviation and (b) Moment of approximated shapes attained by the software. Uniform global vertical load, various interpolation points and different degrees*

### 4.3.2 Perpendicular Load

Various approaches to solving the case of the constant perpendicular load are studied. One of the key features of the benchmark case for this scenario is that it is axisymmetric about the z- axis. One of the intentions of this section is therefore to investigate whether or not difficulties occur as $\lim_{x \to \Delta x} \frac{dy(x)}{dx} \to -\infty$.

Four different approaches are investigated:

1. Points independent in the y- direction ($y_{i=1,2...k-1} \in [0, 10]$) and evenly distributed in the x- direction ($x_i = \frac{i \cdot 10}{k}$)

2. Points limited to increase in the x- direction and decline in the y-direction. The points are interdependent in the way that $y_i = a_i \cdot y_{i-1}$ and $x_i = b_i \cdot x_{i+1}$ where $a_i \cap b_i \in [0, 1]$ are the parameters to be optimized

3. 4 interpolated points independent in the y- direction ($y_{i=1,2,3,4} \in [0, 10]$) and evenly distributed in the x- direction ($x_i = \frac{i \cdot 10}{4}$). The interpolation is of the $5^{\text{th}}$ degree. The curve is divided into equal length segments defining the start- and endpoints of the beam elements

4. Points independent both in the x- and y- direction ($y_{i=1,2...k-1} \cap x_{i=1,2...k-1} \in [0, 10]$)

All optimizations are run with 10 beam elements.

The vertical deviation and bending moment obtained after the first three approaches are illustrated in figure 4.16 *(a)* and *(b)*.

The first approach finished after 270 generations. Its nodes are placed relatively close to the benchmark curve; however, it deviates more between the nodes as the tangent becomes steeper. One could account for this by increasing the density of beams relative to the expected inclination of the curve.

The second approach lasted 2200 generation, and ended with clusters of nodes in both ends (easily seen in the moment diagram). It was observed that during the optimization process, the clusters tended to open slowly and 'send' nodes along the curve one by one.

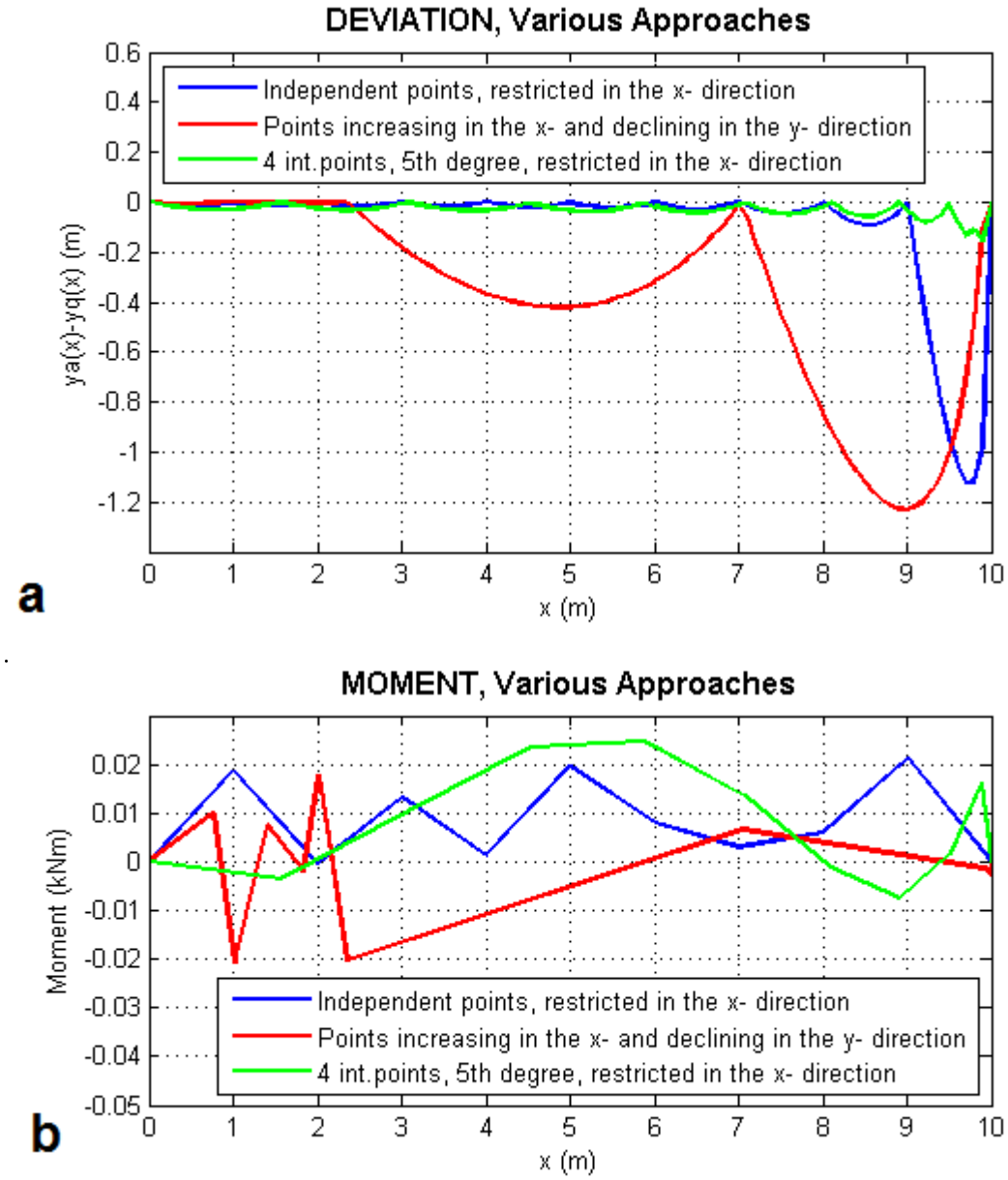


Figure 4.16: *(a) Deviation and (b) Moment of approximated shapes attained by the software. Constant perpendicular load, various approaches*

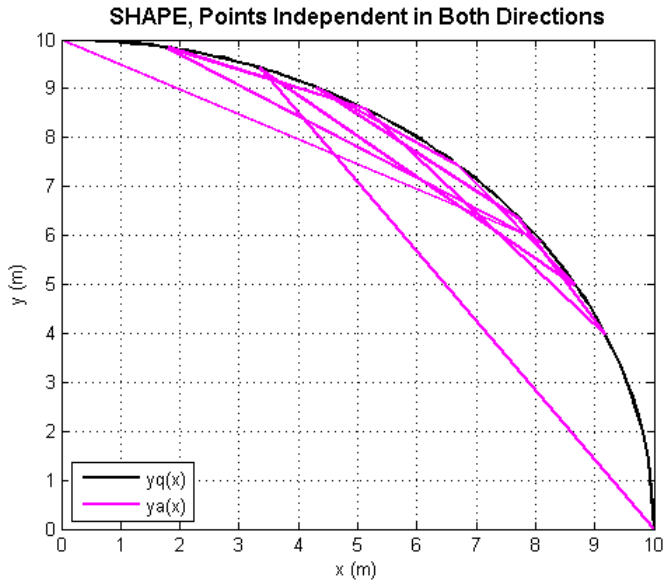


Figure 4.17: *Shape of a misfortunate result. Constant perpendicular load, points independent in both directions*

The approach with the interpolation had a duration of 520 generations. With the beam divided into segments along the curve itself, the deviation was considerably reduced compared to its predecessors. The overall smoothness of the result is greater than that of the other two.

The qualities in regards of the moment distribution of the three solutions are comparable.

The fourth approach ended misfortunately. The solution converged into a "knot", figure 4.17. Other attempts, with different initial values for the parameters were tried out; all ending with similar shapes, where the nodes are placed close to the benchmark curve but in an arbitrary order.

### 4.3.3 Vertical Load

Various approaches to solving the case of the constant vertical load acting over the beam length are studied. For the investigations presented here, a model is chosen as basis for comparison. An optimization process was run with 4 points interpolated with a $5^{\text{th}}$ degree interpolation. They are restricted

in the x- direction, $x_i = \frac{i \cdot 10}{k}$ and independent in the y- direction, $y_{i=1,2...k-1} \in [0, 10]$. The curve is divided into 10 equal length segments forming the basis for the beam model. The process ended after 260 generations. Its result is marked with a black curve in the following graphs.

#### 4.3.3.1 The Fitness Parameter

After having studied different approached regarding the parameters to be optimized, strategies targeting the fitness parameter are given attention. In the basis for comparison, the absolute value of the bending moment in all the nodes is averaged (default setting). Three other approaches are tried out:

1. Subtracting the lowest bending moment occurring in any of the nodes from the greatest
2. Subtracting the lowest absolute value of the bending moments occurring in any of the nodes from the greatest
3. Adding all the absolute values of the bending moments occurring in the nodes

In figure 4.18 *(a)* and *(b)* the results are presented.

The first strategy ended in a result relatively weaker the others. Its optimization process ended after 1200 generations.

The other two strategies involving the use of the absolute values ended with nearly identical outcomes, after 680 and 850 generations correspondingly. Both deviation and bending moment is reduced, but at the cost of duration.

#### 4.3.3.2 Initial Values of the Parameters

The final investigation to be carried out is to witness whether or not the choice for the initial values has an influence on the process and/or the final outcome. The basis for comparison is carried out with all parameters equal to zero. A 'worst case scenario' and a 'best case scenario' are tried out. In the first scenario, $y_1 = 0$, $y_2 = 10$, $y_3 = 0$ and $y_4 = 10$. In the second scenario, the values are adjusted manually to make the model look like the up-side-down catenary. In figure 4.19 *(a)* and *(b)* the results are presented.

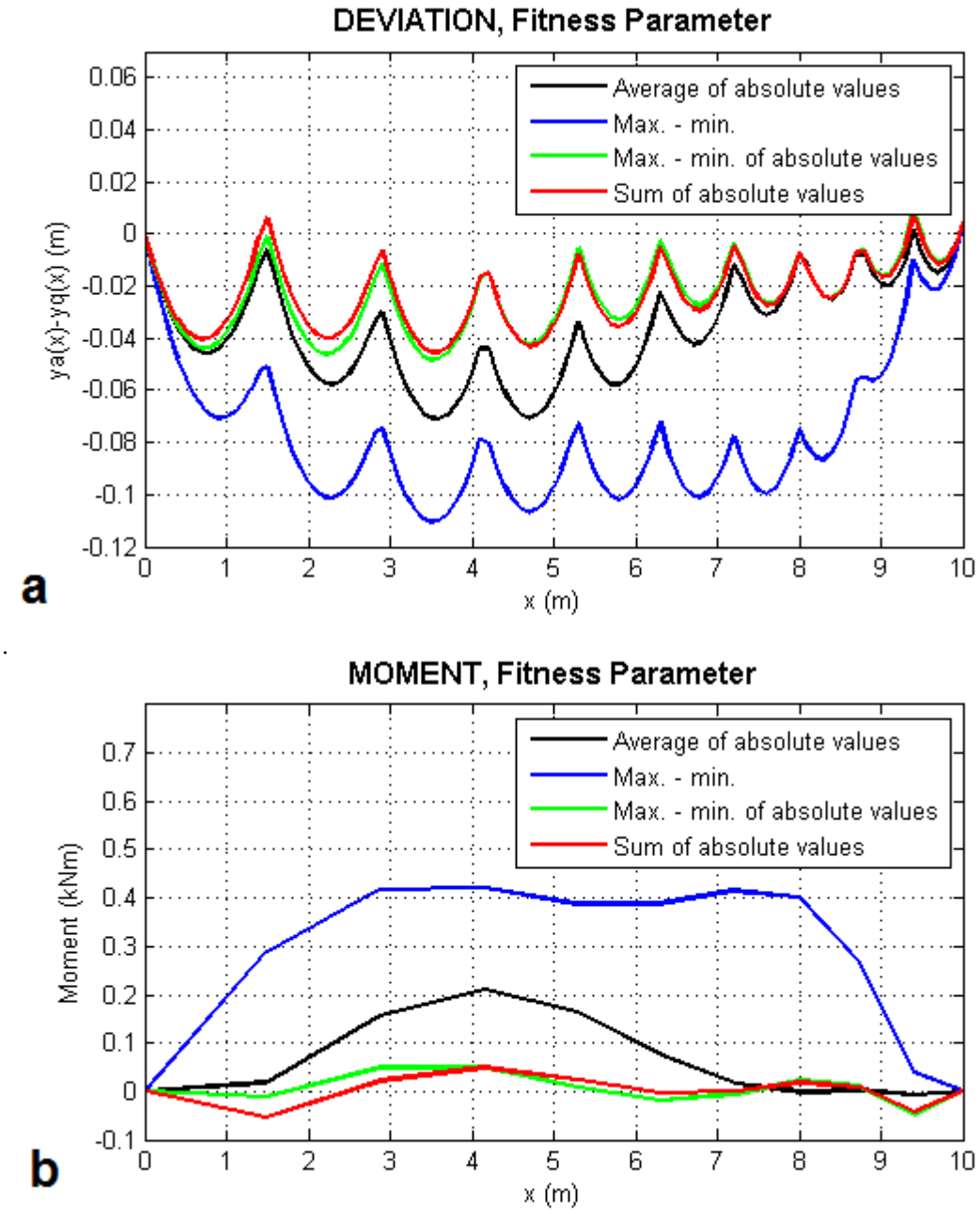


Figure 4.18: *(a) Deviation and (b) Moment of approximated shapes attained by the software. Uniform vertical load acting over the beam length, various inputs for the fitness parameter*

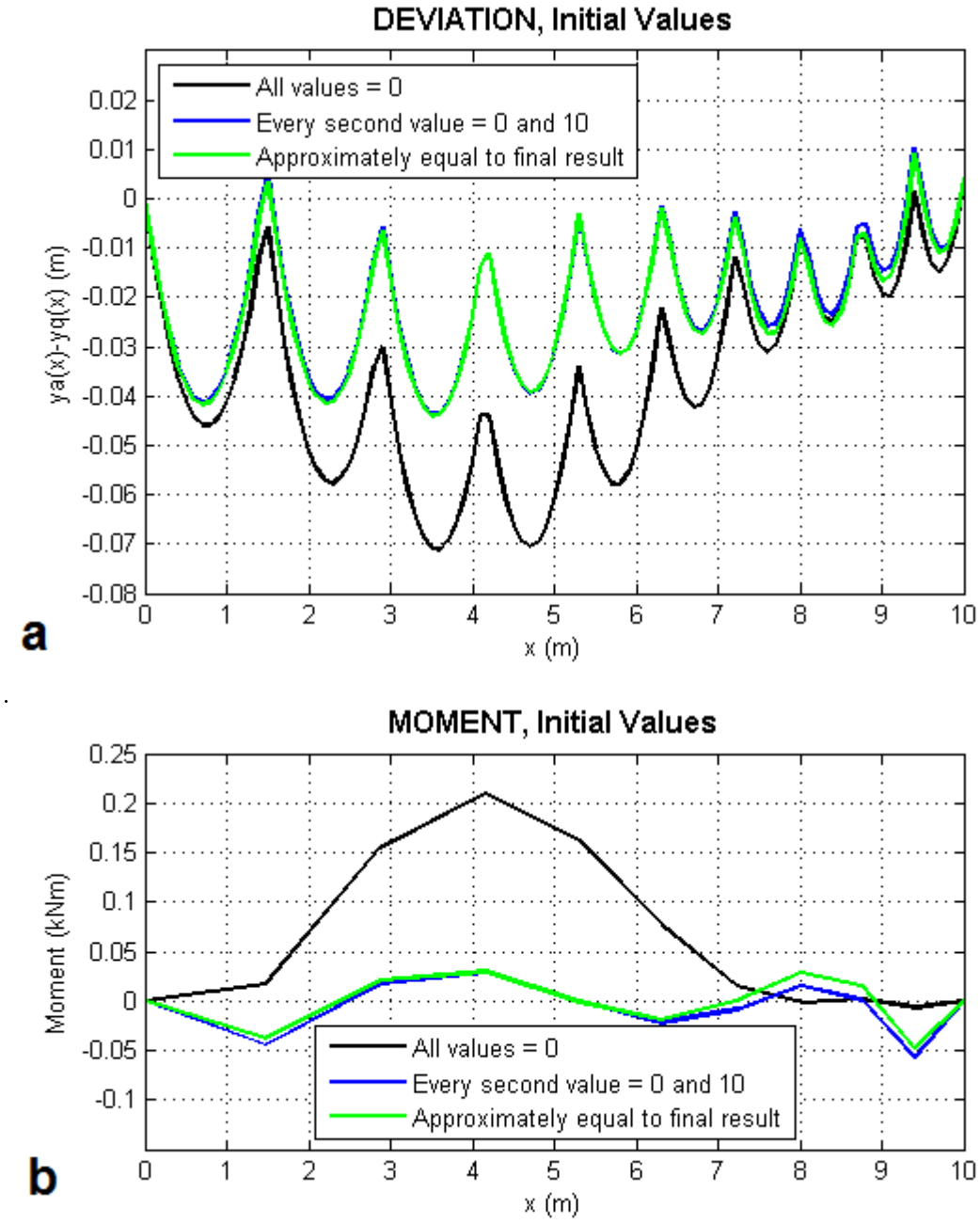


Figure 4.19: *(a) Deviation and (b) Moment of approximated shapes attained by the software. Constant vertical load acting over the beam length, different initial values of the parameters*

The optimization processes ended after 570 and 240 generations correspondingly. They ended with relatively equal outcomes, both with an enhanced quality in terms of both deviation and bending moment. The 'best case scenario' supersedes the others when taken into account both duration and quality.

### 4.3.4 Intermediate Conclusions and Discussion Regarding the Approaches to the Software

From this relatively brief study, a number of conclusions can be drawn.

1. Introducing interdependence between the parameters does not seem to be an asset for the evolutionary algorithm, as the rate of convergence is reduced. Figure 4.12, 4.16

2. Nodes independent from one another converge quickly and with a relatively high quality outcome. The overall smoothness may be an issue. It is recommended to add restrictions to the positions of the nodes in one of the directions to avoid "knots". Some insight regarding the expected result may help reducing the deviation between the nodes by increasing the density of points where the inclination is steeper before starting the algorithm. Figure 4.13, 4.16 *(a)*, 4.17

3. Introducing curves defined by interpolation is an alternative to completely independent points when a level of overall smoothness is required, figure 4.14 *(a)* and *(b)*. It allows for fewer parameters to be optimized, but still give rise to relatively arbitrary shapes. However; one can argue that the approach can be considered more 'confined'. The same argument goes for the selection of curve degree, where a higher degree implies more 'freedom' for the curve as stated in section 3.2 and to some level confirmed by figure 4.15 *(a)* and *(b)*

4. If the problem demands it, experimentation with the choice of the input for the fitness parameter might be suitable. Figure 4.18 confirms its impact. This research will move forward without taking various inputs into consideration as its impact seems to have a limited effect on the final outcome when compared to the required duration

5. If a certain shape is expected, leaving the initial values of the parameters in the proximity of that shape help reduce the duration of the optimization process as well as the final quality of the result. Figure 4.19

# Chapter 5

# CASE: THE DOME

It is desired to apply the software in aiding analytical estimates. Estimates of the shape of a dome in membrane state will be derived analytically. The software will then accommodate the estimates with more information, helping to more clearly see what is its true zero moment shape.

## 5.1 Presentation of the Dome

The dome as an architectural symbol is present in many cultures. Its significance exceeds the mere aesthetics and personal experience of its shape; it also serves as a peculiar way of distributing forces. And in this particular study; more importantly, its characteristics are axisymmetric.

An example of a type of architecture where the dome has an essential presence is the Ottoman mosques. The greatest dome; that of Selimiye Mosque, has an inner diameter of 31.25m. It was completed in 1574 by the architect Mimar Sinan, http://en.wikipedia.org/wiki/Selimiye_Mosque. In figure 5.1 *(a)* and *(b)* is included a picture of Selimiye Mosque and a sketch of a general cross section of an Ottoman mosque.

In the proceedings of this chapter, the optimization of the dome is done with respect to its dead weight. The weight and the stiffness properties are assumed uniform.

a  b 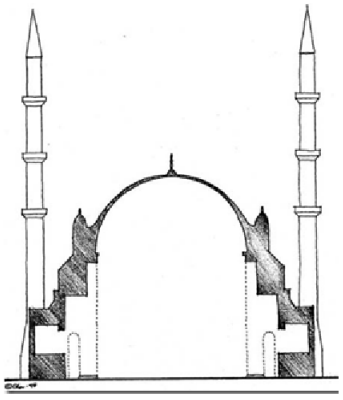

Figure 5.1: *(a) islamicthems.blogspot.no Salimiye Mosque (b) Cross section of an Ottoman mosque, by Latif Abdulmalik*

## 5.2 Analytical Estimates

For comparison, the bending moment of a selection of shapes are established analytically.

Where the shell intersects the axis of revolution, $R_0 = \psi = 0$. The optimizing of the dome shape is restricted to the initial width and height of the Ottoman domes, approximated to be perfect half spheres. The radius of the sphere is given the notation '$a$'. Denoting the meridional curve of the optimized shape as $e(R_0)$ it implies then that $e(0) = a$ and that $e(a) = 0$.

As established in equations 2.16 and 2.17, the moments within a shell can be estimated on the basis of its deflections.

### 5.2.1 Load

The distributed weight of the dome is $p_y = \gamma \cdot g \cdot t$; $\gamma$, $g$ and $t$ being the mass density of the building material, acceleration due to gravity and thickness of the shell respectively.

The resultant of the dead weight is equal the accumulated weight

$$P_e(R_0) = -\int 2\pi \cdot p_y \cdot \frac{R_0}{cos(\psi)} dR_0 + C \tag{5.1}$$

The constant of integration $C$ is determined from $P_e(0) = 0$.

The components of $p_y$ normal to the surface and tangent to the meridional curve are as follows

$$\begin{bmatrix} p_n \\ p_\psi \end{bmatrix} = -p_y \begin{bmatrix} cos(\psi) \\ sin(\psi) \end{bmatrix} \tag{5.2}$$

### 5.2.2 Deflections

One can solve equation 2.13 with respect to $w$ and eliminate it to reach the differential equation for $u$

$$\frac{du}{d\psi} - u \cdot cot(\psi) = R_\psi \cdot \varepsilon_\psi - R_\varphi \cdot \varepsilon_\varphi = \frac{1}{E \cdot t}[T_\psi(R_\psi + \nu \cdot R_\varphi) - T_\varphi(R_\varphi + \nu \cdot R_\psi)] = f(\psi) \tag{5.3}$$

The last relation is found by introducing Hooke's law, equation 2.18, and equation 2.14.

The solution to the differential equation is, [Ugural81]

$$u = sin(\psi) \int \frac{f(\psi)}{sin(\psi)} d\psi + C \cdot sin(\psi) \tag{5.4}$$

where the constant of integration $C$ is determined from the boundary conditions.

Readily, $w$ can be found from equation 2.13

$$w = u \cdot cot(\psi) + \frac{R_\varphi}{E \cdot t}(T_\varphi - \nu \cdot T_\psi) \tag{5.5}$$

As an alternative, the kinematic relations, equation 2.13, can be solved for $u$ and eliminated, giving a formula for the deflection normal to the surface $w$ (the result is the same). The differential equation for $w$ is then

$$\frac{d}{d\psi}(w \cdot tan(\psi) + R_\varphi \cdot \varepsilon_\varphi \cdot tan(\psi)) - w = R_\psi \cdot \varepsilon_\psi \tag{5.6}$$

### 5.2.3 Shapes

The bending moments due to the dead weight of the dome are presented for domes shaped as half spheres and cones.

#### 5.2.3.1 The Half Sphere

One of the primary features of the sphere is that the curvatures of both the principal curves are equal and constant for the whole shell. The radius of the sphere is denoted '$R$'; $R_\psi = R_\varphi = R$. Advancing with the radius of the parallel curves, $R_0 = sin(\psi) \cdot R$ and its incremental variation $dR_0 = cos(\psi) \cdot R \cdot d\psi$.

The accumulated load is then

$$P_e(\psi) = -\int 2\pi \cdot p_y \cdot sin(\psi) \cdot R^2 d\psi + C = 2\pi \cdot p_y \cdot R^2(cos(\psi) - 1)$$

The membrane forces, in accordance with the membrane theory, equations 2.8 and 2.9, are found to be

$$T_\psi = -\frac{p_y \cdot R}{1 + cos(\psi)}$$

$$T_\varphi = p_y \cdot R(\frac{1}{1 + cos(\psi)} - cos(\psi))$$

Equation 5.4 gives the deflections tangent to the meridional curve

$$u = sin(\psi)\frac{p_y \cdot R^2(1+\nu)}{E \cdot t}\int \frac{cos(\psi)(1 + cos(\psi)) - 2}{sin(\psi)(1 + cos(\psi))}d\psi + C \cdot sin(\psi) =$$

$$= [\frac{p_y \cdot R^2(1+\nu)}{E \cdot t}[ln(2) + ln(1 + cos(\psi)) - \frac{1}{1 + cos(\psi)}] + C] \cdot sin(\psi)$$

At the edge of the dome, $\psi = \frac{\pi}{2}$, indicating that $u(\frac{\pi}{2}) = 0$ is the desired boundary condition that exposes the constant of integration $C = \frac{p_y \cdot R^2(1+\nu)}{E \cdot t}(1 - ln(2))$. The deflections are then as follows

$$\begin{bmatrix} u \\ w \end{bmatrix} = \frac{p_y \cdot R^2(1+\nu)}{E \cdot t} \begin{bmatrix} (ln(1+cos(\psi)) + \frac{cos(\psi)}{1+cos(\psi)}) \cdot sin(\psi) \\ cos(\psi)(ln(1+cos(\psi))+1) - 1 + \frac{sin(\psi)}{(1+\nu)} \end{bmatrix}$$

By inserting the obtained formulas for the deflections into equations 2.16 and 2.17 the moment distributions are found to be

$$M_\psi = M_\varphi = \frac{p_y \cdot t^2}{12} \cdot \frac{2+\nu}{1-\nu} cos(\psi) \tag{5.7}$$

#### 5.2.3.2 The Cone

When dealing with the cone as a rotational symmetric object, measures need to be taken into account for $R_\psi \to \infty$. With the height of the cone equal to the radius of its base '$a$', $\psi = \frac{\pi}{4} = constant$ and does not serve a coordinate for the shell. With $ds$ being an infinitesimal distance of the meridional curve (a line), the incremental change of $\psi$ is set to be $d\psi = \frac{ds}{R_\psi} = \frac{dR_0}{R_\psi} \cdot \frac{ds}{dR_0} = \frac{dR_0}{R_\psi} \cdot \frac{1}{cos(\psi)} = \sqrt{2}\frac{dR_0}{R_\psi}$.

Following the steps taken to estimate the moments in the half sphere, the accumulated weight of the cone is

$$P_e(\psi) = -\int 2\sqrt{2}\pi \cdot p_y \cdot R_0 dR_0 + C = -\sqrt{2}\pi \cdot p_y \cdot R_0^2$$

The membrane forces are

$$T_\psi = -p_y \cdot R_0$$

$$T_\varphi = \sqrt{2} p_y \cdot R_0 (\frac{R_0}{R_\psi} - \frac{\sqrt{2}}{2}) = -p_y \cdot R_0$$

The alternative differential equation for deflection, equation 5.6, is then

$$\frac{d}{d\psi}(w - \sqrt{2} p_y \cdot R_0^2 \frac{(1-\nu)}{E \cdot t}) - w = -R_\psi \cdot p_y \cdot R_0 \frac{(1-\nu)}{E \cdot t}$$

which can be rewritten as

$$\frac{dw}{dR_0} - \frac{\sqrt{2}w}{R_\psi} = \sqrt{2}p_y \cdot R_0 \frac{(1-\nu)}{E \cdot t}$$

The solution to the differential equation is, [Malumbres09]

$$w = e^{-\int \frac{\sqrt{2}}{R_\psi} dR_0} \left[ \int \sqrt{2} \cdot p_y \cdot R_0 \frac{(1-\nu)}{E \cdot t} e^{\int \frac{\sqrt{2}}{R_\psi} dR_0} dR_0 + C \right] = \frac{\sqrt{2}}{2} p_y \cdot R_0^2 \frac{(1-\nu)}{E \cdot t} + C$$

Readily, $u$ can be found from equation 2.13

$$u(R_0) = -\frac{\sqrt{2}}{2} p_y \cdot R_0^2 \frac{(1-\nu)}{E \cdot t} + C$$

Establishing the boundary condition $u(a) = 0$ leaves the formulas for the deflections of the cone to be

$$\begin{bmatrix} u \\ w \end{bmatrix} = \frac{\sqrt{2}}{2} p_y \frac{(1-\nu)}{E \cdot t} \begin{bmatrix} a^2 - R_0^2 \\ a^2 + R_0^2 \end{bmatrix}$$

The bending moment about the tangent to the parallel curves is found

$$M_\psi = -D[\frac{\sqrt{2}}{2} \frac{d}{dR_0} (\frac{u}{R_\psi} + \frac{\sqrt{2}}{2} \frac{dw}{dR_0}) + \frac{\nu}{R_0} (\frac{u}{R_\psi} + \frac{\sqrt{2}}{2} \frac{dw}{dR_0})] = -\frac{D}{2} [\frac{d^2w}{dR_0^2} + \sqrt{2} \frac{\nu}{R_0} \frac{dw}{dR_0}]$$

From the same analogy, the bending moment about the tangent to the meridional curves is found, and the moment distributions are as follows

$$M_\psi = M_\varphi = -\frac{\sqrt{2}}{24} p_y \cdot t^2 = constant \tag{5.8}$$

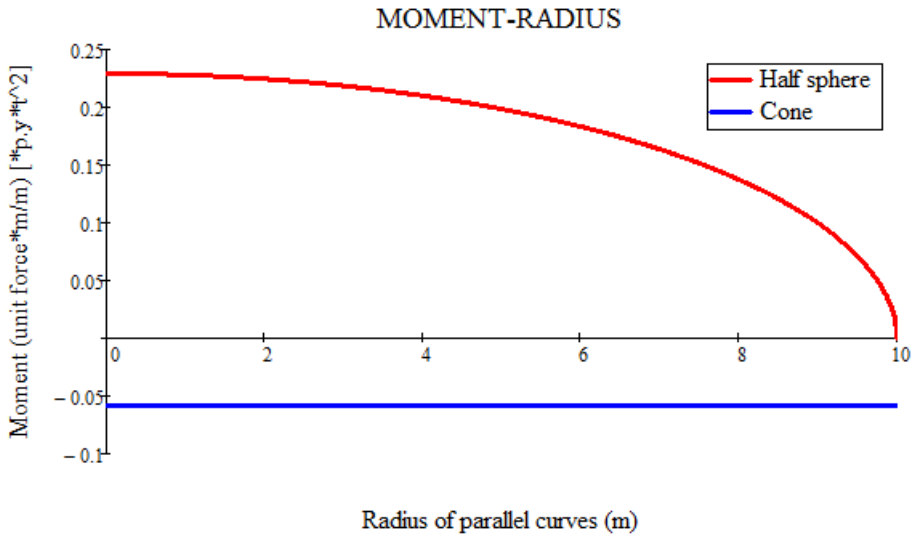


Figure 5.2: *Moment distributions due to dead weight in half spheres and cones with* $a = 10m$ *and* $\nu = 0.2$

#### 5.2.3.3 Comparison between the Half Sphere and the Cone

In figure 5.2, the moment distributions for the half spheres and cones are graphed for the case $a = 10m$ and $\nu = 0.2$, a common Poisson's ration for mortar [Mohamad06].

Judging from the graph one is led to the conclusion that the cone is in closer proximity to the optimum shape than the half sphere. With each of the graphs placed over- and under the horizontal axis, one is to assume that the optimum shape lies somewhere between the two. The hypothesis is drawn that the shape will resemble the cone with a slight, positive curvature in the meridian compensating for the negative moment illustrated in figure 5.2, and that it will be closer to the shape of half sphere around the edges.

### 5.2.4 Remarks Regarding the Apex

Special attention has to be given the apex of the dome, both constructively and theoretically. Constructively, it is practically difficult to let several beams (or rebar) meet in one such intersection. Theoretically, the apex works as a

point support indicating that shearing forces reach infinity in its proximity. Thus, if the shell has a point apex, it must be assumed that the shell is fastened to a column along an adjacent, parallel curve of a given radius. The given radius is corresponding to the radius where the vertical component of the internal forces is satisfactorily close to that of the load, [Ugural81]. Such measures are not taken into account in this research.

## 5.3 Optimization Solutions From Software

Moving on from the 2 dimensional problems in section 4.3, the goal of this section is to get familiarized with the meshing and assembling of 3 dimensional structures within the software. One objective is to acquire competence related to how to assemble a meshed model whose topology is not affected by the constant changes in shape throughout the optimization process. Another objective is to investigate differences between meshing patterns representing the shell.

### 5.3.1 Challenges Faced When Assembling the Model

While spending time with the software mistakes have been made and lessons learned. The challenges are related to two separate issues being the assembling of the geometry and the other the loads. Having a profound understanding of when different strategies are applicable has proven itself key to achieving a successful model. This section gives a short summary of the lessons learned.

**Don'ts**

1. Don't use algorithms involving 'closest points' if variations during the optimization process involve large deviations in the model's shape. A consequence of this may result in a changing topology as shown in figure 5.3

2. Don't manually cull lines, points etc. as it is cumbersome and probably not the best way of exploiting the opportunities provided by the

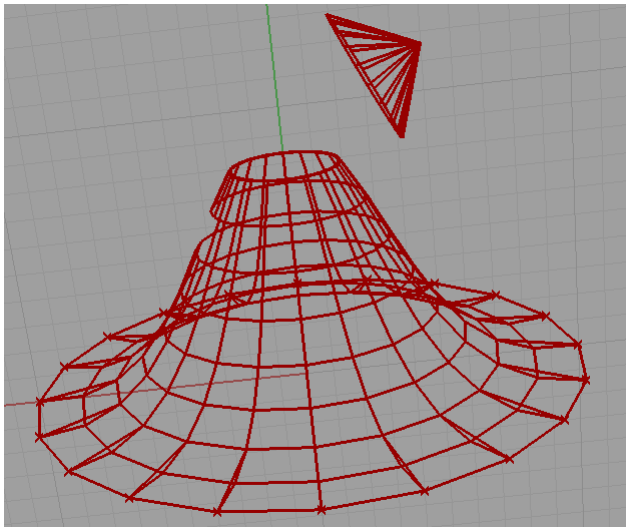

Figure 5.3: *Dome model that does not meet the requirements*

software. Manual culling is also highly sensitive to human errors. In figure 5.3 one can observe that the user has not culled excessive lines close to the boarder

3. Don't intend to relate a load distribution to a projection of the geometry as it strongly increases the run time

**Dos**

1. Check the rigidity of your model assembly by dragging the sliders introduced to the evolutionary solver up and down before running the optimization process

2. Learn what the automatized methods provided by the software can accomplish, as they are efficient in terms of both time spent modeling and run time and they help avoid human errors

3. Invest time in investigating example files, additional components and discussions on the internet, it has been proved rewarding

### 5.3.2 Establishing a Basis for Comparison

The first model consists of a trapezoidal grid of beams, ending in triangles in the apex. The grid is illustrated on the top left in figure 5.5. The meridional curve is represented by a $5^{\text{th}}$ degree interpolated curve using 2 interpolation points. They are evenly distributed on the x- axis, leaving the y- coordinates as parameters to be optimized. The meridional curve is discretized by 10 equal line segments. The parallel curves are discretized by 20 equal line segments. The line segments form the basis for the beam elements in the finite element program. The height and base radius of the dome are both 10m. The surface mesh for the load is defined by the points of intersection between the meridional and parallel lines segments. The load density is set to $1\frac{kN}{m^2}$, acting over the mesh surface, parallelly to the axis of revolution. The fitness parameter is defined by the moment resultants of the beam elements representing the meridional curve. The moment resultants are the resultants of the bending moments within the elements, and do not include torsional moments about their axes. The fitness is set to minimize the input.

Three optimizations are completed with default settings. The first one is given all initial values equal to zero. The second attempt is given initial values equal to the ones found by the first optimization. Accordingly, the third one is given initial values equal to those found by the second optimization. The results are included in figure *5.4 (a)* and *(b)*.

Judging from the moment diagram, the desired solution lies in the proximity of the $2^{\text{nd}}$ and $3^{\text{rd}}$ attempt. It is observed that the $3^{\text{rd}}$ attempt gave a solution with a greater bending moment that the $2^{\text{nd}}$ attempt, suggesting that further attempts would be redundant. Note that the horizontal lengths of the graphs in the moment diagram are of little meaning as they are solely a projection of the equal- length lines in the model onto the x- axis. The $1^{\text{st}}$ attempt is not included in the moment diagram as its maximum value is 10 times that of attempt #3. The three attempts completed after 110, 90 and 65 generations respectively. On a personal laptop, each generation has a duration of approximately 30 seconds. One can observe that the $1^{\text{st}}$ optimization got stuck with a local minima that does not match the minimas found by the later trials.

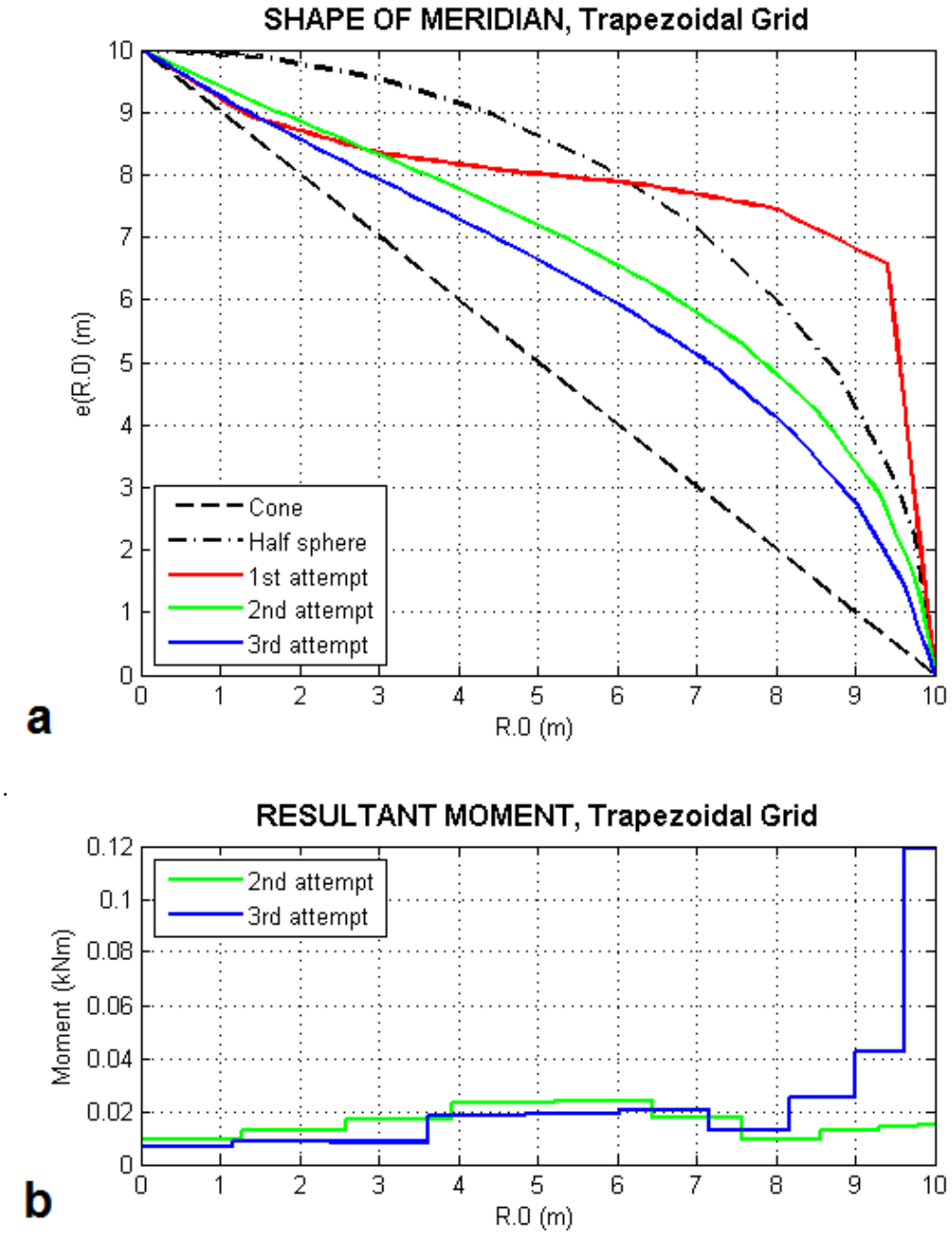


Figure 5.4: *(a) Optimized shapes of dome meridian after changes in initial values (b) Corresponding resultant moments after the* $2^{nd}$ *and* $3^{rd}$ *attempt*

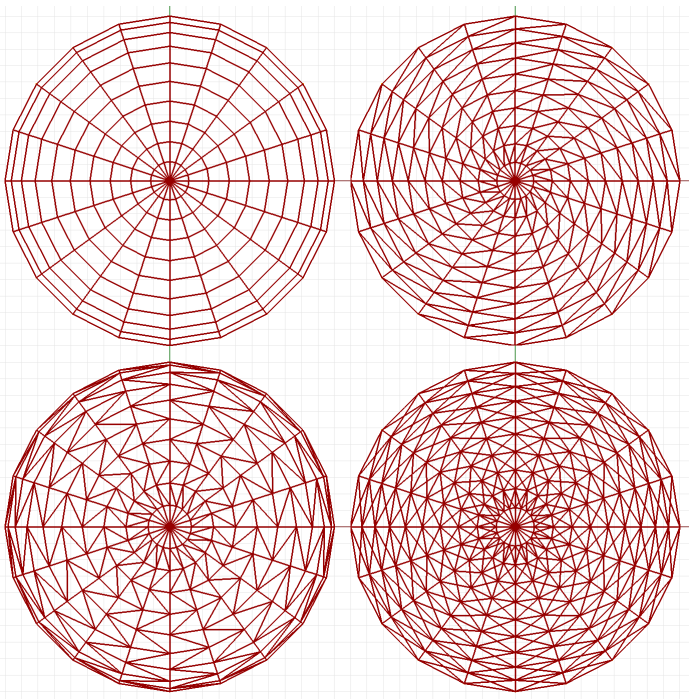

Figure 5.5: *Various beam grids for the dome model*

### 5.3.3 Beam Grids

At the time of investigation, the software does not provide for plate- nor shell elements. To compensate for this, triangular beam grids are suggested by the authors of the program, [Preisinger12#2]. It is assumed that adding diagonal beams within each of the trapezoidal shapes (one in each direction) is the best way to represent the behavior of the shell. However, it is of interest to investigate the consequence of applying alternative solutions. This would translate to structures where the carrying system is in fact beams, e.g. a glass ceiling. In addition to the grid used in the basis for comparison, three alternatives are examined. In the first one, the trapezoids are added a beam in one of their diagonals. The diagonals all have the same radial direction. In the second one, the directions of the diagonals are alternating. The third one is the one considered the optimum, with one added beam in each of the diagonals. A sketch of the grids seen from above is included in figure 5.5.

The applied load is the same as for the basis for comparison, i.e. the mesh

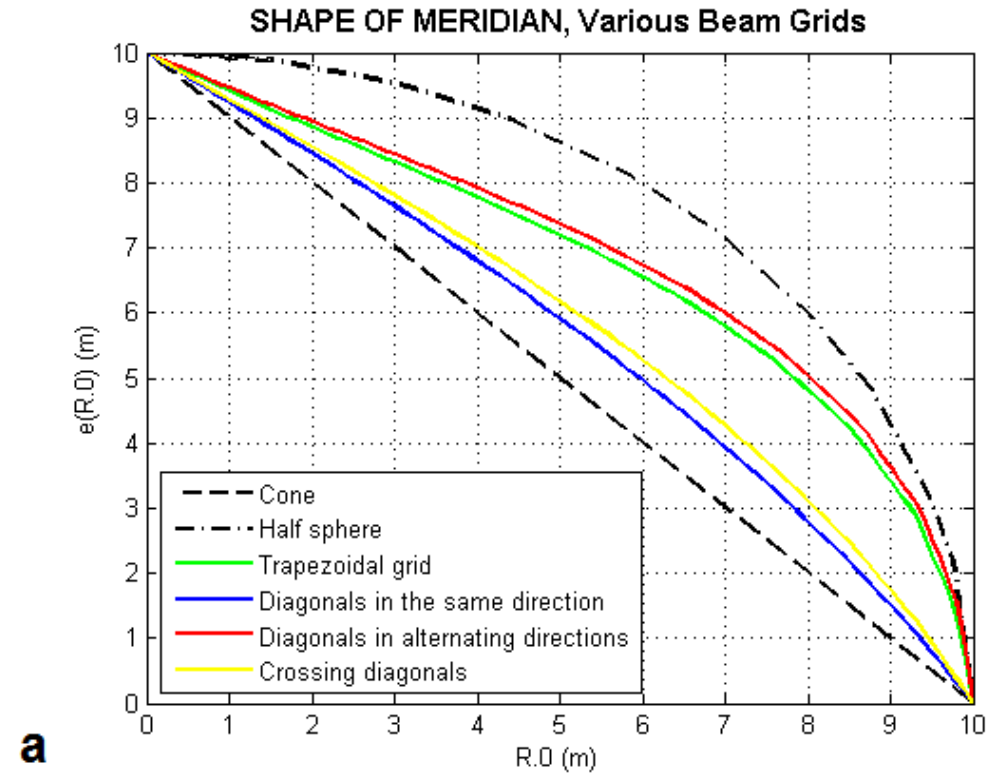


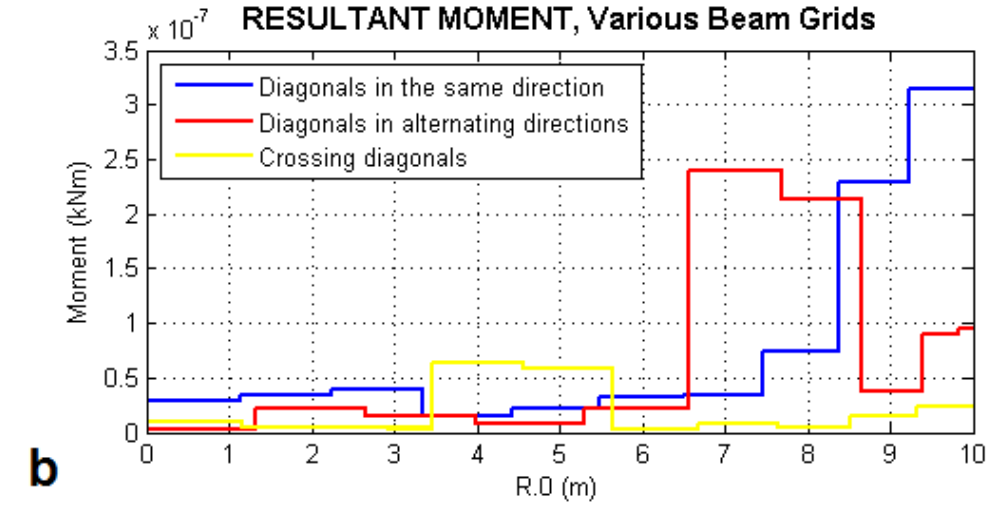


Figure 5.6: *(a) Optimized shapes of dome meridian for the grids in figure 5.5 (b) Corresponding resultant moments*

is not altered.

In figure 5.6 *(a)* and *(b)* one can observe the results. The optimization processes ended after 55, 90 and 150 generations respectively. It was observed during the optimization process of the model with crossing diagonals that it was stuck in a local minima of the same type as that of the $1^{st}$ attempt in figure 5.4 *(a)*. It 'broke loose' after about 120 generations, ending in the shape seen in figure 5.6 *(a)*.

By adding beams, naturally, the distributed moment in the meridian beams decreases. The final moment distributions in the models added only one diagonal; however, are comparable. From the moment diagram one can observe that the quality of the two solutions is virtually the same. Nevertheless, their meridian shapes deviate. One is closer to the basis for comparison, and the other is closer to the shape of the model with beams added in both diagonals. One pair of shapes resembles the cone, and the other resembles the half sphere. Whether this indicates that the optimum shape for the dome has two competing minimas or that the chosen grids in fact have different optimum shapes is hard to conclude based on this study alone. An in-depth study of shell idealization using beam elements is left for further work. As seen in figure 5.4 *(b)*, the maximum bending moment appearing in the model with the trapezoidal grid is about 100 000 times that of those with diagonal beams added to them; thus, does not compare. The assumption that the grid with crossing diagonals is the best shell representation withstands on the basis of the recommendation of the authors of the program for the software, [Preisinger12#2].

### 5.3.4 Load Density

As no unique analytical solution is established, one is to assume that the zero moment shape of the dome is dependent on the load density. Trials with different load densities are run. A uniform increase in load density over the surface of the dome leads to a non- uniform load increase with respect to the parallel curve- coordinate. It is expected that different solutions are found for different load cases. The examination of the load densities are run on the model with crossing diagonal beams added to it. A rough estimate of the weight of a $1m$ thick dome made from mortar and bricks is $20\frac{kN}{m^2}$ and is included as a load case, figure 5.7 *(a)* and *(b)*. For the sake of clarity, it

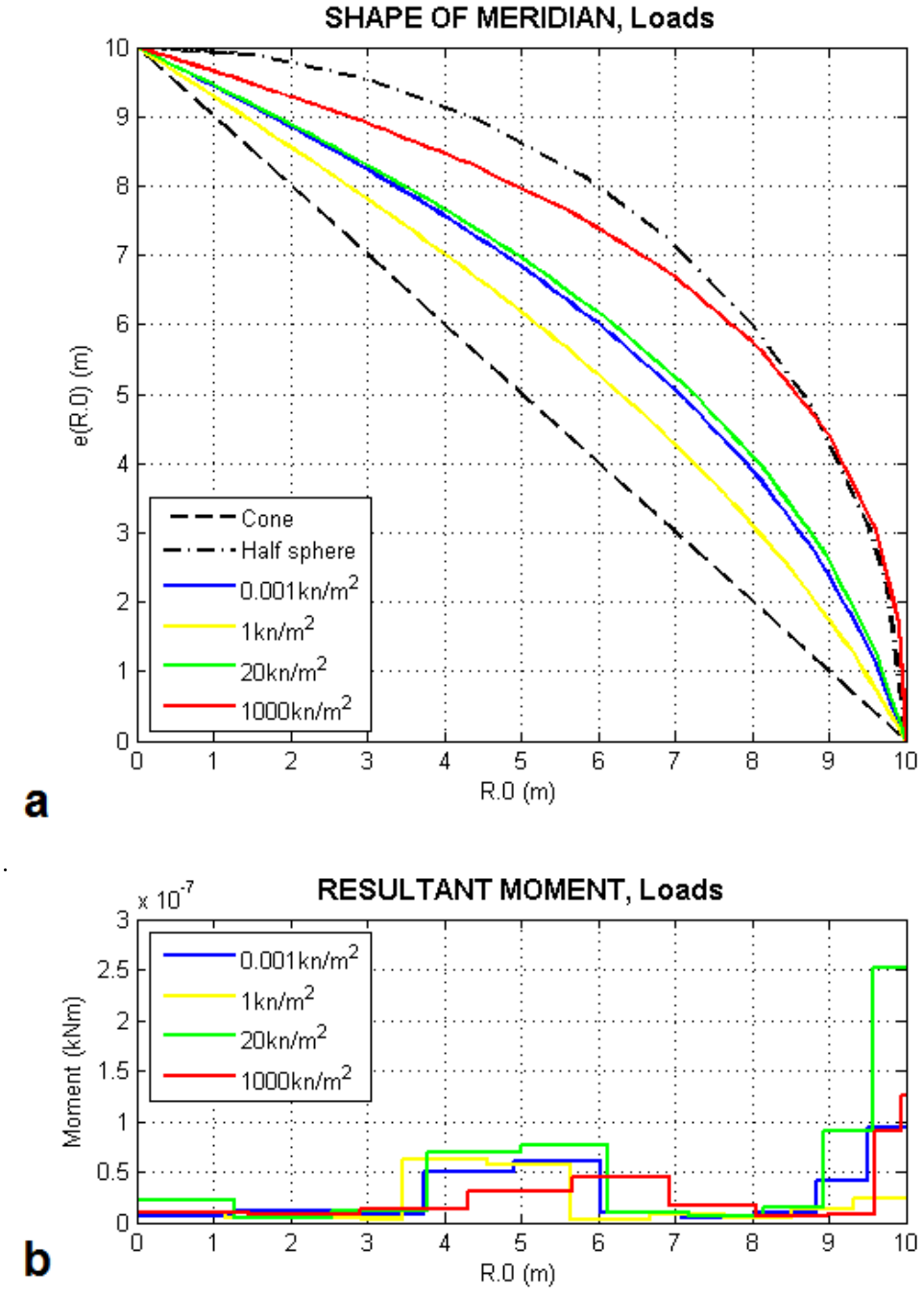


Figure 5.7: *(a) Optimized shapes of dome meridian for various load densities (b) Corresponding resultant moments*

is mentioned that this thickness contradicts the definition of a thin shell, as stated in section 2.1.

The models with the load cases $0.001\frac{kN}{m^2}$, $20\frac{kN}{m^2}$ and $1000\frac{kN}{m^2}$ ended after 135, 125 and 195 generations respectively. From figure 5.7 *(b)* one can observe that in spite of the vast differences in load densities, the quality of the results in terms of resultant bending moment in the meridional beam elements are comparable. The results in figure 5.7 *(a)* are relatively ambiguous as they are neither confirming nor disproving a dependence on the load. In particular, the load case $0.001\frac{kN}{m^2}$ raises doubt as it finds itself between the results of the load cases $1\frac{kN}{m^2}$ and $20\frac{kN}{m^2}$. In combination with the doubts raised in section 5.3.3 it is suspected that this result is stuck in a competing minima with a slightly higher curvature than that of the optimum shape. With the exception of the mentioned load case, it is then concluded that the optimum shape in terms of bending moment is dependent on the density of the load. Special attention is given to the load case $1000\frac{kN}{m^2}$ which has the greatest curvature, but with a resultant bending moment laying within the midst of the rest, confirming that its minima is not the one witnessed in figure 5.6 *(a)*.

### 5.3.5 Discussion Regarding the Estimated Dome Shapes

Though not proved nor statistically verified, the hypothesis given in section 5.2.3.3 appears strengthened by the investigation completed so far by comparing the resultant shapes with that of the cone and the half sphere. They deviate slightly from the cone, with a stronger attraction towards the sphere closer to the boarder. This attraction seems to intensify with an increased load density, being the weight of the dome.

A screen shot of the result obtained with crossing diagonals and a load density of $1\frac{kN}{m^2}$ is included in figure 5.8. In appendix D.1, the first 15 generations of the optimization is included as a video tutorial. Another tutorial shows the basic set-up of the model.

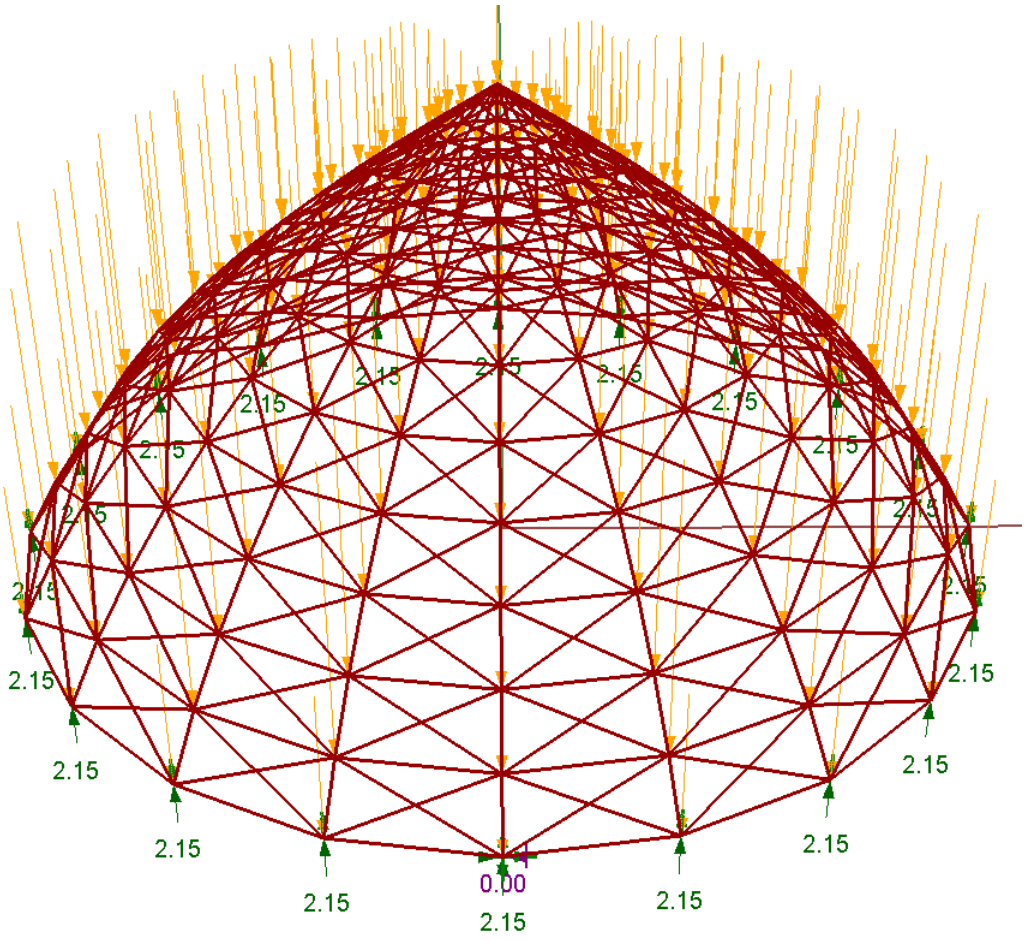


Figure 5.8: *Example of dome obtained with the software*

# Chapter 6

# CASE: KUWAIT INTERNATIONAL AIRPORT

The purpose of this case is to exemplify a potential use of the software in a real project.

It is desired to utilize the software to find the optimal shape of a double curvature shell. The following shell is inspired by the carrying system of the new terminal of the Kuwait International Airport, designed by Foster + Partners. The terminal is estimated to be completed in 2016, http://en.wikipedia.org/wiki/Kuwait_International_Airport#Structure. All assumptions about the carrying system and the load are based on the illustrations in figure 6.1 *(a)* and *(b)*. The scenario is simplified, and additional assumptions are made which cannot be drawn from the illustrations alone.

## 6.1 The Shell

Though not accurate, the pieces connecting the roof and the floor in figure 6.1 *(a)* are referred to as columns for the remainder of this chapter. The system is described in Cartesian, global coordinates. The direction of the row of columns is denoted the y- direction. Accordingly, the x- axis is perpendicular to the row. Along the roof edge $x = 0$ , referred to as the edge of the shell. At the level of the roof, $z = 0$ and $z$ is positive moving closer to the floor level in the direction of gravity, figure 6.2. It is assumed that the columns

a


b

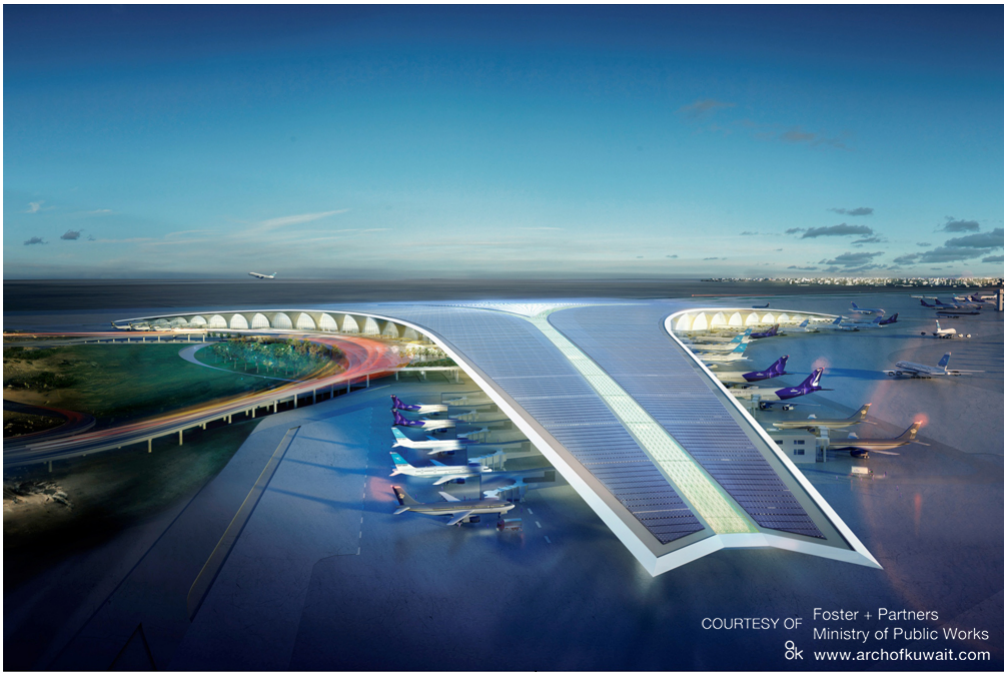


Figure 6.1: *(a) Carrying system for the Kuwait International Airport (b) Roof of the Kuwait International Airport*

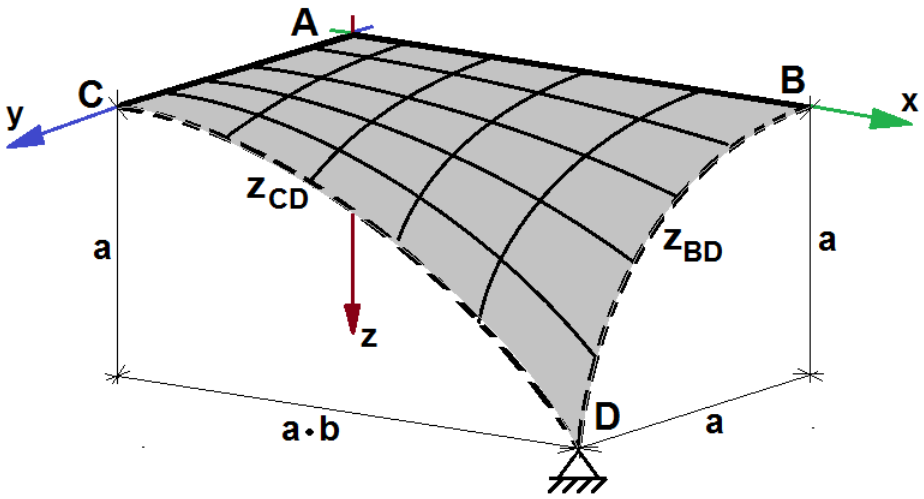


Figure 6.2: *Outline of model for the carrying system*

are symmetrical about the y- axis and about an axis parallel to the x- axis intersecting the base. From these assumptions, each column can be divided into four symmetrical segments. These segments constitute the shell that it is desired to optimize.

The four corners are named A, B, C and D, corresponding to the illustration in figure 6.2. The origin is placed in A.

Due to some hypothetical advantage from a constructional point of view, it is assumed that the shell is only restricted against perpendicular displacements parallel to the x, y- plane along its boarders. I.e. there is no transfer of moments along the borders. In addition, the shell is pinned at the base. Consequently, the entire vertical load is supported by D. Under these assumptions, the support conditions would not contribute to any deviation from a membrane state of the shell.

The height of the roof is denoted '$a$'. The distance between the columns is assumed to be $2a$. The curve constituting the shape of the border BD ($x = constant$) is defined by an interpolating function $z_{BD} = f(y); f(0) = 0; f(a) = a$. The architect wants to achieve a holistic design by letting the curve constituting the shape of the border CD ($y = constant$) be defined by a scaled function of $z_{BD}$; $z_{CD} = f(\frac{x}{b})$. Consequently, the projected distance between the edge and the base is $a \cdot b$. All curves $y = constant$ constituting

the shape of a cross section parallel to the y, z- plane are scaled in the same manner. Any point on the centroidal axes of the shell is then defined by the function

$$z(x,y) = f(y)\frac{f(\frac{x}{b})}{f(\frac{a \cdot b}{b})} = f(y)\frac{f(\frac{x}{b})}{a} \tag{6.1}$$

and $f$ is what is left to be optimized by the software.

## 6.2 The Load, the Roof

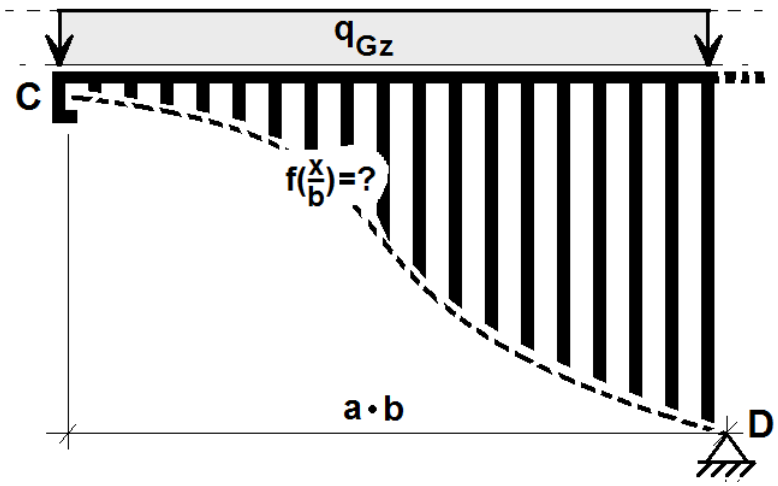


Figure 6.3: *Idealized load case from the roof corroborating the support conditions*

In figure 6.1 *(b)* one can observe the roof that is to be supported by the carrying system. The load from the roof, solar panels, and any other installment that would add to the weight, is idealized to be evenly distributed. It is assumed that weight of the shell itself is negligible. Without any additional information about the internal carrying system (i.e. the transfer of loads between the roof and the shell), the roof is idealized as a stiff body corroborating both the support conditions and the evenly distributed load. The idealized roof with the corresponding load is illustrated in figure 6.3, for the cross section $z_{CD} = f(\frac{x}{b})$.

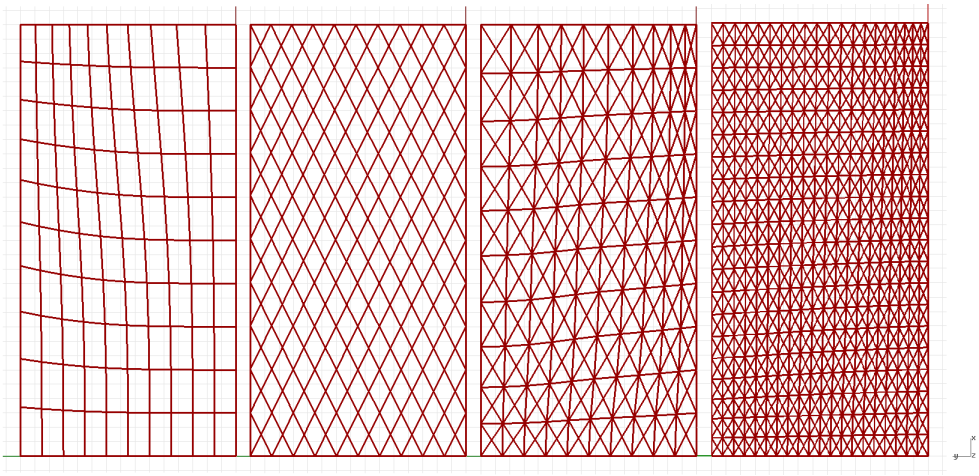

Figure 6.4: *Various grids for the model seen from above; grids #1-4 from left to right respectively*

## 6.3 The Model

### 6.3.1 General

In the model of the shell, $f$ is represented by an interpolation curve defined by 3 variable interpolation points. They are evenly distributed on the floor projection of the curve, leaving the z- coordinates to be found by the Evolutionary Solver. The interpolation curve is a $3^{\text{rd}}$ degree interpolation. On the basis of $f$, curves are outlined in accordance with equation 6.1, evenly distributed on the borders AB ( $y = 0; x \in [0, a \cdot b]$ ) and AC ( $x = 0; y \in [0, a]$ ). These curves are divided into equal curve segments, establishing the basis for the beam grid of the model.

It is of interest to investigate different alternatives for the beam grid representing the shell. Four different grids are used. The grids are illustrated in figure 6.4 from left to right.

1. Beams defined by the curve segments, 10 beams on both border AB and AC
2. Beams defined by lines connecting the intersections of the curve segments as show in figure 6.4, 10 beams on both border AB and AC

3. Beams defined as in both 1. and 2.. This would be the approximation of shell behavior, as stated in section 5.3.3, [Preisinger12#2]

4. Beams defined as in 3, but with 20 beams on both border AB and AC

The purpose of the first three grids is to investigate the consequences of replacing the shell with beams, in terms of optimum shape. The fourth one is included with the intention of verifying that the third grid indeed represents shell behavior by increasing the beam (and element) density. It is then assumed that by increasing the beam density, the model converges towards true shell behavior.

The mesh for the load is a surface mesh with nodes in the same locations as the ends of the curve segments. The load is approximated by point loads acting on these node locations. In coherence with section 6.2, the load is evenly distributed over the x, y- plane and global.

The fitness is set to minimize the resultant moment in all the beam elements.

### 6.3.2 Case Specific

By studying the illustrations in figure 6.1 *(a)* and *(b)*, the height of the columns are estimated to be $a = 15m$. The roof edge is estimated to be $30m$ away from the columns, which means that $b = 2$.

The load density is a unit load $p_{Gz} = 1\frac{kN}{m^2}$. The real world equivalent of this load density is small, approximately equal to the weight of a 4cm thick aluminum plate ($2700\frac{kg}{m^3}$).

## 6.4 Results Found from Software

The four different grids gave results for $f(y)$ as illustrated in figure 6.5. Though not accurate, grid #1 is referred to as rectangular and grid #2 is referred to as diagonals. The duration of the optimization processes, average resultant moments and peak resultant moments of all the beam elements for the different grids are given in table 6.1.

From figure 6.5 one can observe that the grids converge towards different shapes. The defining function $f$ for the "rectangular" grid deviates vertically

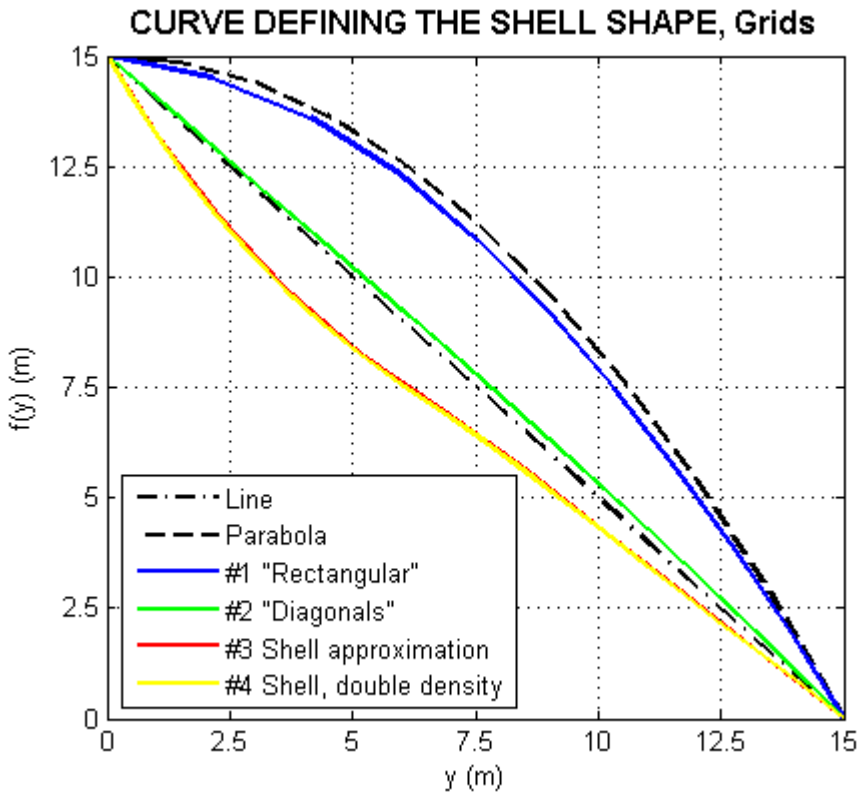


Figure 6.5: *Results for the shape defining curves $f(y)$ corresponding to the grids in figure 6.4*

| Grid | Duration per generation (s) | Number of generations | Average moment (kNm) | Peak moment (kNm) |
|---|---|---|---|---|
| #1 | 4 | 175 | 4.016766 | 16.2162 |
| #2 | 4 | 450 | 0.691236 | 2.2635 |
| #3 | 6 | 510 | 0.348172 | 2.6692 |
| #4 | 15 | 290 | 0.197449 | 3.6658 |

Table 6.1: *Duration and quality of optimizations corresponding to the grids in figure 6.4*

from a parabola with a maximum of 45cm. For the grid with only "diagonals", the function deviates from a straight line with 32cm. The shape defined by a straight line forms a hyperbolic paraboloid. The defining function of the grid representing the shell with 20 beams on borders AB and AC deviates with only 3cm from the one with 10 beams. Under the assumption given in section 6.3.1, it then supports that grid #3 adequately represents shell behavior.

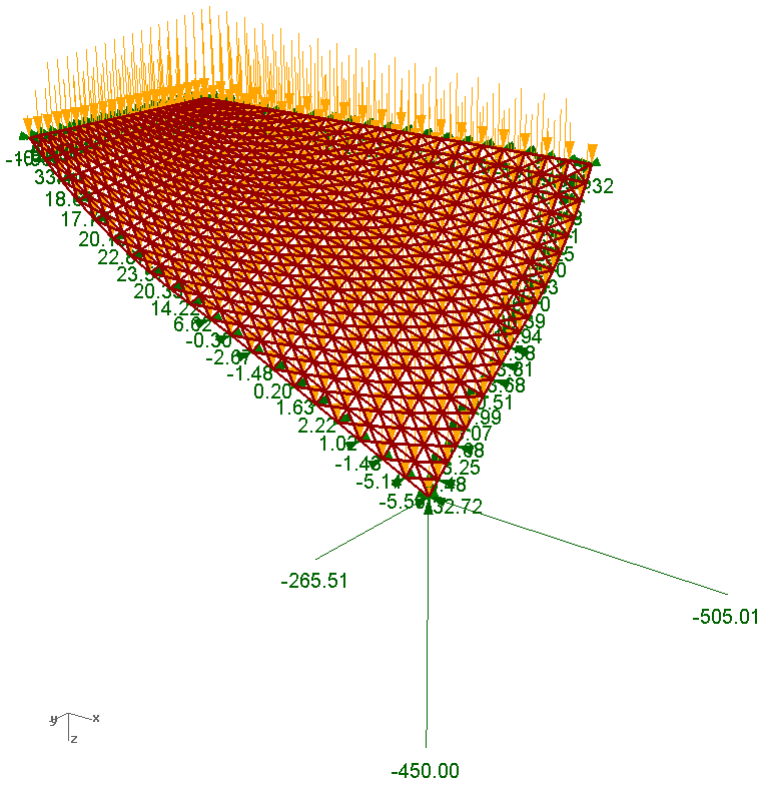


Figure 6.6: *Example of shell obtained with the software*

### 6.4.1 Remarks to the Architect

It is important to note that the shapes are optimized on the basis of the resultant bending moments alone and is only meant to exemplify the procedure and the conclusions one can draw from it. Some observations can be

made and presented to the architect of the columns when evaluating different designs.

1. By changing an initial "rectangular" beam grid to a grid made up of "diagonals" (and the corresponding shape), one can observe a significant drop in the bending moments in the beams, table 6.1. On the basis of that statement, the hyperbolic paraboloid might be a profitable alternative to the original shape, given that the carrying system consists of beams and not a shell.

2. If the carrying structure in fact can be represented by a continuous, isotropic, thin, elastic shell with a constant thickness, it might be appropriate to evaluate a shape with a positive, 'downward' curvature, contrary to the one illustrated in figure 6.1 *(a)*. An illustration of the resulting shell found using the software is included in figure 6.6, for grid #4.

3. If a negative, 'upward' curvature is important, e.g. due to its ability to provide for a more 'spacious' design, the beam grid might be more profitable than the shell, and should be investigated. The resulting design reached from the "rectangular" beam grid is illustrated figure 6.7 by a rough sketch made in Rhino.

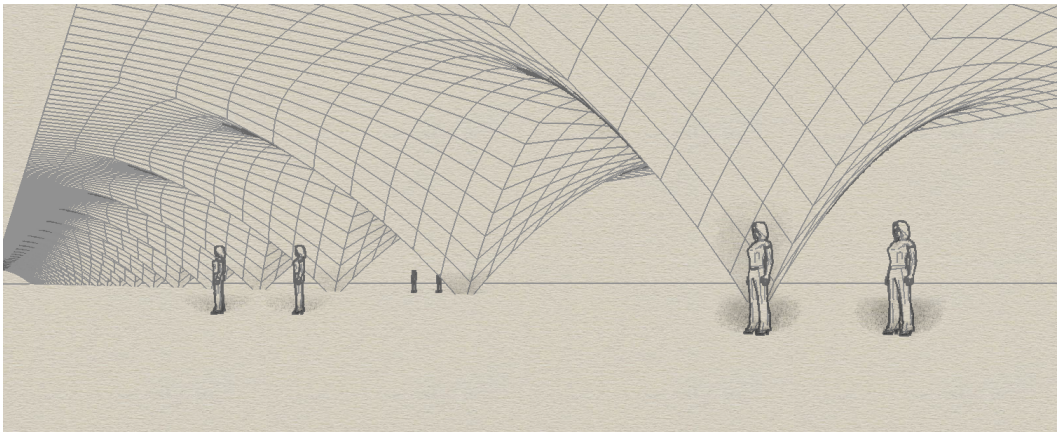

Figure 6.7: *Rough sketch of the result of grid #1 seen in context*

## 6.5 Discussion Regarding the Procedure

**Case- Related.** Based on this relatively brief investigation, a number of early- stage conclusions could be drawn that could have made an impact on the final design and future progress of the project. Many restrictions were added to the assembling of this model, helping to more easily be able to compare the different results. If a project does not possess that many conceptual limitations, the model could easily be adapted and still be of aid to the designer. However, challenges might then occur regarding the distinction between the results, and more parameter studies might be required to be able to draw clear conclusions. Moreover, having only one single measure of success has helped reduce the complexity of the approach presented here. In real life the situation probably would not be as convenient, and the weighing of different measures becomes an issue. Such weighing algorithms are not included here, but can easily be implemented into the model.

**Load Cases.** The software does allow for multiple load cases. How this feature affects the optimization and whether or not this feature is successful is not studied here. With various load cases; however, no design would perfectly accommodate the measures of success, even if there is just the one. In cases including several measures of success and/or load cases, the aid of the software plays an even more important role as it helps see the best (or at least the close-to-best) outcome of seemingly endless possibilities.

**Quality.** One issue remains the quality of the obtained results and the models assembled in the software. Other commercial FEA solvers have an advantage in terms of efficiency. They have invested resources in providing accurate calculations, where element density and numerical iterations are prioritized. The FEA solver Karamba is tailored to the needs of the design phase of a project, and to accommodate the low speed of the evolutionary algorithm. On the other hand, simple models (or more complex models still in the need of an optimization process) would be costly to assemble in such "advanced" programs, as the level of complexity offered is excessive in light of the projects' needs. It seems that the engineer is to draw a line in the progress of the design investigation where the benefits of "advanced" FEA solvers outweigh the benefits of programs like Karamba and corresponding

evolutionary solvers. Though, one might expect that the mentioned line is drawn further and further away as the speed of computers advance and gives way for evolutionary solvers to be run on more comprehensive models. The conjunction of the two types of software still would seem optimal as the one compensates for the other.

**The Interface.** One distinctive benefit of the procedure presented here has been the interface. As both the software for the architect (CAD) and for the engineer is within the same interface, close-to-no time is spent converting the models from one to the other. This improves the interchanging of ideas at a low cost and with little effort. Another benefit is the workflow within the software. To dynamically be able to update and make changes to the model on an orderly and organized canvas has made the assembling both efficient and an incentive for quick experimentation. It should be mentioned, that it also adds a certain fun-factor to the ordeal, which is beneficial to all parties of a project.

# Chapter 7

# DISCUSSION

**The Analytical Methods.** The analytical methods presented here have proven themselves quite resourceful. The approaches derived for the 2 dimensional beam cases, in particular, have with relatively little effort been able to present "clean" shapes with zero (or close-to zero) bending moments. The approach used for the 3 dimensional case of the dome did not give the same unambiguous results as the complexity of the problem made it hard to implement any continuous, analytical optimization method. However, the trial-and-error was able to give rise to some relatively accurate intermediate conclusions. Whether one would be able draw as accurate conclusions by implementing the same method on equivalent types of problems is hard to say based on this study.

It goes without saying, that in spite of best effort, the intricate typing of numbers and formulas has made it probable that errors occur. Most of the graphs; however, are derived directly from scripts, to minimize this potential error in the shape representations. Hence, the conclusions drawn on the basis of these should be on stronger ground.

**The Use of the Software.** The software, as a means of shape investigation, has proven itself an invaluable tool. Both the flexibility of the set-up of the models and the user friendliness continuously help motivate the user to explore alternative designs. No matter the complexity of the set-up, the evolutionary algorithm still helps the user explore possible solutions. One disadvantage though, seems to be that the process does benefit from the

guidance of human intelligence, and as more complex problems arise it becomes harder for the user to 'stay in control' of the process and intellectually intervene.

The qualities of the results obtained by the software have only been measured relative to each other. In spite of low bending moments reached by all the models, the remaining moments are not seen in light of real-world implications. I.e., the investigation is lacking a level of constructive measures for the discrepancies.

The FEA solver and the evolutionary solver are both made for "non- programmers". In contrast to more "advanced" FEA solvers, they do not offer many options for altering their algorithms or intervening with the set-up. This can be done on a code-level, however, but it requires competences beyond what I have attained through this study. Moreover, the information provided about the underlying procedures of the software is given at a user friendly basis only. Gathering in-depth information about the solvers is not easy to do, and demands a direct correspondence with their providers. With more information on how the solvers operate and on what assumptions and idealizations they base their calculations, the empirical approach in this study might have been more narrowed down and pin-pointed.

**Alternative Approaches.** The analytical methods (and problems) presented here are of a continuous nature. This has made the complexity of the calculations and theories grow exponentially with the complexity of the problems at hand. Though the personal learning curve has been inclined due to this, it could have been more constructive to implement numerical approaches. Experience related to the interchanging of the methods would perhaps be beneficial in a real project. The same goes for experience related to the interchange of types software, and how to convert a model from one format to another.

**Constructive Limitations.** The implementation of constructive limitations would help make the resulting shapes more justified. They could include anything from difficulties regarding the assembling of joints to adding restrictions on the quantity of beam lengths. All the shapes derived in this study are theoretical and could be justified for being part of the design phase only, where creativity might be considered more profitable. However, from

an engineering stand point, such restrictions can be valuable inputs at an early stage of a project and might help streamline the process later on.

**The Process of Writing the Report.** In light of the self-imposed limitations to solving the problem of the report, some clear conclusions have emerged. It would have been favorable to include cases with more measures of success, and where more than one shape can be considered optimal as this might better reflect the potential of the software. The general impression is however, that within the 20 weeks at disposal, the chosen line of progress was able to help maximize the learning experience of the writer as well as to be a source for future studies.

# Chapter 8

# CONCLUSION

When knowing both the shape and the load case of a statically determinate curved beam, deriving its bending moment distribution is for the most part an undemanding process. After finding the boundary forces of the beam, or parts of the beam, the moment distribution is found on the basis of the load acting perpendicular to its centroidal axis.
Classical theories describe the moment distribution in shells on the basis of initial curvatures and kinematic relations. For the most part, deriving geometrical descriptions including the initial curvatures is undemanding; however, the implementation of the kinematic relations does involve differential equations. Unless the shapes are relatively simple, solving these equations analytically can be a delicate process.
Though the striving for exact solutions is rewarding in terms of attaining a profound understanding of how internal forces and loads relate to shape, the analyst is to draw a line when a problem becomes too demanding to solve this way. When the constructive benefits of alternative methods (e.g. numerical methods) outweigh those of the analytical methods, a compromise has to be made.
It is noted that small differences in shape can give rise to relatively vast differences in bending moments.

A general strategy for reducing the bending moments in a structure by modifications to its shape is to compensate with more curvature where the bending moment is greater. This is an iterative process, as changes in shape also imply changes in the moment distribution of the structure.

For the curved beam, the method of analytical convergence has proved itself effective in reducing bending moments.

Through the work presented in this study, it is concluded that using modern software to reduce the bending moments of a structure by modifications to its shape is advantageous on many levels. It is highly effective as it entrusts a computer to do the iterative processes. It is beneficial as it helps explore shapes beyond the imagination of the user. Furthermore, it is highly cooperative and dynamically adapts to quick modifications made by the user.
One issue remains the quality of the solutions and the certainty of the obtained shapes. Compared to more "advanced" FEA solvers, Karamba does not offer the same accuracy and possibilities to intervene with the internal FEA algorithms. Deriving final shapes based on the software used in this study alone is not ideal, and should be used in conjunction with others.
Many approaches can be used to modify shapes within the software; some more successful than others. The major lessons learned regarding the applications of the software are as follows: Interdependence between the parameters to be optimized is not an asset to the evolutionary algorithm. Models can be assembled on the basis of independent points or points defined by interpolation according the needs of the problem. One should trust the software with automated approaches, as methods involving manual adjustments are prone to human errors.

It is mentioned that at the time of investigation, the software did not include shell elements. One is to expect that the implementation of this will promote some significant improvements in terms of both the analysis and the assembling of shell models.

# Chapter 9

# FURTHER WORK

The writing of this report has been a mere introduction to the field of structural optimization. During its completion, a number of related topics have arisen but not been further investigated. Some of these could probably have contributed to mapping out an enhanced process for general form finding. Others are may be of interest for further investigation in light of other objectives.

## 9.1 Suggested Improvements Left for Further Work

**Discrete systems.** In this study, all parameters to be optimized have been continuous. A step forward would be to include discrete, integer based parameters. These could represent anything from quantities of supports and beams to size parameters that reflect the different selections of lengths and cross sections offered by real suppliers.

**Collaboration with other types of software.** In real life there is a need for collaboration between different types of software. The investigation presented here does not explore the challenges faced when converting a model from one format to another. A natural step forward might be to obtain experience related to these types of conversions as well as to examine how to

optimize the process of doing so. Three relevant types software are rendering tools for presentations, advanced FEA programs for further analysis and BIM programs for planning of the structure.

**Constructive limitations.** Shape optimization done by an engineer could be strengthened by implementing limitations regarding difficulties with the realization of a structure in the real world. This could be anything from limitations of joints to introducing limitations due to the function of the structure.

**Multiple measures of success.** Having only one measure of success is only theoretical. In real life, multiple measures of success are present when deciding the quality of a structure. Continuing this study by including algorithms that include weighing of such measures might be a good improvement.

**Complex structures.** All the cases in this report deal with single constructional elements. Exploring how the software deals with structures of multiple constructional elements might help better exploit its potential. This can be anything from shape optimization of joint elements to modeling entire buildings. From an analytical perspective, theories on lines of distortion may be relevant.

**Cross sections and thicknesses.** Varying cross sections and shell thicknesses is not investigated in this report. By including such parameters in the evolutionary solver one is able to further optimize the structures in this report.

## 9.2 Related Topics that have Emerged During this Study

**Topology optimization.** Another type of structural optimization apart from shape optimization is topology optimization. Topology optimization does not require as many conceptual definitions of the design; and hence, is to be considered a more liberated way to optimize structures. However,

both the mathematical foundation and methodology for this is different than what is described in this report, and should be considered as a separate study entirely.

**Numerical approaches.** The present study was done on a continuous basis only. At a certain point it might be considered more constructive to base the analysis on numerical methods. The quantity of both literature and preceding studies on this topic is comprehensive; however, its application is current nonetheless. A recommended reading includes, as mentioned, [Arora12].

**Economic measures.** Directly relating shape and cost (not profit) might be an attractive approach to such optimization studies. This includes numerous factors in all parts of a project and such a study is highly applicable to real life.

**Isogeometric analysis.** The underlying shape representation in the software is NURBS based. NURBS plays a central role in isogeometric analysis. The software presented here might be able to provide for a suitable environment for such studies, though isogeometric elements are not included in the FEA solver Karamba.

**Material properties.** Including various materials with different material properties in the optimization might be a suitable may to optimize the structure, or impose limitations.

**Eigenmodes.** With original shapes, the eigenmodes of a structure might not be intuitive. Establishing a structures' eigenmodes help investigate both its dynamic properties as well as buckling characteristics, and could be included in an optimization study.

**Shells idealizations.** A study on matters related to the effects of idealizing shells, e.g. with beam elements, and what is the best practice of this may be of help to optimizing a structure in certain scenarios.

# Chapter 10

# FINAL WORDS

For me, the writing of this report has been a gateway to many interesting fields. Being introduced to the various specializations that relates to structural optimization has been motivating from beginning till end; and the more I have explored, the more I have been intrigued. As a student I am content with that the fact that I was able to expand upon the theories learned through my education. I have acquired a certain level of insight with the application of Grasshopper and Karamba, though even more competence with the software would have been preferable. Most importantly, I feel I have reached state of independence with both the theories and the software, a state where I am able to manage and adapt an approach to the needs of a problem and attain the information not yet possessed by me personally. In hindsight I see that more time invested in determining which fields that would be of direct relevance to the project and which that would not, might have helped make the process more streamlined in the early stages.

The report might have benefited from having two authors. From previous projects, I have experienced that the quality of a product at times is reflected by the interchanging of ideas and arguments between two or more parties. Let it be mentioned; however, that I personally have gained more independence through writing this report, and that the freedom of choosing a direction based on personal interest has been rewarding. The time spent figuring out a problem alone is indeed an investment that will pay off in future collaborations.

The last 20 weeks have been both tiresome and enjoyable at the same time.

Not having access to fellow students or professors at the university during the completion of the thesis has made it more challenging to overcome obstacles. At times, a good night of sleep a strong cup of coffee have been the only sources for inspiration needed to surmount adversities. If anything, I feel more comfortable in the on- line environments and forums now than before; a comfort I am sure to benefit from in the future.

I am left with the impression that my participation in the on- line environments has been of help also to other users of the software, as their participation has helped me. It is my hope that this proactive participation continues after the submission of the thesis, and that the lessons learned here will be added to the global web of knowledge that is the internet.

Benefiting from two separate departments at NTNU has been rewarding to me. I hope the work presented here at some level will be of pleasure also to them.

# References


[Cook99] **Cook, Robert Davis** and **Young, Warren C.**, *Advanced Mechanics of Materials - $2^{nd}$Edition* , Prentice-Hall, Inc., Madison, 1999

[Novozhilov64] **Novozhilov, Valentin Valentinovich**, *Thin Shell Theory*, P. Noordhoff, California, 1964

[Reitman90] **Borkowski, Adam** and **Jendo, Stefan**, *Structural Optimization, Volume 2, Mathematical Programming*, edited by Save, M. and Prager, William, Mathematical concepts and methods in science and engineering; 40, Plenum Press, New York, 1990, chapter 14 by Reitman, Mark I.

[Save85] **Save, M**. and **Prager, William**, *Structural Optimization, Volume 1, Optimality Criteria*, edited by Save, M. and Prager, William, Mathematical concepts and methods in science and engineering; 34, Plenum Press, New York, 1985, chapter 6 by Save, M.

[Ugural81] **Ugural, A. C.**, *Stresses in Plates and Shells*, McGraw-Hill, Inc., New York, 1981, chapter 10 to 13

[Ventsel01] **Ventsel, Eduard** and **Krauthammer, Theodor**, *Thin Plates and Shells - Theory, Analysis, and Applications*, Marcel Dekker, Inc., Pennsylvania, 2001

[Malumbres09] **Malumbres, Juan Luis Varona**, *Métodos Clásicos de Resolución de Ecuaciones Diferenciales Ordinarias*, Servicio de Publicaciones, La Rioja, 2009

[Mira12] **Alegria Mira, L.**, **De Temmerman, N.** and **Preisinger, C.**, *Structural optimisation of deployable scissor structures using new computational methods*, Brussel, 2012 (not yet published)

[Mohamad06] **Mohamad, G**, **Lourenco, P B** and **Roman, H R**, *Poisson Behaviour of Bedding Mortar Under Multiaxial Stress State*, 2006

[Payne09] **Payne, Andrew** and **Issa, Rajaa**, *The Grasshopper Primer, Second Edition - for version 0.6.0007*, 2009

[Preisinger12#1] **Preisinger, Clemens**, *Karamba User Manual for Version 0.9.084*, 2012

[Rutten10] **Rutten, David**, *Evolutionary Principles applied to Problem Solving*, 2010

## E-MAIL EXCHANGES

[Rutten12] **Rutten, David**, Bit-smith for Robert McNeel & Associates, May 1st - June 28th 2012

[Preisinger12#2] **Preisinger, Clemens**, Bollinger-Grohmann-Schneider ZT-GmbH Vienna, March 15th - June 4th 2012

# Bibliography

## BOOKS

### On Stresses in Shells

[Flügge60] **Flügge, Wilhelm**, *Stresses in Shells*, Springer-Verlag, Berlin, 1960

[Timoshenko59] **Timoshenko, Stephen P.**, *Theory of Plates and Shells*, McGraw-Hill Book Company, Inc., New York, 1959

### On Stability of Shells

[Timoshenko61] **Timoshenko, Stephen P.** and **Gere, James M.**, *Theory of Elastic Stability Second Edition*, Dover Publications, New York, 2009

### On Practice in Designing Shells

[Billington65] **Billington, David.**, *Thin Shell Concrete Structures*, McGraw-Hill Book Company, Inc., New York, 1965

### On Methods for Structural Optimization

[Arora12] **Arora, Jasbir S.**, *Introduction to optimum design, 3rd. edition*, Elsevier Inc., Iowa, 2012

### On Isogeometric Analysis

[Cottrell09] **Cottrell, J. Austin**, **Hughes, Thomas J. R.** and **Bazilevs, Yuri**, *Isogeometric Analysis: Toward Integration of CAD and FEA*, John Wiley & Sons, Ltd, Chichester, 2009

## PAPERS AND LECTURE NOTES

### On Topology, Shape and Size Optimization

[Ås06] **Ås, Sigmund Kyrre**, *Use of the finite element method for the optimization of structural components in engineering design*, Norwegian University of Science and Technology, Trondheim, 2006

### On Structural Optimization

[Bletzinger98] **Prof. Dr. Ing. Bletzinger, Kai- Uwe**, *Form Finding and Optimization of Membranes and Minimal Surfaces*, Technical University of Denmark, Lyngby, 1998

[Bletzinger11] **Prof. Dr. Ing. Bletzinger, Kai- Uwe**, *Structural Optimization*, Technische Universität München, München, 2011

### On Shape Generation Based on the Theory of Plasticity

[Bahr10] **Bahr, Marco** and **Kotnik, Toni**, *The generation of continuous membrane surfaces*, ETH Zurich, Zurich, 2010

### On Geometrical Representations Using NURBS

[Hughes04] **Hughes, T. J. R.**, **Cottrell, J. A.** and **Bazilevs, Y.**, *Isogeometric analysis: CAD, finite elements, NURBS, exact geometry and mesh refinement*, Computer Methods in Applied Mechanics and Engineering 194 (2005) 4135-4195, The University of Texas at Austin, Austin, 2004

**On Approaches to Optimized Shapes**

[Espath11] **Espath, L. F. R.**, **Linn, R. V.** and **Awruch, A. M.**, *Shape Optimization of shell structures based on NURBS description using automatic differentiation*, International Journal for Numerical Methods in Engineering; 88:613-636, John Wiley & Sons, Ltd, Federal University of Rio Grande do Sul, Porto Alegre, 2011

**On Mesh-Free FEA Software**

[Intact09] **Intact Solution, LLC**, *Scan&Solve™: FEA without Meshing*, 2009

**WEB PAGES**

**On NURBS**

[Altmann] **Altmann, Markus**, *About Nonuniform Rational B-Splines - NURBS*,
http://web.cs.wpi.edu/~matt/courses/cs563/talks/nurbs.html

[Rw06] *What is a NURBS?*, Realworld Graphics, 2006,
http://www.rw-designer.com/NURBS

[Schneider] **Schneider, Philip J**, *NURB Curves: A Guide for the Uninitiated*,
http://www.mactech.com/articles/develop/issue_25/schneider.html

**On Homogeneous Coordinates**

[Ahn05] **Ahn, Song Ho**, *Homogeneous Coordinates*, 2005, http://www.songho.ca/math/homogeneous/homogeneous.html

[Wildberger09] **Wildberger, Norman J.**, *WT33: Projective geometry and homogeneous coordinates*, 2009, http://www.youtube.com/watch?v=q3turHmOWq4

# Appendix A

# FIRST APPENDIX - Results

## A.1 Formulas for Uniform Global Loads Acting at an Angle

In table A.1 are exhibited the general formulas for curved beams subjected to a uniform, global load acting at an angle $\alpha$, with varying positions for the supports $\Delta x, \Delta y$. The heights of the beams are determined by the relation $\Delta r_{\parallel AC}(\alpha) = \Delta y \cdot sin(\alpha)$.

| $\alpha$ | $y(x, \Delta x, \Delta y)$ |
|---|---|
| $\frac{\pi}{2}$ | $x\frac{\Delta y}{\Delta x}(2 - \frac{x}{\Delta x})$ |
| $\frac{5\pi}{12}$ | $\frac{(3.730\Delta x+\Delta y)\sqrt{\Delta y}}{0.518\sqrt{\Delta x}+\sqrt{\Delta y}} - 3.732x - \frac{7.454\Delta x+1.998\Delta y}{(0.518\sqrt{\Delta x}+\sqrt{\Delta y})\sqrt{\Delta y}}(\frac{(0.933\Delta x+0.250\Delta y)\sqrt{\Delta y}}{0.518\sqrt{\Delta x}+\sqrt{\Delta y}} + \begin{Bmatrix} \sqrt{(\frac{(0.933\Delta x+0.250\Delta y)\sqrt{\Delta y}}{0.518\sqrt{\Delta x}+\sqrt{\Delta y}} - 0.500\Delta y)^2 + 1.000\Delta y \cdot x} \\ -\sqrt{(\frac{(0.933\Delta x+0.250\Delta y)\sqrt{\Delta y}}{0.518\sqrt{\Delta x}+\sqrt{\Delta y}} - 0.500\Delta y)^2 + 1.000\Delta y \cdot x} \end{Bmatrix})$ |
| $\frac{\pi}{3}$ | $\frac{(1.732\Delta x+\Delta y)\sqrt{\Delta y}}{0.760\sqrt{\Delta x}+\sqrt{\Delta y}} - 1.732x - \frac{2.000\Delta x+1.155\Delta y}{(0.760\sqrt{\Delta x}+\sqrt{\Delta y})\sqrt{\Delta y}}(\frac{(0.750\Delta x+0.433\Delta y)\sqrt{\Delta y}}{0.760\sqrt{\Delta x}+\sqrt{\Delta y}} + \begin{Bmatrix} \sqrt{(\frac{(0.750\Delta x+0.433\Delta y)\sqrt{\Delta y}}{0.760\sqrt{\Delta x}+\sqrt{\Delta y}} - 0.866\Delta y)^2 + 1.732\Delta y \cdot x} \\ -\sqrt{(\frac{(0.750\Delta x+0.433\Delta y)\sqrt{\Delta y}}{0.760\sqrt{\Delta x}+\sqrt{\Delta y}} - 0.866\Delta y)^2 + 1.732\Delta y \cdot x} \end{Bmatrix})$ |
| $\frac{\pi}{4}$ | $\frac{(1.000\Delta x+\Delta y)\sqrt{\Delta y}}{1.000\sqrt{\Delta x}+\sqrt{\Delta y}} - 1.000x - \frac{1.000\Delta x+1.000\Delta y}{(1.000\sqrt{\Delta x}+\sqrt{\Delta y})\sqrt{\Delta y}}(\frac{(0.500\Delta x+0.500\Delta y)\sqrt{\Delta y}}{1.000\sqrt{\Delta x}+\sqrt{\Delta y}} + \begin{Bmatrix} \sqrt{(\frac{(0.500\Delta x+0.500\Delta y)\sqrt{\Delta y}}{1.000\sqrt{\Delta x}+\sqrt{\Delta y}} - 1.000\Delta y)^2 + 2.000\Delta y \cdot x} \\ -\sqrt{(\frac{(0.500\Delta x+0.500\Delta y)\sqrt{\Delta y}}{1.000\sqrt{\Delta x}+\sqrt{\Delta y}} - 1.000\Delta y)^2 + 2.000\Delta y \cdot x} \end{Bmatrix})$ |
| $\frac{\pi}{6}$ | $\frac{(0.578\Delta x+\Delta y)\sqrt{\Delta y}}{1.316\sqrt{\Delta x}+\sqrt{\Delta y}} - 0.577x - \frac{0.667\Delta x+1.155\Delta y}{(1.317\sqrt{\Delta x}+\sqrt{\Delta y})\sqrt{\Delta y}}(\frac{(0.250\Delta x+0.433\Delta y)\sqrt{\Delta y}}{1.316\sqrt{\Delta x}+\sqrt{\Delta y}} + \begin{Bmatrix} \sqrt{(\frac{(0.250\Delta x+0.433\Delta y)\sqrt{\Delta y}}{1.316\sqrt{\Delta x}+\sqrt{\Delta y}} - 0.866\Delta y)^2 + 1.732\Delta y \cdot x} \\ -\sqrt{(\frac{(0.250\Delta x+0.433\Delta y)\sqrt{\Delta y}}{1.316\sqrt{\Delta x}+\sqrt{\Delta y}} - 0.866\Delta y)^2 + 1.732\Delta y \cdot x} \end{Bmatrix})$ |
| $\frac{\pi}{12}$ | $\frac{(0.268\Delta x+\Delta y)\sqrt{\Delta y}}{1.929\sqrt{\Delta x}+\sqrt{\Delta y}} - 0.268x - \frac{2.143\Delta x+7.994\Delta y}{(1.931\sqrt{\Delta x}+\sqrt{\Delta y})\sqrt{\Delta y}}(\frac{(0.067\Delta x+0.250\Delta y)\sqrt{\Delta y}}{1.931\sqrt{\Delta x}+\sqrt{\Delta y}} + \begin{Bmatrix} \sqrt{(\frac{(0.067\Delta x+0.250\Delta y)\sqrt{\Delta y}}{1.931\sqrt{\Delta x}+\sqrt{\Delta y}} - 0.500\Delta y)^2 + 1.000\Delta y \cdot x} \\ -\sqrt{(\frac{(0.067\Delta x+0.250\Delta y)\sqrt{\Delta y}}{1.931\sqrt{\Delta x}+\sqrt{\Delta y}} - 0.500\Delta y)^2 + 1.000\Delta y \cdot x} \end{Bmatrix})$ |

Table A.1: *General shapes for global load acting at a selection of angles, variable positions for the supports $\Delta x, \Delta y$, height defined by $\Delta r_{\|AC}(\alpha) = \Delta y \cdot sin(\alpha)$*

## A.2 Formulas for Perpendicular Load Depending on 'x'

The estimated shapes found in section 4.2.2.2 are represented by the formulas given in table A.2 and A.3. They are found by a one- time analytical iteration. The first one is found on the basis of a straight line, $x_{1a}(y) = y\frac{\Delta x}{\Delta y}$, and the second one is found on the basis of a parabola, $x_{1b}(y) = \Delta x(1 - \sqrt{1 - \frac{y}{\Delta y}})$. The formulas are found for the case $\Delta x = \Delta y = 1$. It is mentioned that only the parts $x_{2a}(y)_3$ and $x_{2b}(y)_3$ of the solutions are displayed in figure 4.9.

| Iteration | $x_i(y)$ |
|---|---|
| $x_{2a}(y)$ | $\left\{ \begin{array}{c} a(y)^{-\frac{1}{3}} + a(y)^{\frac{1}{3}} \\ -\frac{1}{2}(a(y)^{-\frac{1}{3}} + a(y)^{\frac{1}{3}}) - \frac{\sqrt{3}}{2}i[a(y)^{-\frac{1}{3}} - a(y)^{\frac{1}{3}}] \\ -\frac{1}{2}(a(y)^{-\frac{1}{3}} + a(y)^{\frac{1}{3}}) + \frac{\sqrt{3}}{2}i[a(y)^{-\frac{1}{3}} - a(y)^{\frac{1}{3}}] \end{array} \right\}^{\star}$ |
| $x_{2b}(y)$ | $\left\{ \begin{array}{c} b(y)^{-\frac{1}{3}} + b(y)^{\frac{1}{3}} \\ -\frac{1}{2}(b(y)^{-\frac{1}{3}} + b(y)^{\frac{1}{3}}) - \frac{\sqrt{3}}{2}i[b(y)^{-\frac{1}{3}} - b(y)^{\frac{1}{3}}] \\ -\frac{1}{2}(b(y)^{-\frac{1}{3}} + b(y)^{\frac{1}{3}}) + \frac{\sqrt{3}}{2}i[b(y)^{-\frac{1}{3}} - b(y)^{\frac{1}{3}}] \end{array} \right\}^{\star}$ |

Table A.2: *Shapes found by one- time analytical iteration for a perpendicular load linearly dependent on 'x'; $\Delta x = \Delta y = 1$; $(q_{nA}, q_{nB}) = (0, 1)$. $^{\star}$Intermediate functions $a(y)$ and $b(y)$ are given in table A.3*

| $a(y)$ | $\sqrt{\frac{1}{4}y^6 + \frac{1}{2}y^4 + \frac{1}{4}y^2 - 1} - \frac{1}{2}y^3 - \frac{1}{2}y$ |
|---|---|
| $b(y)$ | $b_1(y) + \sqrt{b_2(y) + b_3(y)}$ |
| $b_1(y)$ | $\frac{13}{10}y - 2y(1-y)^{\frac{3}{2}} + 2(1-y)^{\frac{3}{2}} - \frac{6}{5}(1-y)^{\frac{5}{2}} - \frac{3}{2}y^2 - \frac{4}{5}$ |
| $b_2(y)$ | $-\frac{132}{25}y + \frac{1049}{100}y^2 - \frac{103}{10}y^3 + \frac{109}{20}y^4 - \frac{16}{25}y^5 + \frac{7}{25}$ |
| $b_3(y)$ | $(\frac{42}{5}y - \frac{56}{5}y^2 + 6y^3 - \frac{16}{5})(1-y)^{\frac{3}{2}} + (-\frac{78}{25}y + \frac{18}{5}y^2 + \frac{48}{25})(1-y)^{\frac{5}{2}}$ |

Table A.3: *Functions introduced to $x_{2a}(y)$ and $x_{2b}(y)$ in table A.2*

## A.3 Perpendicular Load Depending on 'x' Found from Software

As some analytical effort was invested in the prediction of the optimum shape of a beam subjected to a perpendicular load whose density is linearly dependent on 'x', a solution found by the software is included for the sake of curiosity. No new method is tried out in this research; thus, the example is not part of the report.

The model is defined by independent points evenly distributed on the y-axis; parameters to be optimized are $y_{i=1,2...k}$. It is assigned $k = 10$ beam elements. The load is a line load $q_{n.i}$ acting normally to each beam element '$i$'. Its magnitude is defined by the average x- coordinate of each beam element in the following manner

$$q_{n.i} = q_{max} \frac{1}{\Delta x} \frac{x_i + x_{i-1}}{2} \tag{A.1}$$

where $q_{max}$ is the load density in $(\Delta x, \Delta y)$.

The optimization process ended after 415 generations. The result is included in figure A.1.

Note that the optimization was executed with $q_{max} = 1 \frac{kN}{m}$ and with $\Delta x = \Delta y = 10m$; $y_{i=1,2...k} \in [0, 10m]$ In figure A.1, the graph is scaled to match those presented in figure 4.9, section 4.2.2.2. With these values, the peak moment acting in the beam is $13,694 \times 10^{-3} kNm$. One might suspect that the peak moment is proportional to the second order of the size of the centroidal axis of beam and proportional to the first order of the load density. If this is the case, the comparable moment would be $0,13694 \times 10^{-3}$. This is significantly less than that of both the approximated shapes found using analytical convergence. This is in spite of a resulting shape being in closer proximity to the one with more bending moment. It is suspected that this logical discrepancy is due to inaccuracies in the model, like that of the load idealization and the discretization of the beam. This suspicion will not be further investigated.

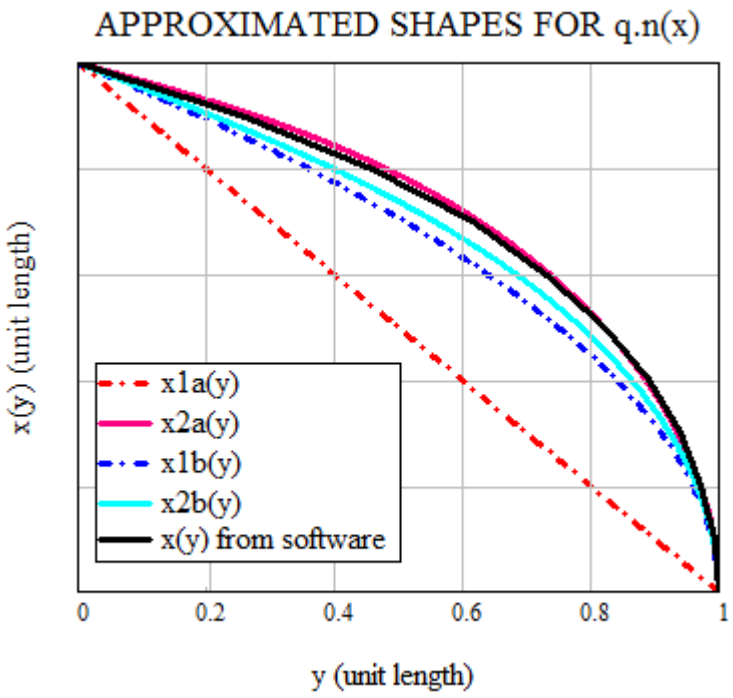


Figure A.1: *Approximated shapes for the load $q_n(x)$ including an approximated shape found by applying the software*

# Appendix B

# SECOND APPENDIX - Theories

A number of theories have been investigated and derived, but not included in the report. Some of them might play a role in aiding further work, and will therefore be included in this appendix.

## B.1 Double Curvature Shell

It will in the following be attempted to establish the theoretical foundation for estimating the moment distribution in double curvature shells.

### Geometrical Descriptions

In order to describe the shape of a free form shell with only two variables, its surface is divided by planes parallel to the Cartesian coordinates $x$ and $y$. Accordingly, the general description of the surface is given the notation

$$\boldsymbol{r}(\mathbf{x},\mathbf{y}) = x \cdot \mathbf{e_x} + y \cdot \mathbf{e_y} + z(x,y) \cdot \mathbf{e_z} \tag{B.1}$$

This is also called a double curvature surface.

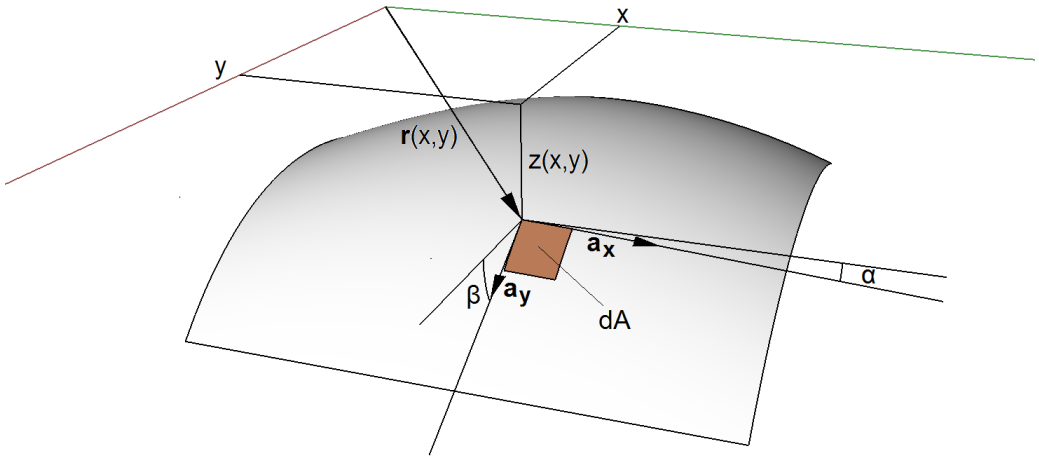


Figure B.1: *Notation for the geometrical description of a free form surface*

The tangent vectors parallel to the mentioned planes at any point on the surface are then

$$\mathbf{a_x} = \frac{\delta \boldsymbol{r}(\mathbf{x},\mathbf{y})}{\delta x} = \mathbf{e_x} + \frac{\delta z(x,y)}{\delta x} \cdot \mathbf{e_z} = \mathbf{e_x} + tan(\alpha) \cdot \mathbf{e_z} \tag{B.2}$$

and

$$\mathbf{a_y} = \frac{\delta \boldsymbol{r}(\mathbf{x},\mathbf{y})}{\delta y} = \mathbf{e_y} + \frac{\delta z(x,y)}{\delta y} \cdot \mathbf{e_z} = \mathbf{e_y} + tan(\beta) \cdot \mathbf{e_z} \tag{B.3}$$

where $\alpha$ and $\beta$ are the angles between the tangent vectors and the x, y- plane, figure B.1. It is important to note that $\mathbf{a_x}$ and $\mathbf{a_y}$ are neither unitary nor perpendicular to each other.

From this one can derive the lengths of the sides of an infinitesimal part of its surface

$$dS_x = \left| \frac{\delta \boldsymbol{r}(\mathbf{x},\mathbf{y})}{\delta x} \right| dx = |\mathbf{a_x}|\, dx = \sqrt{\mathbf{a_x} \cdot \mathbf{a_x}} dx = \sqrt{1 + tan^2(\alpha)} dx$$

$$dS_x = \frac{dx}{cos(\alpha)} \tag{B.4}$$

$$dS_y = \left| \frac{\delta \boldsymbol{r}(\mathbf{x},\mathbf{y})}{\delta y} \right| dy = |\mathbf{a_y}|\, dy = \sqrt{\mathbf{a_y} \cdot \mathbf{a_y}} dy = \sqrt{1 + tan^2(\beta)} dy$$

$$dS_y = \frac{dy}{cos(\beta)} \tag{B.5}$$

and its surface area

$$dA = |\mathbf{a_x} \cdot dx \times \mathbf{a_y} \cdot dy| = |\mathbf{a_x} \times \mathbf{a_y}|\, dx \cdot dy = \begin{vmatrix} \mathbf{e_x} & \mathbf{e_y} & \mathbf{e_z} \\ 1 & 0 & tan(\alpha) \\ 0 & 1 & tan(\beta) \end{vmatrix} dx \cdot dy$$

$$= |-tan(\alpha) \cdot \mathbf{e_x} - tan(\beta) \cdot \mathbf{e_x} + \mathbf{e_z}|\, dx \cdot dy$$

$$dA = \sqrt{1 + tan^2(\alpha) + tan^2(\beta)} dxdy \tag{B.6}$$

## Theories from Structural Mechanics

The intention is to establish the necessary theoretical tools to be able to describe a shell with double curvature subjected to a continuously distributed load $\mathbf{p} = \mathbf{p}(x, y)$. For the sake of making it more easily readable, the notation for dependence on x and y is not included in this section.

By adapting the notation used in [Reitman90] to what is already established in section B.1 and attempting to include not only the vertical component of the load, but also the horizontal components, one could argue as in the proceeding paragraphs.

### Membrane Theory

**Internal membrane forces** It is important to distinguish between forces acting relative to the tangent plane of the shell, and their projected counterparts, seen in the x, y- plane. The projected counterparts are assigned a '$\tilde{\square}$' marked over the symbol.

As $\mathbf{a_x}$ and $\mathbf{a_y}$ do not meet at right angles, the force vectors acting parallel to the x, z- plane and the y, z- plane interdepend as shown below in equations B.7 and B.8.

$$\mathbf{T_x} = T_x \frac{\mathbf{a_x}}{|\mathbf{a_x}|} + Q \frac{\mathbf{a_y}}{|\mathbf{a_y}|} \tag{B.7}$$

$$\mathbf{T_y} = Q \frac{\mathbf{a_x}}{|\mathbf{a_x}|} + T_y \frac{\mathbf{a_y}}{|\mathbf{a_y}|} \tag{B.8}$$

As the vectors act at angles relative to each other, $Q$ is equal in the two equations.

Intuitively, the membrane forces acting over a unit length in the tangent plane need to be equal to their counterparts acting over a corresponding unit length in the x, y- plane, $\mathbf{T_x} \cdot dS_y = \tilde{\mathbf{T}}_\mathbf{x} \cdot dy$ and $\mathbf{T_y} \cdot dS_x = \tilde{\mathbf{T}}_\mathbf{y} \cdot dx$. From equations B.4 and B.5 it is then obtained that

$$\mathbf{T_x} = \tilde{\mathbf{T}}_\mathbf{x} \cdot cos(\beta) \tag{B.9}$$

$$\mathbf{T_y} = \tilde{\mathbf{T}}_\mathbf{y} \cdot cos(\alpha) \tag{B.10}$$

The projected force vectors, expressed by both a vertical component and horizontal components are given the following notation

$$\tilde{\mathbf{T}}_\mathbf{x} = \tilde{T}_x \cdot \mathbf{e_x} + \tilde{Q} \cdot \mathbf{e_y} + \tilde{V}_x \cdot \mathbf{e_z} \tag{B.11}$$

$$\tilde{\mathbf{T}}_\mathbf{y} = \tilde{Q} \cdot \mathbf{e_x} + \tilde{T}_y \cdot \mathbf{e_y} + \tilde{V}_y \cdot \mathbf{e_z} \tag{B.12}$$

Equations B.7 and B.8 are equal to equations B.9 and B.10 correspondingly. Be replacing them with equation B.11 and B.12 it is possible to derive the following relations

$$T_x \frac{\mathbf{a_x}}{|\mathbf{a_x}|} + Q \frac{\mathbf{a_y}}{|\mathbf{a_y}|} = (\tilde{T}_x \cdot \mathbf{e_x} + \tilde{Q} \cdot \mathbf{e_y} + \tilde{V}_x \cdot \mathbf{e_z}) cos(\beta)$$

$$Q \frac{\mathbf{a_x}}{|\mathbf{a_x}|} + T_y \frac{\mathbf{a_y}}{|\mathbf{a_y}|} = (\tilde{Q} \cdot \mathbf{e_x} + \tilde{T}_y \cdot \mathbf{e_y} + \tilde{V}_y \cdot \mathbf{e_z}) cos(\alpha)$$

which lead to

$$T_x \cdot cos(\alpha)(\mathbf{e_x} + tan(\alpha) \cdot \mathbf{e_z}) + Q \cdot cos(\beta)(\mathbf{e_y} + tan(\beta) \cdot \mathbf{e_z}) = (\tilde{T}_x \cdot \mathbf{e_x} + \tilde{Q} \cdot \mathbf{e_y} + \tilde{V}_x \cdot \mathbf{e_z}) cos(\beta)$$

$$Q \cdot cos(\alpha)(\mathbf{e_x} + tan(\alpha) \cdot \mathbf{e_z}) + T_y \cdot cos(\beta)(\mathbf{e_y} + tan(\beta) \cdot \mathbf{e_z}) = (\tilde{Q} \cdot \mathbf{e_x} + \tilde{T}_y \cdot \mathbf{e_y} + \tilde{V}_y \cdot \mathbf{e_z}) cos(\alpha)$$

By equalizing each component individually, it is obtained that

$$T_x = \tilde{T}_x \frac{cos(\beta)}{cos(\alpha)} \tag{B.13}$$

$$Q = \tilde{Q} \tag{B.14}$$

$$\tilde{V}_x = \tilde{T}_x \cdot tan(\alpha) + \tilde{Q} \cdot tan(\beta) \tag{B.15}$$

$$T_y = \tilde{T}_y \frac{cos(\alpha)}{cos(\beta)} \tag{B.16}$$

$$\tilde{V}_y = \tilde{Q} \cdot tan(\alpha) + \tilde{T}_y \cdot tan(\beta) \tag{B.17}$$

**External load** As for the membrane forces, it is intuitively stated that a load acting over a unit area in the tangent plane needs to be equal to its counterpart acting over a corresponding unit area in the x, y- plane. The relation between the load acting in the tangent plane and its projection is

$$\mathbf{p} \cdot dA = \tilde{\mathbf{p}} \cdot dx \cdot dy$$

which combined with B.6 reveals that

$$\tilde{\mathbf{p}} = \mathbf{p} \cdot \sqrt{1 + tan^2(\alpha) + tan^2(\beta)} \tag{B.18}$$

where $\mathbf{p} = p_x \cdot \mathbf{e_x} + p_y \cdot \mathbf{e_y} + p_z \cdot \mathbf{e_z}$ and $\tilde{\mathbf{p}} = \tilde{p_x} \cdot \mathbf{e_x} + \tilde{p_y} \cdot \mathbf{e_y} + \tilde{p_z} \cdot \mathbf{e_z}$.

**Equations of equilibrium** Based in the x, y- plane, the equilibrium between the projected counterparts gives rise to the following relation

$$\frac{\delta \tilde{\mathbf{T}}_{\mathbf{x}}}{\delta x} + \frac{\delta \tilde{\mathbf{T}}_{\mathbf{y}}}{\delta y} + \tilde{\mathbf{p}} = 0 \tag{B.19}$$

By combining equation B.19 with equation B.11 and B.12, and equalizing each component individually it can be shown that

$$\frac{\delta \tilde{T_x}}{\delta x} + \frac{\delta \tilde{Q}}{\delta y} + \tilde{p_x} = 0 \tag{B.20}$$

$$\frac{\delta \tilde{Q}}{\delta x} + \frac{\delta \tilde{T_y}}{\delta y} + \tilde{p_y} = 0 \tag{B.21}$$

$$\frac{\delta \tilde{V_x}}{\delta x} + \frac{\delta \tilde{V_y}}{\delta y} + \tilde{p_z} = 0 \tag{B.22}$$

By then combining equations B.15, B.17, B.20, B.21 with B.22 the following result is obtained

$$\frac{\delta}{\delta x}(\tilde{T_x} \cdot tan(\alpha) + \tilde{Q} \cdot tan(\beta)) + \frac{\delta}{\delta y}(\tilde{Q} \cdot tan(\alpha) + \tilde{T_y} \cdot tan(\beta)) + \tilde{p_z} = 0$$

$$\tilde{T_x}\frac{\delta^2 z}{\delta x^2} + \frac{\delta \tilde{T_x}}{\delta x}\frac{\delta z}{\delta x} + \tilde{Q}\frac{\delta^2 z}{\delta x \delta y} + \frac{\delta \tilde{S}}{\delta x}\frac{\delta z}{\delta y} + \tilde{Q}\frac{\delta^2 z}{\delta y \delta x} + \frac{\delta \tilde{Q}}{\delta y}\frac{\delta z}{\delta x} + \tilde{T_y}\frac{\delta^2 z}{\delta y^2} + \frac{\delta \tilde{T_y}}{\delta y}\frac{\delta z}{\delta y} + \tilde{p_z} = 0$$

$$\tilde{T_x}\frac{\delta^2 z}{\delta x^2} + 2\tilde{Q}\frac{\delta^2 z}{\delta x \delta y} + \tilde{T_y}\frac{\delta^2 z}{\delta y^2} = -\tilde{p_z} - (\frac{\delta \tilde{T_x}}{\delta x} + \frac{\delta \tilde{Q}}{\delta y})\frac{\delta z}{\delta x} - (\frac{\delta \tilde{Q}}{\delta x} + \frac{\delta \tilde{T_y}}{\delta y})\frac{\delta z}{\delta y}$$

$$\tilde{T_x}\frac{\delta^2 z}{\delta x^2} + 2\tilde{Q}\frac{\delta^2 z}{\delta x \delta y} + \tilde{T_y}\frac{\delta^2 z}{\delta y^2} = -\tilde{p_z} + \tilde{p_x}\frac{\delta z}{\delta x} + \tilde{p_y}\frac{\delta z}{\delta y} \tag{B.23}$$

where $tan(\alpha) = \frac{\delta z}{\delta x}$ and $tan(\beta) = \frac{\delta z}{\delta y}$.

The equation proposed by Pucher is reached by introducing Airy's function $\varphi(x, y)$, [Reitman90] and including the contributions from the horizontal components in the following manner; $\tilde{T_x} = \frac{\delta^2\varphi}{\delta y^2} - \int \tilde{p_x} dx$, $\tilde{T_y} = \frac{\delta^2\varphi}{\delta x^2} - \int \tilde{p_y} dy$ and $\tilde{Q} = -\frac{\delta^2\varphi}{\delta x \delta y}$. The equilibrium is verified by replacing the assumed relations into equations B.20 and B.21: $\frac{\delta^3\varphi}{\delta x \delta y^2} - \tilde{p_x} - \frac{\delta^3\varphi}{\delta x \delta y^2} + \tilde{p_x} = 0$ and $-\frac{\delta^3\varphi}{\delta x^2 \delta y} + \frac{\delta^3\varphi}{\delta x^2 \delta y} - \tilde{p_y} + \tilde{p_y} = 0$.
By introducing the relations to equation B.23, the differential equation of the problem is obtained:

$$\frac{\delta^2\varphi}{\delta y^2}\frac{\delta^2 z}{\delta x^2} - 2\frac{\delta^2\varphi}{\delta x \delta y}\frac{\delta^2 z}{\delta x \delta y} + \frac{\delta^2\varphi}{\delta x^2}\frac{\delta^2 z}{\delta y^2} = -\tilde{p_z} + \tilde{p_x}\frac{\delta z}{\delta x} + \tilde{p_y}\frac{\delta z}{\delta y} + \frac{\delta^2 z}{\delta x^2}\int \tilde{p_x} dx + \frac{\delta^2 z}{\delta y^2}\int \tilde{p_y} dy \tag{B.24}$$

### Bending Theory

The easiest way to include bending- and torsional moments is to add Lagrange's operator, $LA(M) = \frac{\delta^2 M_x}{\delta x^2} + 2\frac{\delta^2 M_{xy}}{\delta x \delta y} + \frac{\delta^2 M_y}{\delta y^2}$ to equation B.24, [Reitman90]. Doing so yields the final differential equation for the double curvature shell

$$\frac{\delta^2 M_x}{\delta x^2} + 2\frac{\delta^2 M_{xy}}{\delta x \delta y} + \frac{\delta^2 M_y}{\delta y^2} + \frac{\delta^2\varphi}{\delta y^2}\frac{\delta^2 z}{\delta x^2} - 2\frac{\delta^2\varphi}{\delta x \delta y}\frac{\delta^2 z}{\delta x \delta y} + \frac{\delta^2\varphi}{\delta x^2}\frac{\delta^2 z}{\delta y^2} =$$

$$= -\tilde{p_z} + \tilde{p_x}\frac{\delta z}{\delta x} + \tilde{p_y}\frac{\delta z}{\delta y} + \frac{\delta^2 z}{\delta x^2}\int \tilde{p_x} dx + \frac{\delta^2 z}{\delta y^2}\int \tilde{p_y} dy \tag{B.25}$$

### Force- Strain Relations

Analogue to the material laws and moment- curvature relations stated in section 2.3.2.3, the relations between the strains and the forces and moments are as follows

$$\begin{bmatrix} T_x \\ T_y \\ S \end{bmatrix} = \frac{E \cdot t}{1 - \nu^2} \begin{bmatrix} 1 & \nu & 0 \\ \nu & 1 & 0 \\ 0 & 0 & \frac{1-\nu}{2} \end{bmatrix} \begin{bmatrix} \varepsilon_x \\ \varepsilon_y \\ \gamma_{xy} \end{bmatrix} \tag{B.26}$$

$$\begin{bmatrix} M_x \\ M_y \\ M_{xy} \end{bmatrix} = D \begin{bmatrix} 1 & \nu & 0 \\ \nu & 1 & 0 \\ 0 & 0 & 1-\nu \end{bmatrix} \begin{bmatrix} \kappa_x \\ \kappa_y \\ \kappa_{xy} \end{bmatrix} \tag{B.27}$$

In the preceding equations, $t$ is the thickness of the shallow shell, $\gamma_{xy}$ is the shear strain and $\kappa_{xy}$ and $M_{xy}$ are the twisting and twisting moments of the shell respectively.

**Kinematic Relations**

A more modern piece of literature on the subject of thin shells that gives a summary of preceding works is [Ventsel01]. It is one step closer to the subject of tensor analysis. It states the kinematic relations for the shell as follows

$$\varepsilon_1 = \frac{1}{A}\frac{\delta u}{\delta I} + \frac{1}{A \cdot B}\frac{\delta A}{\delta II}v - \frac{w}{R_1} \tag{B.28}$$

$$\varepsilon_2 = \frac{1}{B}\frac{\delta v}{\delta II} + \frac{1}{A \cdot B}\frac{\delta B}{\delta I}u - \frac{w}{R_2} \tag{B.29}$$

$$\gamma_{12} = \frac{B}{A}\frac{\delta}{\delta I}(\frac{v}{B}) + \frac{A}{B}\frac{\delta}{\delta II}(\frac{u}{A}) \tag{B.30}$$

$$\kappa_1 = -[\frac{1}{A}\frac{\delta}{\delta I}(\frac{u}{R_1} + \frac{1}{A}\frac{\delta w}{\delta I}) + \frac{1}{A \cdot B}\frac{\delta A}{\delta II}(\frac{v}{R_2} + \frac{1}{B}\frac{\delta w}{\delta II})] \tag{B.31}$$

$$\kappa_2 = -[\frac{1}{B}\frac{\delta}{\delta II}(\frac{v}{R_2} + \frac{1}{B}\frac{\delta w}{\delta II}) + \frac{1}{A \cdot B}\frac{\delta B}{\delta I}(\frac{u}{R_1} + \frac{1}{A}\frac{\delta w}{\delta I})] \tag{B.32}$$

$$\kappa_{12} = -[\frac{1}{AB}(-\frac{1}{A}\frac{\delta A}{\delta II}\frac{\delta w}{\delta I} - \frac{1}{B}\frac{\delta B}{\delta I}\frac{\delta w}{\delta II}) + \frac{1}{R_1}\frac{A}{B}\frac{\delta}{\delta II}(\frac{u}{A}) + \frac{1}{R_2}\frac{B}{A}\frac{\delta}{\delta I}(\frac{v}{B})] \tag{B.33}$$

One key feature of this approach is that all quantities are referred to a coordinate system local to the shell's surface (middle surface), not necessarily Cartesian. Sub-indices 1 and 2 refer to the directions tangent to the surface

by which the initial curvature is at its maximum and minimum respectively. These are called principal directions and are by definition orthogonal.

$I$ and $II$ are independent variables mapping out locations on the shell's surface, referred to as curvilinear coordinates. Relating to the global x, y and z- coordinates, equation B.1, the position vector is a follows

$$\boldsymbol{r}(\mathbf{I},\mathbf{II}) = x(I,II)\cdot\mathbf{e_x} + y(I,II)\cdot\mathbf{e_y} + z(I,II)\cdot\mathbf{e_z} \tag{B.34}$$

Given that $I$ and $II$ form an orthogonal net (contrary to $\mathbf{a_x}$ and $\mathbf{a_y}$ in equations B.2 and B.3), the Lamé parameters $A$ and $B$ are given as

$$A = \sqrt{\frac{\delta\boldsymbol{r}(\mathbf{I},\mathbf{II})}{\delta I}\cdot\frac{\delta\boldsymbol{r}(\mathbf{I},\mathbf{II})}{\delta I}} \tag{B.35}$$

$$B = \mathbf{e_3}\cdot\frac{\delta^2\boldsymbol{r}(\mathbf{I},\mathbf{II})}{\delta I^2} \tag{B.36}$$

where $\mathbf{e_3}$ is a unit vector normal to the surface.

$u$, $v$ and $w$ are the displacements in the directions parallel to the axes in the local coordinate system.

# Appendix C

# THIRD APPENDIX - Models and Scripts

## C.1 Models From Grasshopper and Karamba

The canvases of a representative selection of the models used in this research are exhibited on the proceeding pages.

1. Figure C.1: Curved Beams involving declining points
2. Figure C.2: Curved Beams involving interpolation points
3. Figure C.3: The Dome, with crossing diagonals
4. Figure C.4: The Kuwait International Airport shell, with crossing diagonals, 10 beams on border AB and AC

Some descriptions are added. For a more detailed and interactive look at the models; the models are included as attachments, appendix D.2.

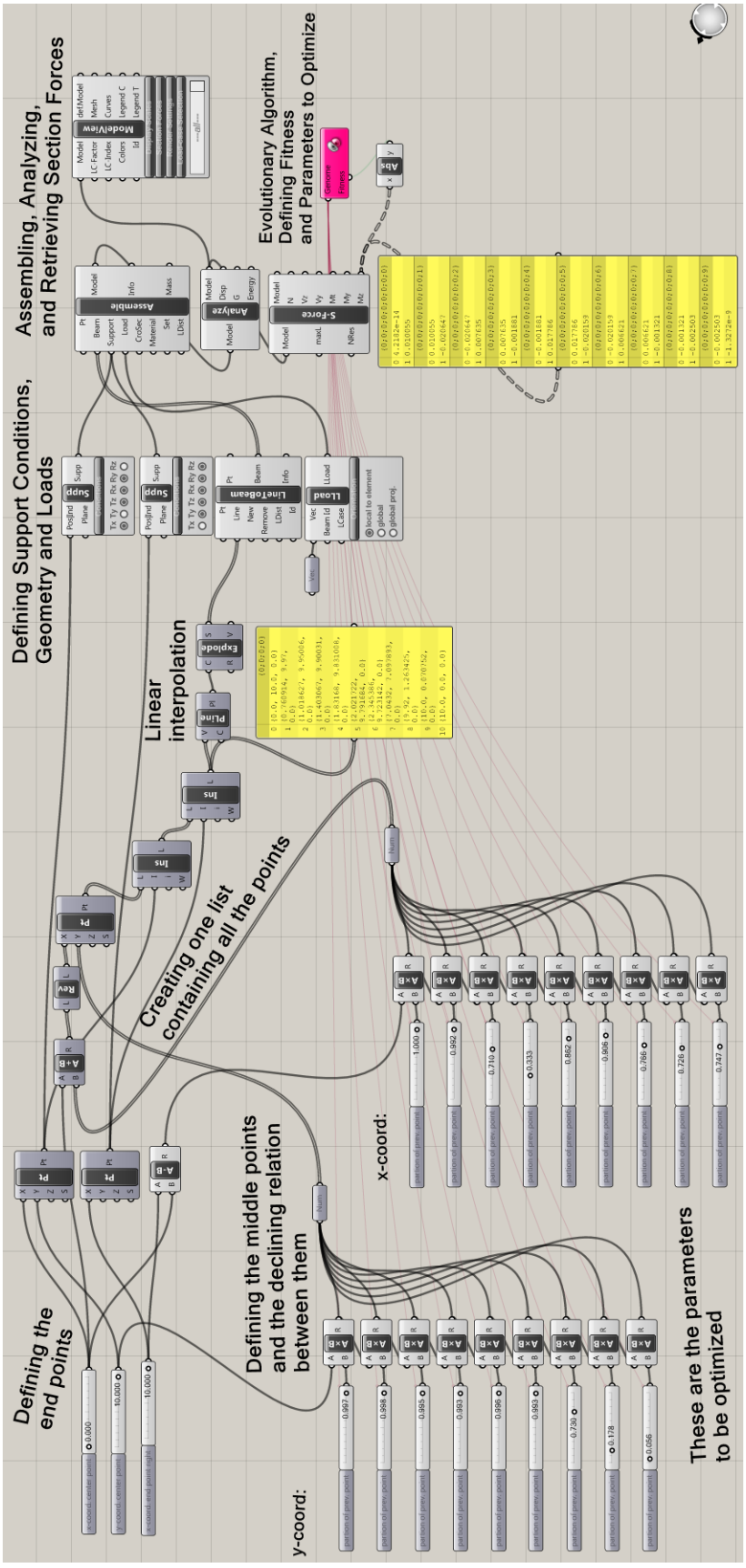


Figure C.1: *Canvas for Curved Beams involving declining points*

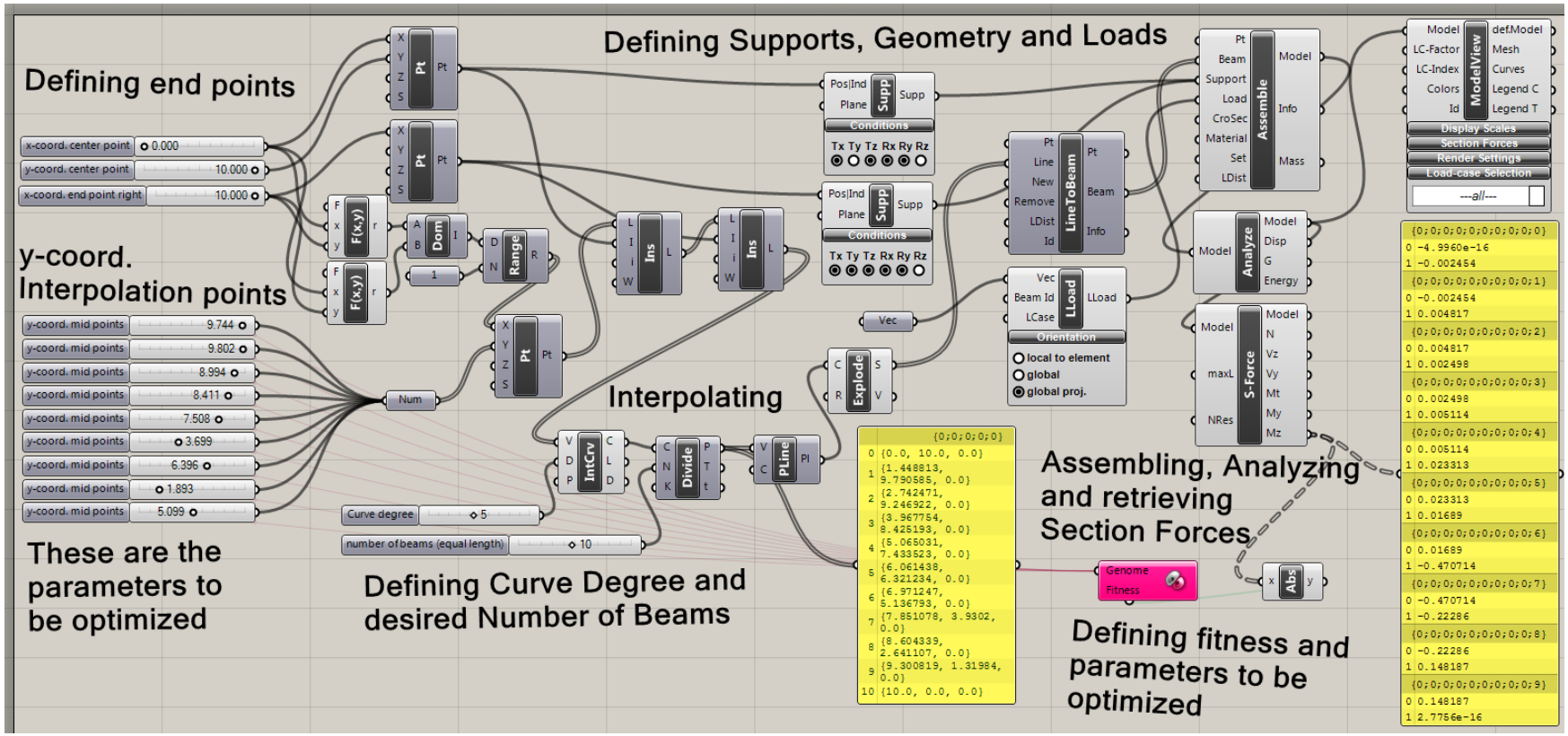


Figure C.2: *Canvas for Curved Beams involving interpolation points*

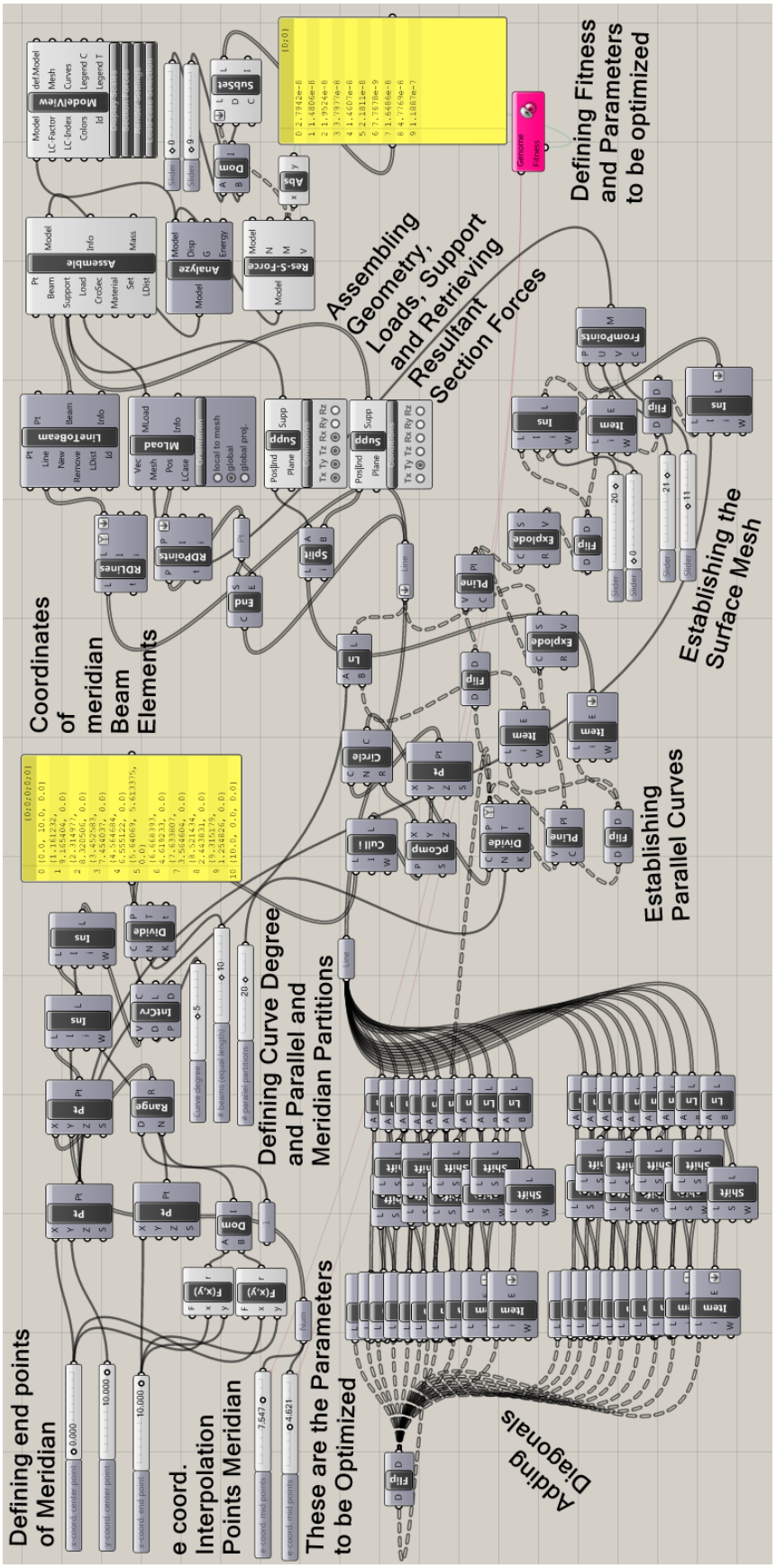


Figure C.3: *Canvas for The Dome, with diagonals*

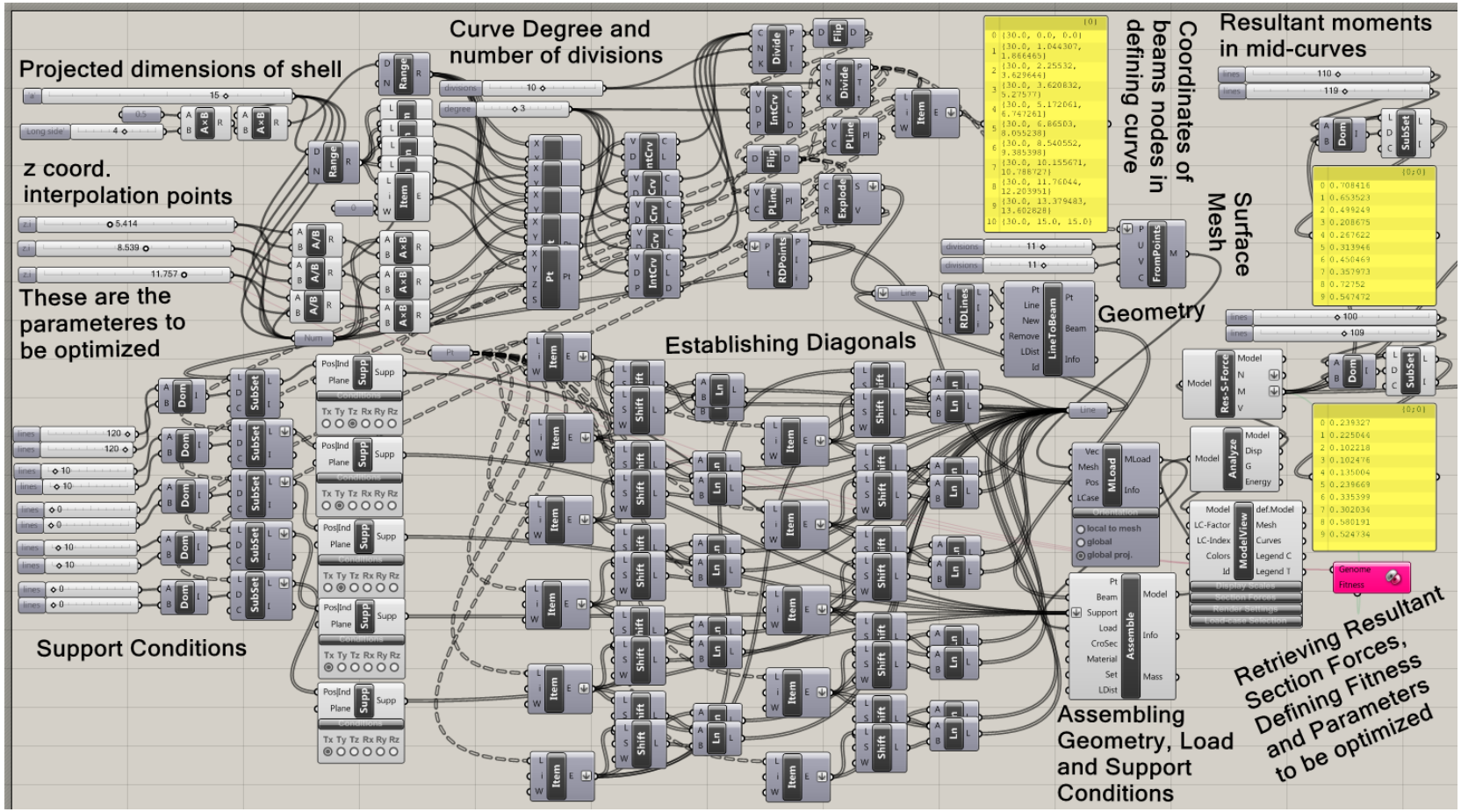


Figure C.4: *Canvas for The Kuwait International Airport shell, with diagonals*

## C.2 Script for Graphing Moment in Beam

Due to the comprehensive formulas arising in section 4.2.2.2; for the sake of convenience, the final moment distributions were found with the aid of the script included in this appendix. The script is in the format of an earlier version of Mathcad. The case in question was the curved beam subjected to a perpendicular load linearly dependent on 'x'.

$\Delta y := 1$ $\Delta x := 1$ $q_{n.A} := 0$ $q_{n.B} := 1$

$\blacksquare := \frac{\Delta x}{\Delta y} \cdot y$ $x_q(y) := \Delta x \cdot \left(1 - \sqrt{1 - \frac{y}{\Delta y}}\right)$

$q_n(x_q) := q_{n.A} + \frac{x_q}{\Delta x} \cdot (q_{n.B} - q_{n.A}) \rightarrow x_q$

$q_{xp}(y) := q_n(x_q(y)) \rightarrow 1 - \sqrt{1 - y}$

$q_{yp}(x) := q_n(x) \rightarrow x$

$q_{xp1}(y) := y$

$q_{xp2}(y) := 1 - \sqrt{1 - y}$

$A_y(\Delta x) := \int_0^{\Delta x} q_{yp}(x)\, dx$

$A_x(\Delta x, \Delta y) := \int_0^{\Delta y} q_{xp}(y) \cdot \left(\frac{y}{\Delta y} - 1\right) dy + \frac{1}{\Delta y} \cdot \int_0^{\Delta x} q_{yp}(x) \cdot x\, dx$

$M_{qx}(y) := \int_0^{y} q_{xp}(\psi) \cdot (y - \psi)\, d\psi$

$M_{qy}(x) := \int_0^{x} q_{yp}(\chi) \cdot (x - \chi)\, d\chi$

---

Solving for 'x': => $A_x(\Delta x, \Delta y) \cdot y(x) + M_{qx}(y(x)) = A_y(\Delta x) \cdot x - M_{qy}(x)$

$A_x(\Delta x, \Delta y) \cdot y + M_{qx}(y) \rightarrow \frac{7 \cdot y}{30} - \frac{2 \cdot (1 - y)^{\frac{3}{2}}}{3} + \frac{2 \cdot (1 - y)^{\frac{5}{2}}}{5} + \frac{y^2}{2} + \frac{2 \cdot y \cdot \left[(1 - y)^{\frac{3}{2}} - 1\right]}{3} + \frac{4}{15}$

$A_y(\Delta x) \cdot x - M_{qy}(x) \rightarrow \frac{x}{2} - \frac{x^3}{6}$ gives $x_2(y)$.

Changing the initial function for $x_q(y)$ to y*Δx/Δy and following the same steps gives $x_1(y)$.

---

Figure C.5: *Script for graphing moment in beam, page 1/2*

$$x_a(y) := \frac{\Delta x}{\Delta y}\cdot y \qquad x_b(y) := \Delta x\cdot\left(1 - \sqrt{1 - \frac{y}{\Delta y}}\right)$$

$$x_{M1}(y) := x_1(y)_3 \qquad x_{M2}(y) := x_2(y)_3$$

$$q_{xpM1}(y) := q_n\left(x_{M1}(y)\right)$$

$$q_{xpM2}(y) := q_n\left(x_{M2}(y)\right)$$

$$A_{yM1} := \int_0^{\Delta x} q_{yp}(x)\,dx$$

$$A_{yM2} := \int_0^{\Delta x} q_{yp}(x)\,dx$$

$$A_{xM1} := \int_0^{\Delta y} q_{xpM1}(y)\cdot\left(\frac{y}{\Delta y} - 1\right)dy + \frac{1}{\Delta y}\cdot\int_0^{\Delta x} q_{yp}(x)\cdot x\,dx$$

$$A_{xM2} := \int_0^{\Delta y} q_{xpM2}(y)\cdot\left(\frac{y}{\Delta y} - 1\right)dy + \frac{1}{\Delta y}\cdot\int_0^{\Delta x} q_{yp}(x)\cdot x\,dx$$

$$M_{qyM1}(y) := \int_0^{x_{M1}(y)} q_{yp}(\chi)\cdot\left(x_{M1}(y) - \chi\right)d\chi$$

$$M_{qyM2}(y) := \int_0^{x_{M2}(y)} q_{yp}(\chi)\cdot\left(x_{M2}(y) - \chi\right)d\chi$$

$$M_{qxM1}(y) := \int_0^{y} q_{xpM1}(\psi)\cdot(y - \psi)\,d\psi$$

$$M_{qxM2}(y) := \int_0^{y} q_{xpM2}(\psi)\cdot(y - \psi)\,d\psi$$

$$M_{2a}(y) := A_{xM1}\cdot y - A_{yM1}\cdot x_{M1}(y) + M_{qxM1}(y) + M_{qyM1}(y)$$

$$M_{2b}(y) := A_{xM2}\cdot y - A_{yM2}\cdot x_{M2}(y) + M_{qxM2}(y) + M_{qyM2}(y)$$

$$M_a(y) := -\frac{y\cdot\left(y^2 - 1\right)}{3} \qquad ; \qquad M_b(y) := -\frac{4}{15}\cdot\left[1 - (1 - y)^{\frac{5}{2}}\right] - \frac{y}{2}\cdot\left(y + \frac{y^2}{3} - \frac{28}{15}\right)$$

Figure C.6: *Script for graphing moment in beam, page 2/2*

# Appendix D

# FOURTH APPENDIX - Attachments

## D.1 Content Delivered as a ZIP- file

Some content is delivered using the thesis registration system of NTNU on the internet. This includes a ZIP- file with the following content:

#### Video Tutorials

Two short video tutorials are included to demonstrate the basic workflow within the software. The video tutorials have the following plots:

**Dome tutorial 1:** Shows the basic set- up of the dome model with crossing diagonals presented in the report. The load density is 1kN/m^2.

**Dome tutorial 2:** Shows what it looks like when the evolutionary solver is running. The first 15 generations are included, and the video skips between generation # 3 and 13.

**Models from Grasshopper and Karamba, Appendix C.1**

The models, as presented in appendix C.1, are included in the ZIP- file for a more detailed and interactive look.

## D.2 Content on Compact Disk

All the models that form the basis for the results in this report are included on a separate compact disk. They are neither added descriptions nor edited for the sake readability.